

Deep Space Metallurgy

Final Report
Sponsored by Dr. Bowman, Arizona State University
NASA Psyche Inspired Program

Jonah Fechner
Scott Hennarty
Mikaela Ikeda
Ryan Krieghbaum

May 1, 2024

In partial fulfillment of the requirements of the course:
ME 472: Capstone Design III

Dr. Sangelkar, Dr. McCormack, Dr. Chambers
RHIT Mechanical Engineering

Executive Summary

Psyche is a metal-rich asteroid located in the asteroid belt between Mars and Jupiter. It is hypothesized that Psyche may be the core of an early planetary formation, known as a planetesimal, that had its rocky exterior stripped away by a massive collision. By studying Psyche, NASA hopes to learn more about the origin and formation of Earth.

The current Psyche mission launched on October 13, 2023, and plans to orbit the asteroid to study it from afar. If this mission is successful, future missions may include surface exploration, which would include in-situ resource utilization (ISRU). ISRU is the concept of using the resources on the asteroid for the mission and could provide significant savings in part replacement and generation. Common ISRU functions include imaging, separation, and manufacturing of material. The purpose of this project is to explore preparation of the material for manufacturing, with a focus on **designing a heating mechanism capable of melting the materials of Psyche in deep-space conditions.**

The design must successfully operate under the conditions of Psyche, which include a vacuum environment as well as low external temperatures and low gravity. In these conditions, the design must be capable of reaching the melting point of iron (1810K) and physically containing a significant quantity of material (8cm³). The design also prioritizes operating within minimal weight and volume constraints, using less than 1950W of power, and mitigating thermal losses. The values for the technical specifications were primarily determined through analysis of research on Psyche's environment and benchmarking to similar spacecraft and traditional metallurgy. These specifications will be evaluated for the final design through a variety of methods, such as analysis of a CAD model, thermal simulations, and heat transfer analysis.

The design-to-date utilizes induction as its heating method and was chosen after evaluating the generated concepts with a decision matrix. A visual of the design is shown below in Figure 1.

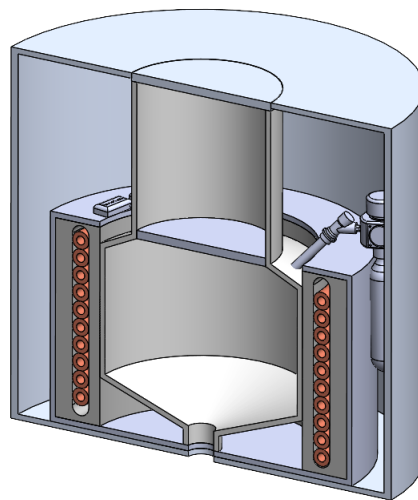


Figure 1: CAD model for heating via induction

This design utilizes the available solar energy on the Psyche spacecraft to energize the sample through a high-frequency electromagnetic field, causing heat generation. The sample will also be surrounded by insulating material and radiation shields to minimize heat transfer to the environment.

In the fall quarter, we generated our problem statement and resulting project scope. We defined key objectives, design functions, and technical specifications, explored preliminary concepts, and proved project viability. We decided on exploring induction heating to melt the sample, and concluded solar power was enough to power the system. We performed baseline mathematical calculations to demonstrate that this system could work with numerous assumptions and found that there was capability for success of this system.

In the winter quarter, we finalized the CAD model of the induction heating system and created a mathematical model and thermal simulation. These models were compared to a similar experiment that the Los Alamos National Laboratory (LANL) conducted and a physical experiment we ran using pewter (99.9% tin) to validate their assumptions and setup. We also determined sublimation, a large concern for the system in the fall quarter, negligible based on work done through a material property database and research on melting lunar regolith to extract metals. The mathematical model and thermal simulation aligned with the results of the physical experiment, were validated using the LANL experiment, and were then modified simultaneously to ensure both could represent Psyche conditions to the best of our ability.

In the spring quarter, we finalized our mathematical model and thermal simulation work and evaluated these models against our technical specifications. We succeeded at most of our technical specifications, most notably holding internal temperature, all volumetric and weight specifications, and startup power limitations, but we did not meet our external temperature, melting point, or operational power technical specifications. After analysis of our system progress over the last year, we found that most of the reasons we failed to meet technical specifications were either lack of time or lack of computational power, so we were satisfied with the progress we made with this project. We also ran a breakeven cost analysis and found that the mass of our system was roughly equivalent to the weight of four samples being melted through our system, which makes the system financially sound in terms of launch cost, since the lifetime of our system should be significantly larger than four cycles.

From our progress over the last year, we believe the system we researched and designed is a feasible possibility for a system that could launch to Psyche and be part of an in-situ resource utilization project. While we did not meet every technical specification and have numerous recommendations for how this system should be further pursued, the foundation of the system and the mathematical model is sound, and we believe in the work we have completed.

Disclaimer

The contents of this report were prepared by senior mechanical engineering students at the Rose-Hulman Institute of Technology. We feel confident in our work as students. However, all material should be reviewed by an appropriate professional before implementation.

This work was created in partial fulfillment of the Rose-Hulman Institute of Technology Capstone Course, ME470-ME472. The work is a result of the Psyche Student Collaborations component of NASA's Psyche Mission (<https://psyche.asu.edu>). "Psyche: A Journey to a Metal World" [Contract Number NNM16AA09C] is part of the NASA Discovery Program mission to solar system targets. Trade names and trademarks of ASU and NASA are used in this work for identification only. Their usage does not constitute an official endorsement, either expressed or implied, by Arizona State University or the National Aeronautics and Space Administration. The content is solely the responsibility of the authors and does not necessarily represent the official views of ASU or NASA.

Table of Contents

Executive Summary	1
List of Figures.....	6
List of Tables	8
Introduction.....	9
Problem Definition	10
Project Needs.....	12
Background Research.....	14
Design Objectives	19
Technical Specifications	20
Functional Model.....	22
Concept Generation.....	23
Concept Selection	29
Design-to-Date	32
Conceptual Design Validation.....	35
Physical Experiment	35
Mathematical Model.....	38
Thermal Simulation	41
Application 1 – Los Alamos National Lab Experiment.....	41
Application 2 – Physical Experiment	46
Simulated Psyche Model	50
Technical Specification Validation	59
Limitations and Next Steps	61
References	63
Acknowledgements.....	67
Ethical Considerations	69
Appendix A	70
Concept Generation, Filtering.....	70
Appendix B.....	71
Sintering Description.....	71

Appendix C	72
Initial Concept Generation Sketches	72
Appendix D	77
Concept Selection, Heating Systems	77
Appendix E.....	78
Calculations for Nitrogen Container Size.....	78
Appendix F	79
Sublimation Negligibility Justification	79
Appendix G	81
Material Property Curves	81

List of Figures

Figure 1: CAD model for heating via induction.....	1
Figure 2: An illustration of the asteroid Psyche [2]	9
Figure 3: A Range of the Surface Temperatures on Psyche [5]	11
Figure 4: A theoretical CO ₂ Capturing Device [6].....	14
Figure 5: Radiators that are used to emit heat from the ISS into space [7].....	15
Figure 6: A component diagram for a blast furnace [10]	16
Figure 7: A set of figures that walk through the metal levitation process [12].....	17
Figure 8: The design objective tree which shows the prioritized design objectives for the project.....	19
Figure 9: Finalized functional model, utilizing gas as an auxiliary method to generate pressure	22
Figure 10: Concept Generation, Heating Ideas.....	23
Figure 11: Heating of sample using combustion and external gas.....	24
Figure 12: diagram of multi-layer insulation (MLI) in use	25
Figure 13: Utilization of multiple layers of aluminum for radiation insulation.....	25
Figure 14: Full System diagram for heating via induction	26
Figure 15: Full diagram for heating via conduction through resistors	26
Figure 16: Full System diagram for conduction via heating rods.....	27
Figure 17: Full System diagram for forming via sintering.....	27
Figure 18: Full induction system design-to-date, sectioned to show gas canister, coils, and sensors.....	32
Figure 19: Electrical and auxiliary components to design. A battery has been included to ensure consistent energy delivery to the system.	33
Figure 20: A 4-stage process for induction melting. The induction coils reach a lower temperature than the sample, shown using color gradients.....	33
Figure 21: Physical Experiment Setup	36
Figure 22: Temperature vs. Time Graph for Pewter.....	37
Figure 23: Correlation chart for the Nagaoka coefficient of an air-core solenoid [25].....	40
Figure 24: The experimental setup utilized for the LANL validating simulation [24].	41
Figure 25: Comparison of the LANL produced temperature vs. time graph (left) and the math model produced graph (right). The math model seeks to recreate the analytical curve.....	42
Figure 26: Heat flux vs. time graph for the mathematical modeling of the LANL data	43
Figure 27: The 3D model utilized for the thermal simulation of the Los Alamos experiment.....	43
Figure 28: A cross-section animation of the LANL sample heating over time.	44
Figure 29: Transient temperature response data for the LANL sample and coil. The sample reaches a center temperature of 952.0°C (1225.15 K) after 250 seconds, and the coil reaches a temperature of 108.2°C (381.2 K).	45
Figure 30: Comparison of measured data and experimental data for the physical experiment.	47
Figure 31: The 3D model utilized for the thermal simulation of the physical experiment.	47
Figure 32: A cross-section animation of the physical experiment sample heating over time.	48

Figure 33: Transient temperature response data for the sample and coil. The sample reaches the melting temperature after 75 seconds with a temperature of 505.44 K, and the coil reaches a temperature of 293.23 K.49

Figure 34: Temperature vs. time curve of iron sample with specific design parameters.....50

Figure 35: The 3D model utilized for thermal simulation of the Psyche system.....52

Figure 36: Heat flux vs. time for the final Psyche simulation.....53

Figure 37: A cross-section animation of the Psyche system heating over time in cold atmospheric conditions.54

Figure 38: A cross-section animation of the Psyche system heating over time in warm atmospheric conditions.54

Figure 39: Transient temperature response data for the updated Psyche sample and crucible in cold atmospheric conditions. The sample does not reach melting within the 3300s range of the simulation, with a maximum temperature of 1797 K at 3300s.....55

Figure 40: Transient temperature response data for the updated Psyche coils and insulation in cold atmospheric conditions. The coils reach a temperature of 651.01 K after 3300s of operation.55

Figure 41: Transient temperature response data for the updated Psyche sample and crucible at warm atmospheric conditions. The sample reaches the melting point at 3660 seconds with a center temperature of 1810.3 K, and the crucible temperature reaches a temperature of 1129.6 K.....56

Figure 42: Transient temperature response data for the updated Psyche coils and insulation in warm atmospheric conditions. At the melting time of 3660s, the coil insulation reaches a temperature of 1100.7 K and the coils reach a temperature of 925.14 K.56

Figure 43: Transient response data for external temperature at two locations over the temperature range on Psyche. The safe limit is marked in black, with both systems breaching this threshold after approx. 2500s.....57

Figure 44: The 3D model utilized for the previous thermal simulations of the Psyche system. The outlet of the system and length of the inlet section are much smaller than the final model, and the sample is far wider with minimal distance between the sample and the inlet walls of the crucible.....58

Figure 45: Transient temperature response data for the previous Psyche sample and crucible in cold atmospheric conditions. The sample reaches the melting point at 2610 seconds with a center temperature of 1810.9 K, and the crucible temperature reaches a maximum value of 1248.4 K.58

Figure 46: Optimized model, only proven mathematically.....62

List of Tables

Table 1: A list of the estimated physical properties of Psyche [2] and how they compare to Earth [3]	10
Table 2: A prioritized list of technical specifications for the project	20
Table 3: Concept Selection Matrix with Full Systems	30
Table 4: Assumptions made during the generation of the mathematical model.	38
Table 5: A list of the relevant variables for the mathematical model.....	39
Table 6: The physical parameters utilized in the high frequency fast startup experiment.....	42
Table 7: Percent difference calculations for the response of the LANL simulation.	45
Table 8: Percent difference calculations for mesh convergence of the LANL simulation.....	45
Table 9: The physical parameters utilized for the tin melting experiment.....	46
Table 10: Percent difference calculations for the response of the physical simulation.....	49
Table 11: Percent difference calculations for mesh convergence of the physical simulation.	49
Table 12: Chosen parameters for Psyche induction heating system	50
Table 13: The material properties utilized for the Psyche design simulation.	51
Table 14: Percent error calculations for mesh convergence of the Psyche induction simulation.....	57
Table 15: Technical Specification Analysis.....	59
Table 16: Ethical considerations for the mission's scope.....	69

Introduction

Psyche is a metal-rich asteroid located between Mars and Jupiter at a distance of approximately 500 kilometers, or 3.55 astronomical units, from Earth [1]. Psyche is roughly 280 kilometers in length and 230 kilometers in width, with a presumed ovular shape. The metal-rich nature of the asteroid gives it the classification of M-type, comprised primarily of iron and nickel mixed with silicates [2]. The true shape and size of Psyche is currently unknown, but an artist's illustration of Psyche is shown below in Figure 2.



Figure 2: An illustration of the asteroid Psyche [2]

Due to the makeup of this asteroid, it has been hypothesized that this asteroid may be the remains of an early planetary formation, known as a planetesimal. It is possible that Psyche once consisted of a rocky surface with a metal core, much like Earth, but the rock may have been stripped away by a large collision. Psyche will be the first metal-rich asteroid explored by humanity, and understanding the nature of this asteroid may yield new insights on how the Earth was formed.

Currently, the Psyche mission consists of an orbiter equipped with sensors to capture images of Psyche and analyze the magnetic and gravitational effects around the asteroid. The orbiter launched on October 13, 2023, with an estimated arrival time to Psyche in 2029. It is possible that future missions will be made to Psyche, with the goal of landing on the surface of the asteroid and collecting and returning samples. This hypothesized mission may require use of resources within the environment of Psyche, which is a concept known as in-situ resource utilization, or ISRU. Utilizing resources from the environment allows missions to bring less material from Earth and manufacture new components or structures post-launch.

Problem Definition

The hypothesized second Psyche mission is the focus of our project, specifically through incorporating ISRU procedures to harness the natural metals found on Psyche. ISRU processes would allow the Psyche program to save mass and cost for fabrication of parts, tools, or other key aspects of robotic surface exploration. To narrow the scope of this project down to something feasible for a capstone project, we identified three potential categories to choose between: material identification, separation of materials, or manufacturing of materials. From these, we chose to focus on one of the fundamental steps to manufacturing – material preparation – and formed the following problem statement:

Design a heating mechanism capable of melting the materials of Psyche in deep-space conditions.

Melting metal in space is a difficult task considering the physical properties of Psyche, some of which are shown below in Table 1. A notable few are the fractional amount of gravity, zero pressure due to no present atmosphere, and the obliquity (axial tilt) of the asteroid [2].

Table 1: A list of the estimated physical properties of Psyche [2] and how they compare to Earth [3].

	Psyche	Earth
Mass	$(2.29 \pm 0.14) \times 10^{19}$ kg	5.972×10^{24}
Volume	5.75×10^6 km ³	1.083×10^{12} km ³
Mean Density	3.977 ± 0.253 g/cm ³	5.134 g/cm ³
Surface Gravity	0.144 m/s ²	9.806 m/s ²
Pressure	0 atm	1 atm
Eccentricity	0.134	0.016
Obliquity	95 deg	22.1 - 24.5 degrees
Day Length	4.196 hours	24 hours
Orbital Period	5.5 years	365.256 days
Orbital Radius	2.5 - 3.3 AU	1 AU

To ensure we could account for Psyche’s unique physical properties while maintaining a reasonable scope for a year-long project, we made several assumptions to simplify the project scope. The first assumption is that the sample consists of pure iron. Psyche is hypothesized to have somewhere between 30-60 vol% metal, with a highly metallic surface (based on reflectivity observations) that is likely a mixture of iron and nickel [4]. To simplify this model, we chose to focus on melting pure iron, since it is the majority element found and has a higher melting point than nickel. The second assumption is that there will be a system on the lander that can extract the material from Psyche and insert it into our heating mechanism. We will design inlet and outlet locations but will not focus on the semantics of the material physically entering and exiting the system. The third assumption is that this

lander will be located on the equator of Psyche. This assumption is based on a graph of Psyche's surface temperatures in a four-Earth-year span, shown in Figure 3 below.

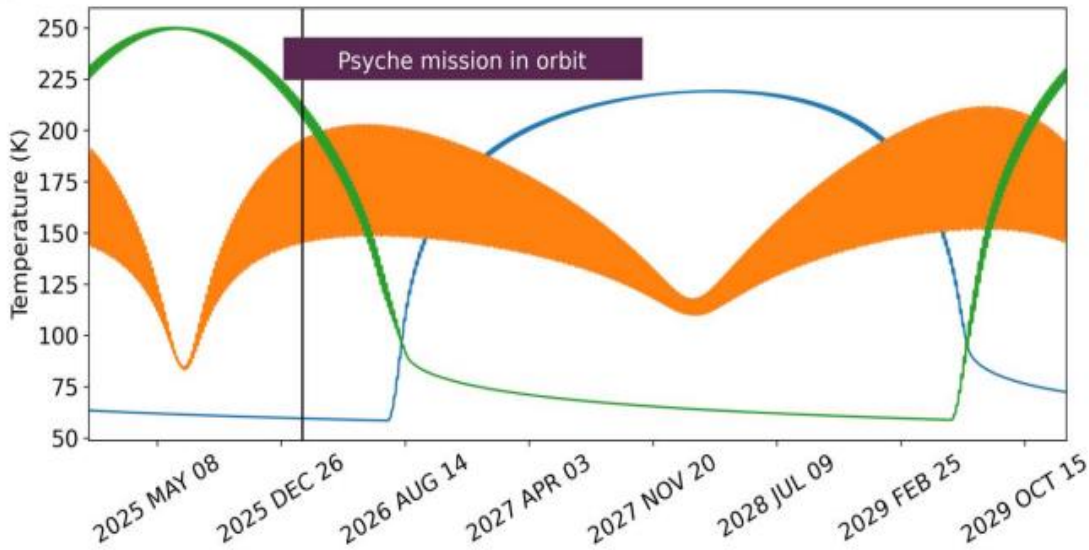


Figure 3: A Range of the Surface Temperatures on Psyche [5]

The blue line on this graph demonstrates temperature fluctuations on the north pole, the green line the south pole, and the orange line the equator. The thickness of each line demonstrates the temperature fluctuations possible throughout a day on Psyche (approximately four Earth hours). From this graph, the equator location seems to have the least yearly temperature fluctuations, and therefore the smallest range of temperatures our system would function in.

In addition to the previous three assumptions, our project will also not focus on what the metal will be manufactured into, or any of the many considerations that come with utilization of the melted sample. Our goal is only to melt the metal.

Project Needs

In the initial phase of the project, a significant amount of project scoping needed to be done due to the broad scope given to the team. To accomplish this, we created a list of ten prioritized questions to ask our client, Dr. Cassie Bowman. Dr. Bowman is a research professor at Arizona State University and a co-investigator on the Psyche Asteroid Mission. The list of questions and Dr. Bowman's responses, are listed below:

1. Which of the three categories (identification, separation, and manufacturing) of ISRU have other teams researched in the past?
 - a. *There has only been one other team to focus on researching ISRU, and they narrowed their scope down to melting metal.*
2. Are there any specific tools NASA would like to be manufactured on Psyche?
 - a. *As of now, the idea is too vague to narrow down to any specific design, but commonly used parts that may be damaged would be nice to replace.*
3. How long will the surface phase of the mission last, and is our project intended to work for this entire length?
 - a. *It's unknown how long the second Psyche mission will last, but the ISRU project should be functional the entire time.*
4. Should we be concerned about the utilization of meteoroids on Psyche's surface?
 - a. *Anything that could reasonably be on Psyche's surface should be accounted for.*
5. What level of communication should we have with Psyche? Should the mission be fully autonomous?
 - a. *Assume that this will be a deep space mission, meaning that there may be one message sent and received per day. Other than this, it should operate autonomously.*
6. What range of temperatures and forces should we expect to experience on the surface?
 - a. *The group decided to prioritize other questions with Dr. Bowman, this question was answered with further background research however, with a range of 50 to 270 K expected.*
7. Should we design with protection for solar wind in mind?
 - a. *Yes, the system should account for Psyche's surface conditions.*
8. Are there any size or power constraints that should be kept in mind?
 - a. *The project may be as broad as possible, don't place limits on your design yet.*
9. Should this device be reusable for multiple missions?
 - a. *Nothing on the Psyche lander will be returning to Earth. It only needs to function for the duration of the Psyche mission.*
10. What minimum output is expected of the design?
 - a. *The main focus of this project will be a proof of concept. The research done into it is the most important thing to focus on.*

We also analyzed the project's stakeholders, along with key professional references. The stakeholder we have the most contact with is Dr. Cassie Bowman, of Arizona State University. As the client supporting our project, Dr. Bowman is very invested in our success. During the initial meeting, Dr. Bowman required us to send her only our finalized materials, the end-of-year report and demonstration, and was purposely vague in her answers to our questions so she did not sway us in any direction.

The overarching stakeholder for our project is NASA, specifically the NASA Psyche team, which our research could benefit in the future. Dr. Bowman mentioned the possibility of open office hours with NASA engineers where we could ask them direct questions, but otherwise we expect very little contact from the team and will primarily work with Dr. Bowman.

The number of stakeholders for this project is low because it is fundamentally a research project and will not directly impact any groups. Should this project transition into one of the Psyche missions, the stakeholders would increase. Additionally, since this is an open-ended research project, the stakeholder requirements were very general, which means the team had the ability to take it in whatever direction we wanted. This provided a very large scope, so we started extensive background research to narrow the scope to something feasible within one academic year.

Background Research

While melting metal in space has been theorized for over half a century, it has never been performed in deep space conditions, so we utilized as many relevant projects as possible for our background research. We started with online research, which had four main focuses: previous NASA projects to investigate current ISRU efforts, documentation for how heat is controlled on the International Space Station (ISS), the process of melting metal on Earth to understand the process in a pressurized environment, and finally past theories as to how to melt metal in space for proof of feasibility.

One theoretical ISRU device from NASA that we researched was the Mars in-situ carbon dioxide freezer, shown in Figure 4, below. This system is supposed to capture and freeze carbon dioxide, which allows for future processing of the molecule into methane using stored hydrogen.

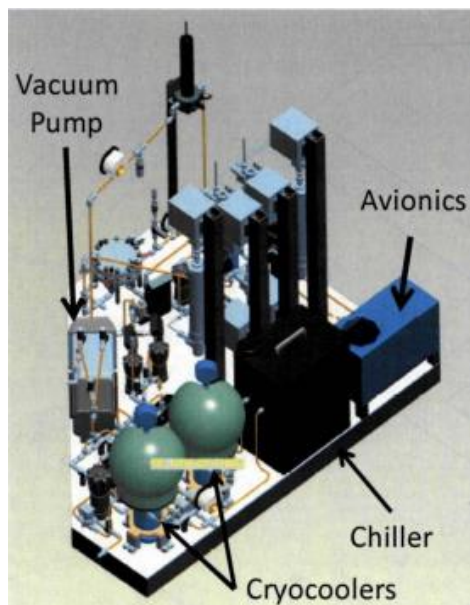


Figure 4: A theoretical CO₂ Capturing Device [6]

The requirements for this design were to provide 88 grams of near-pure CO₂ an hour, with a power limit of 900W. A notable part of this design was the two cryocoolers used, where one stores the dry ice (solid CO₂) for longer periods, and one transfers the dry ice to future processes. These cryocoolers account for the freezing point of CO₂ and natural heat leakage from the environment, and the heat leakage may be a key part of our design. Unfortunately, the cryocoolers used were purchased externally, so further research would need to be done if we were to pursue the technology or mechanics further.

To better understand how heat is controlled in space, we transitioned to investigating how the ISS currently controls heat [7]. Controlling heat is a two-part problem: the ISS needs to be heated enough for the astronauts and systems to work but must not overheat. The primary component of the ISS's insulation, which is also used in general spacecraft, is a substance known as "multi-layer insulation"

(MLI). MLI is made of reflective aluminized Mylar sheets, separated by a Dacron fabric that prevents conduction. The combination of these materials effectively blocks thermal radiation on whatever surface it is placed on. The ISS then uses heat exchangers to emit excess heat by heating ammonia, which once heated then flows into a section of large radiators (shown in Figure 2) which emit heat into space.



Figure 5: Radiators that are used to emit heat from the ISS into space [7]

Since the low-temperature, low-pressure environment of space does not allow for convection (no atmosphere), and conduction will only work internal to the system, the process behind the radiation mechanisms will be important for our project [8]. However, we are attempting to do the opposite of the ISS. The ISS's heat transfer/emission system works assuming the ISS always wants to reach equilibrium with the outside. Our system, on the other hand, needs to stay at a significantly warm temperature and will always be working against natural equilibrium.

Once research on pre-existing space mechanisms was completed, research was refocused on the process necessary to melt metal. Since Earth has a rich atmosphere, iron mined from the surface is oxidized into either hematite (Fe_2O_3) or magnetite (Fe_3O_4) and must undergo further processing to remove impurities [9]. This process is known as iron refinement, and is commonly done in a blast furnace, an example of which is shown in Figure 6.

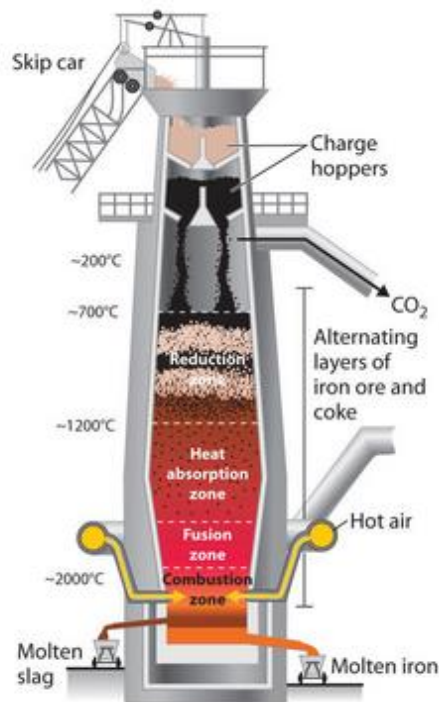


Figure 6: A component diagram for a blast furnace [10]

The blast furnace removes oxygen from the iron by heating it with a mixture of coke, which is carbon made by heating coal in the absence of air. At the bottom of the blast furnace, hot air is blown into the remaining mixture of iron and slag (stony unusable matter), which oxidizes the remaining coke into carbon dioxide and creates a massive amount of heat. This heat is used to melt both the iron and all extraneous material, creating two separate molten liquids that are different densities: liquid iron and slag. The iron extracted from the blast furnace is known as pig iron, which is a brittle and high-carbon form of iron. This iron typically contains 3-4% carbon and other impurities such as sulfur and phosphorus, which renders it useless for most applications. To become useful, pig iron must undergo further refinement, which creates either wrought iron, steel, or cast iron [11].

Since Psyche has no atmosphere, the oxidization of iron is inapplicable, so whatever iron we can melt will be pure iron and therefore immediately useful in applications such as small repairs [5]. However, since the iron will most likely be mixed with silicates, the system on Psyche will likely still produce slag.

To ensure our project will apply to the environmental conditions in space, we also analyzed two research papers that dealt with the theory of melting metal in space. The first research paper discussed how melting metal would be possible in a vacuum without using conduction [12]. This technique involves an alternating electromagnetic field, created via two coaxial coils connected in series across a common capacitor. This system creates a parallel tuned load to the alternator, which makes stable levitation of solid metal possible. The alternation of the electromagnetic field is important because

rotating the field prevents involuntary metal dripping. A diagram of the levitation process is shown below, in Figure 7.

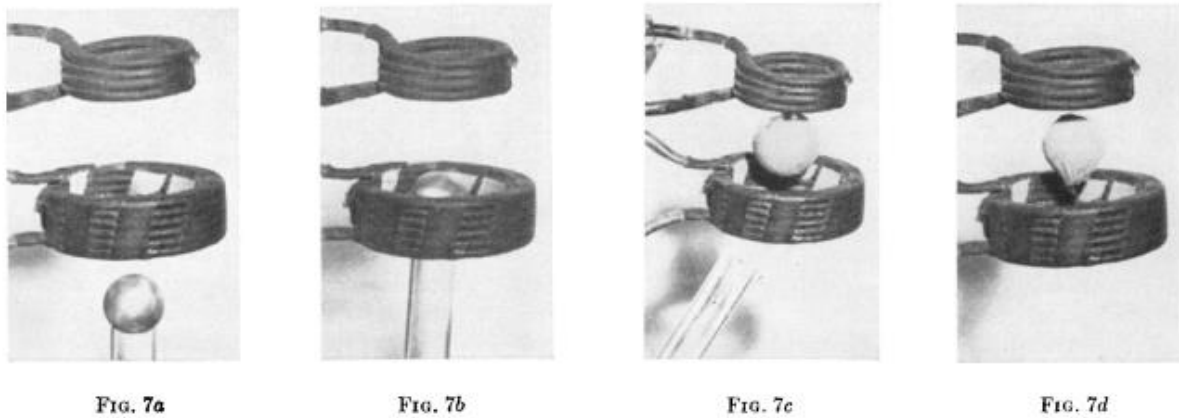


Figure 7: A set of figures that walk through the metal levitation process [12]

Levitation force and induction heating power input vary with the square of the circulating current in the coil system, which means it is possible to increase heating power by increasing the current, and possible for controlled metal release through decreasing the current. This system was proven to work on Earth, and is hypothesized to work in a vacuum, but has not been fully tested. However, this system only consists of one phase change, solid metal to liquid metal, which could theoretically be easier to model.

The other research paper focused on melting and evaporating metals in a vacuum [13]. This paper was more theoretical, but discussed important factors of working in space, such as the ability in a low-pressure low-temperature environment to sublimate solid metal (transition directly from solid to gas), rather than melt it. Presuming we move forward with initially sublimating the metal, this process would continue by condensing the now-vapor to an evaporation surface. Once at this surface, the pressure of the metal should, assuming correct location of the triple point (which would depend on the composition of the alloy), the vapor would increase both the temperature and pressure, allowing the metal to condense from vapor to liquid. Other notable ideas from this paper included the potential for iron to lose manganese if the sheet was annealed at a high temperature and low pressure, unless carbon is added, and the potential for sublimation interference if the metal reacts with residual gases at extremely low pressures.

This initial research left us with numerous questions, so we turned to our on-campus resources to continue identifying a feasible project scope. We first met with Dr. Matt Riley, a mechanical engineering professor who specializes in materials science and aerospace. Dr. Riley has previous research experience designing systems for both the moon and for Titan (a moon of Saturn) so our questions for him revolved around how materials would react in those space conditions. He emphasized the importance of considering sublimation of the iron/nickel alloy as well as melting,

because of the low pressure on Psyche, and suggested we consider the consequences of cold-welding. Metal on Earth has a natural oxide layer that prevents cold-welding, but without that oxygen on Psyche, if two metals that have the same composition touch, they could share electrons, effectively fusing them together. Dr. Riley also recommended we research pressure versus temperature graphs for different alloys of both iron and nickel, to see if we could use both a high-pressure/Earth-pressure versus temperature graph to understand how those metals would work in low pressure. Finally, he urged us to not discount the benefits of conduction in our design, since utilizing conductive heating rods is another possibility to consider alongside radiative heat.

This aided us in potential design ideas, but we still had questions about the general environment of space, so we also consulted with Dr. Elizabeth Melton, a physics professor who specializes in astrophysics. Dr. Melton informed us about the potential of Psyche to have trapped gas within the silicates on its surface. These trapped gas molecules could change how we consider the phase changes in heating metal, since they could interfere with sublimation or melting. She also recommended having a higher focus on energy and fuel constraints, though she believed we could use up to 95% of the lander's energy for a short moment to initialize the system, which was a helpful limit.

After combining our background research with the discussions with the professors, and consulting with our capstone advisor, we were able to narrow our project scope with feasible limits and continued forward with our mission statement.

During our fall quarter external review, our reviewer mentioned the concept of sintering the metal, rather than pure melting. Sintering is a manufacturing process used to form metal and ceramic objects by heating powdered materials to a temperature below their melting point, allowing them to fuse together to create a solid, dense structure. Since sintering is vastly different from the other ideas we have been considering, it is explained more in Appendix B, and we will keep it in mind as we go through concept generation and selection.

Design Objectives

Based on the information we gathered during background research, we created a design objective tree, shown below in Figure 8. This tree separates the environmental conditions that all objectives will need to operate under and prioritizes the objectives of the project to better allow for time and resource allocation to each objective. Some objectives were deemed important to keep in mind but inapplicable to the project, such as accounting for the long duration of the mission time and the process of inputting/removing the sample from the system.

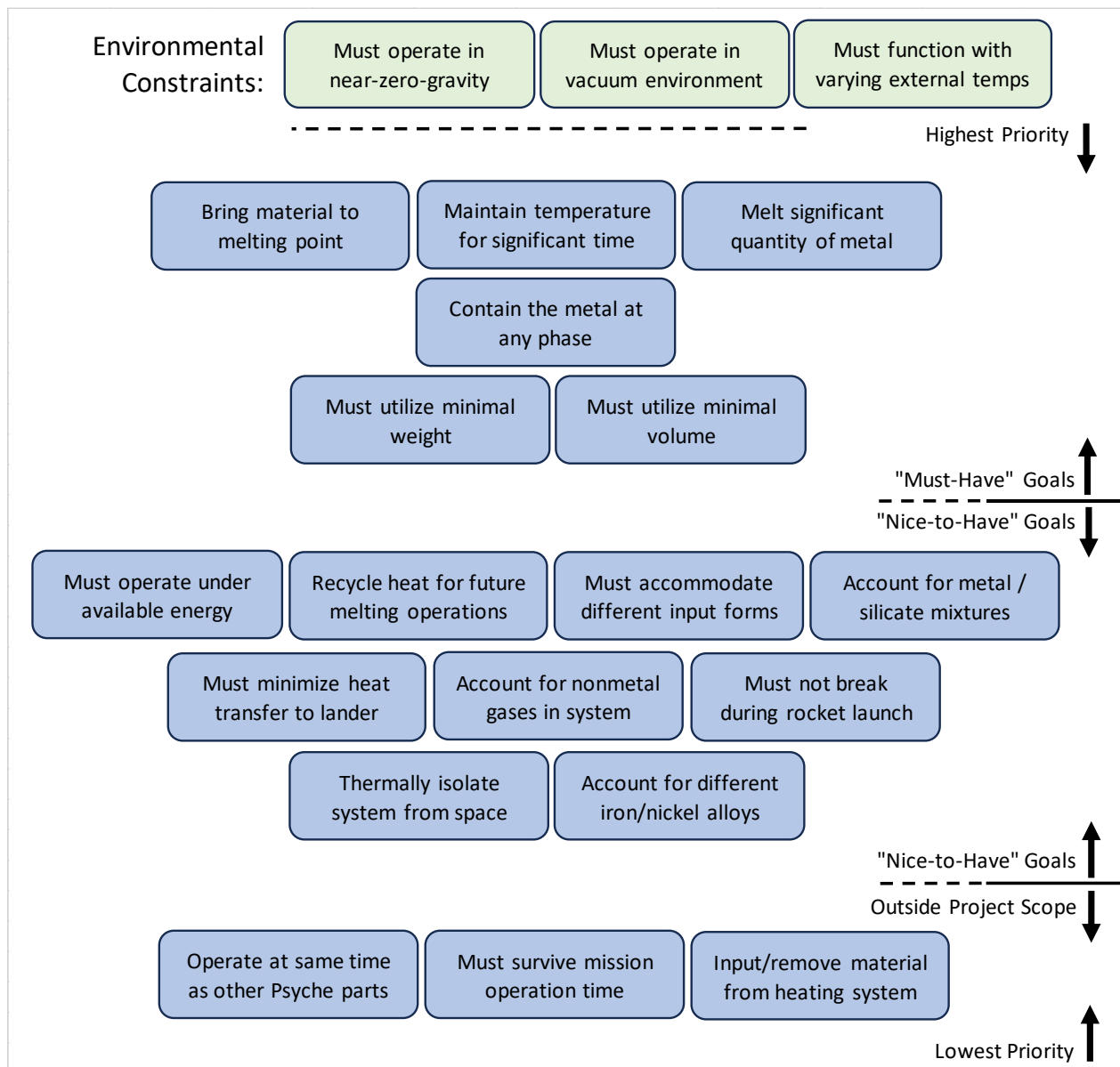


Figure 8: The design objective tree, which shows the prioritized design objectives for the project

Technical Specifications

Utilizing the design objective tree, each objective was broken down into technical specifications that our design should be able to meet. These specifications allow for target values to be placed on each objective that can be utilized to evaluate the performance of the final design. The full table of these specifications is shown below in Table 2. Each specification must function under all environmental conditions on Psyche in addition to meeting target values.

Table 2: A prioritized list of technical specifications for the project

	Project Needs	Technical Specification	Rationale for Target Value	Specification Evaluation
1	Melting Point	The melting chamber must reach a minimum temperature of 1810K	The melting point of iron in 1atm [14], which is the highest possible melting point as low-pressure decreases melting temperature [15]	Mathematical modeling using heat transfer and thermodynamic principles
2	Temperature Maintenance	The melting chamber's temperature must hold steady until the heat of fusion is overcome	Energy required for fully liquid metal to be present	Mathematical modeling using heat transfer and thermodynamic principles
3	Melt a Significant Quantity	The melting chamber must be able to hold a minimum of 8cm ³ of solid alloy	OSIRIS-REx was required to collect a sample of 60g [16]. Since nickel has the lowest density, assuming the sample is 100% nickel, the sample size is approximately 7.6cm ³ .	Volume calculations of space, combined with packing factors
4	Contain Metal	The chamber must be fully sealed from outside environments while melting	Necessary to reduce loss of finite resources and maintain pressure	Binary – Are there locations where gas can leak from design?
5	Thermal Isolation from space/lander	The external temperature of the system should not exceed 358 K	Maximum temperature electronics can reach without failing [17]	Heat transfer analysis of created design, including specific material properties and geometries.

6	Weight Constraint	The entire system must weigh less than 850 kg	850kg comes from the full weight of the Mars Curiosity rover, realistically we will aim for well under half of this [18]	Analysis of CAD model
7	Volume Constraint	The entire system must take up less volume than 16 m ³	16 m ³ comes from the full volume of the Mars Curiosity rover, realistically we will aim for well under half of this [18]	Analysis of CAD model
8	Energy Constraint	The system must be able to start with 1950 W of power	Based on utilization of 95% of solar power from current Psyche satellite [19]	Mathematical analysis of heating system
9	Low Energy Consumption	The system must be able to steadily operate on 500 W of power	Based on how much heat is returned to the main chamber	Thermodynamic calculations regarding heat loss and heat needed

In the winter quarter, we changed/removed four technical specifications, listed below.

- Technical Specification, “Temperature Maintenance”: changed from “hold chamber at a consistent temperature for 10 minutes” to “the melting chamber must stay steady until heat of fusion is overcome”. This was changed due to results found in the physical experiment we ran, where the heat of fusion took a significant amount of time that we initially deemed negligible.
- Technical Specification, “Contain Metal – Static FOS”: deleted. During winter quarter, we deemed sublimation negligible (justification shown in Appendix F) so the need to pressurize the chamber lessened significantly. We will still have an external gas canister shown in the final designs to show that one could be added, but we have decided to take the actual pressurization of the chamber out of the scope.
- Technical Specification, “Contain Metal – Pressure Vessel FOS”: deleted, for the same reasons as the static FOS technical specification.
- Technical Specification, “Account for Different Metal Sizes”: deleted. This was also changed from the results of the experiment, where one of the major takeaways was that powdered material melted slower under induction heating than solid metal. This allows us to focus on one size of solid metal for the scope of the project.

Functional Model

Functional models are a useful visual tool to help break down the design into what functions it will need to perform. It also allows for functions to interact in the system, such as a sensor that will follow the sample, or power that will be applied to different components. The functional model, shown below in Figure 9, assumes sublimation negligible, but will keep a supply of stable gas to use in case sublimation is later found to have a significant impact. It will also not focus on communications with earth, though this will be necessary to implement for a mission to Psyche. We will use this functional model to aid in future concept generation and selection.

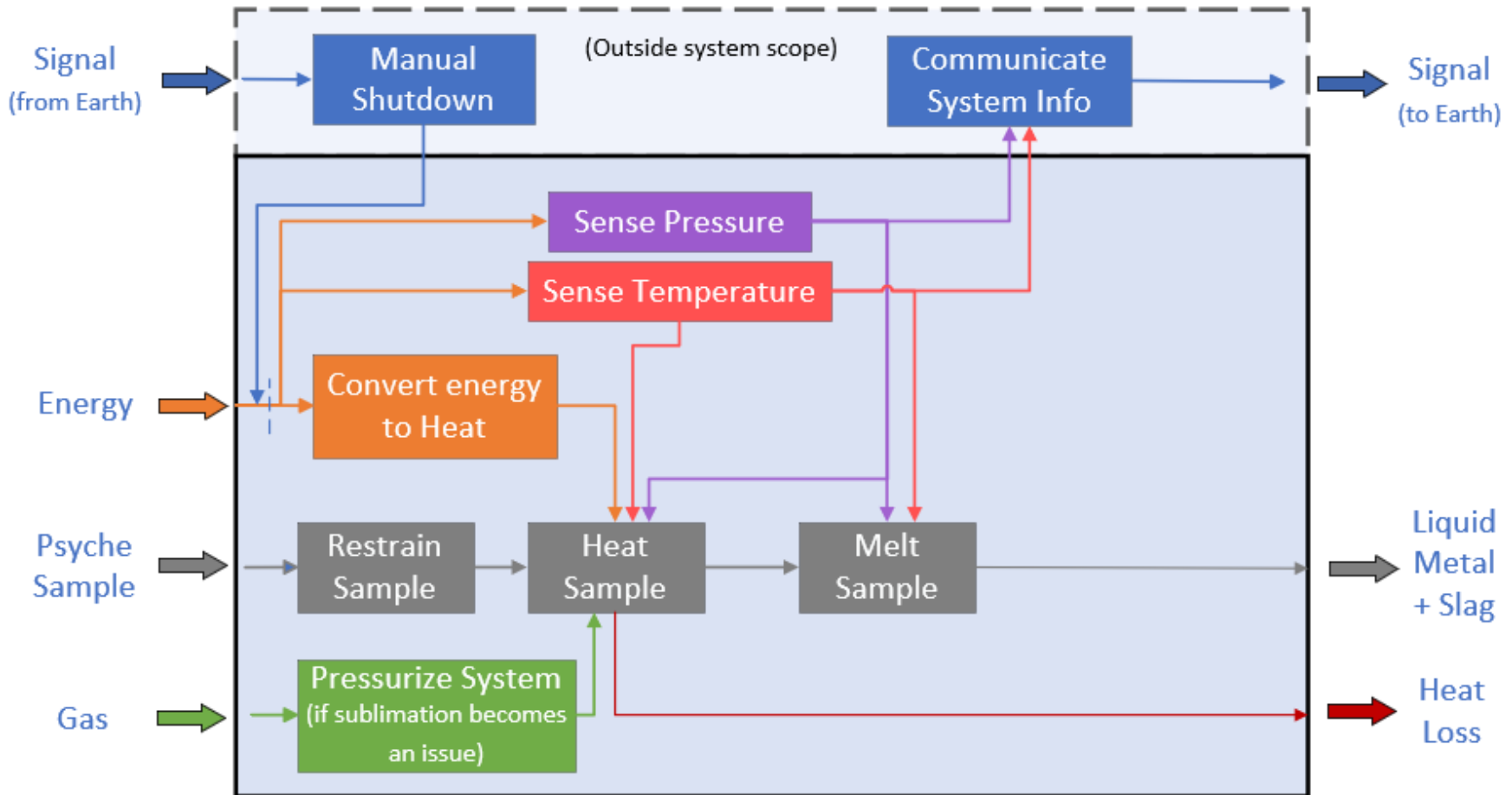


Figure 9: Finalized functional model, utilizing gas as an auxiliary method to generate pressure

Concept Generation

The primary functions chosen for concept generation were energy conversion to heat, sample heating, thermal isolation, and filtration/separation of molten metal and slag. We also created rough initial full systems to start figuring out how each of these functions could connect to each other. We used collaborative sketching as our brainstorming method.

After the initial round of full-system concept generation, we decided it would be smarter to start with brainstorming systems for individual functions, then brainstorm connections between those functions to create a full system. This allows us to focus on the generation of specific parts before getting overwhelmed with the complexity of the system and should result in us combining the best functions together to deliver the best system. We narrowed down the functions that were most important for concept generation into three categories: heating the sample, filtration/separation of the molten sample, and thermal isolation.

The first function we generated ideas for was sample heating, because it is the most important for both our mission statement and technical specifications. The first three heating ideas are shown in Figure 10, below.

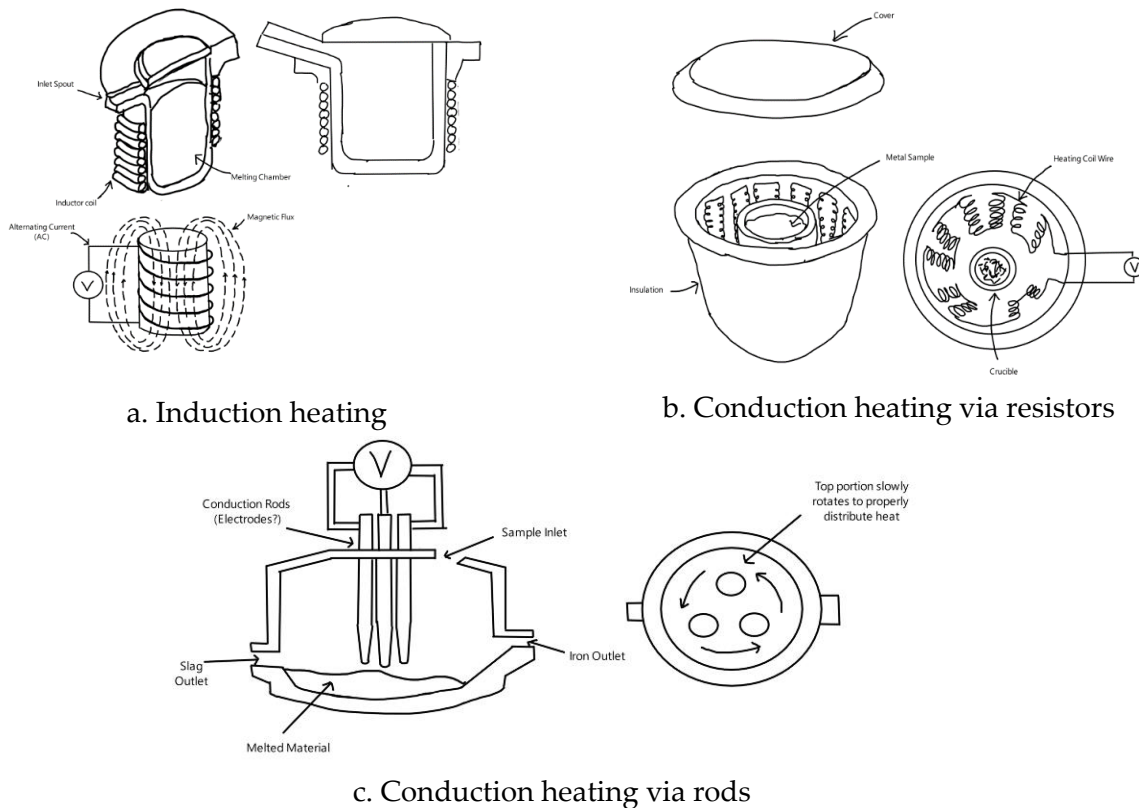


Figure 10: Concept Generation, Heating Ideas

The top left, a., demonstrates the induction heating concept. Magnetic fields generated by current running through induction coils create a flux in the sample between the coils, which heats the sample without excessively heating the coils or surroundings. The top right, b., shows the conduction via resistors concept.

This would entail embedding resistors in the crucible's walls, which would heat up as current is run through them. The sample would then heat and melt through contacting the walls. The bottom diagram, c., shows conduction via heated rods. Here, instead of embedding resistors in the crucible wall, we would insert resistors into semi-hollow rods. The current would run through the resistors so the rods would heat up, and the walls of the crucible would be insulated to not allow any heat through. The rods would then rotate around the crucible, effectively stirring the metal sample as it heats.

Our fourth and final idea was combustion. This idea relies on transporting pure hydrogen and oxygen gas external to the system from Earth, and then pumping the correct ratio of both into a chamber. This should cause heat via combustion of the molecules, with an excess amount of steam that would need to be let out of the system. A basic diagram of how combustion would work is shown below in Figure 11.

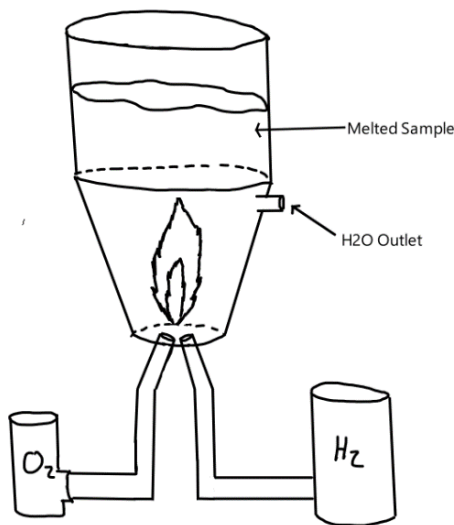


Figure 11: Heating of sample using combustion and external gas

The second function we focused on generating concepts for was filtration and separation of the sample. This function assumes we are proceeding with the sample containing both a metal alloy and silicate and are filtering the molten sample at the end of the melting process. However, filtration was cut from our scope later in fall quarter, so the generation drawings are now in Appendix C.

The final function we considered during concept generation was thermal isolation. Since the heat we generate to melt the metal will be a limited resource, we want to ensure that our system contains as close to all of it as possible. From prior research, we determined there were two feasible ways to thermally isolate the system. The first idea is through multi-layer insulation, or MLI. This is already used in numerous space missions, most notably the ISS. A diagram of how MLI would work in our system is shown below in Figure 12.

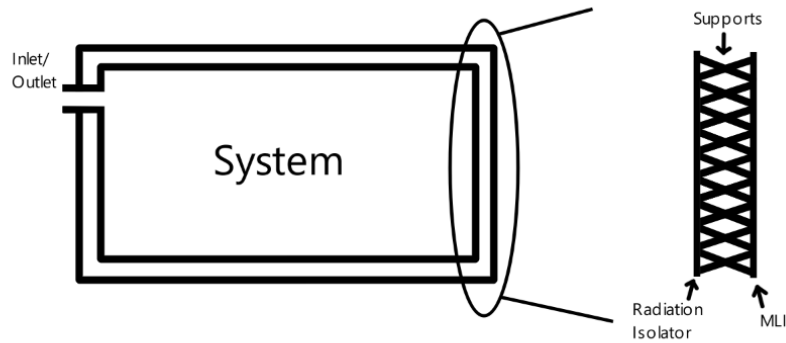


Figure 12: diagram of multi-layer insulation (MLI) in use

Though MLI has proven success in space missions, it is also very fragile and is recommended to be away from moving parts. Since our conceptual system will still need inlets and outlets for the sample and the molten production, we also considered a backup to MLI that could be used in tandem with or in substitution. This second idea is shown below, in Figure 13.

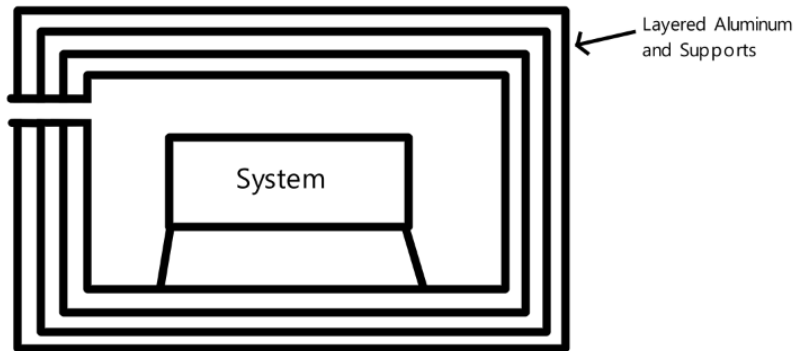


Figure 13: Utilization of multiple layers of aluminum for radiation insulation

This insulation method requires multiple layers of thin, highly polished aluminum around the system. Aluminum is much sturdier than MLI and has decent insulation properties but would weigh significantly more than MLI.

Then, putting these concepts together, we generated four full systems, one of which we will select to move forward with designing. Our first full system centered around using induction to heat the sample, and a diagram is shown below in Figure 14.

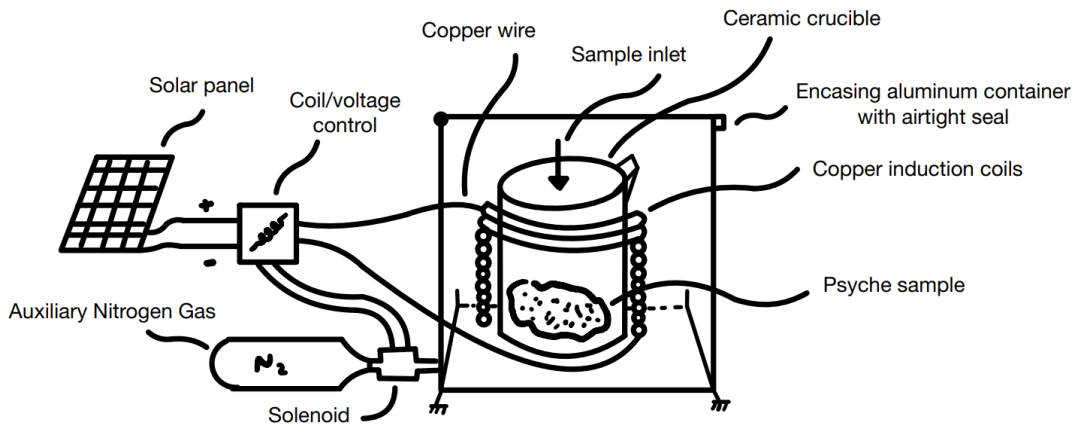


Figure 14: Full System diagram for heating via induction

Induction requires a crucible, where the sample would sit in, and then heats via the copper coils that are shown around the crucible. The crucible would most likely be ceramic, similar to how induction crucibles work on Earth. This system would harness energy through solar panels and has auxiliary nitrogen gas in case more pressure is needed. The entire crucible is sealed in an aluminum container to prevent excessive heat loss. When the sample is melted, we presume the crucible could be taken out of the aluminum container.

The second full system is centered around using conduction via resistors to heat the sample, and a diagram is shown below in Figure 15.

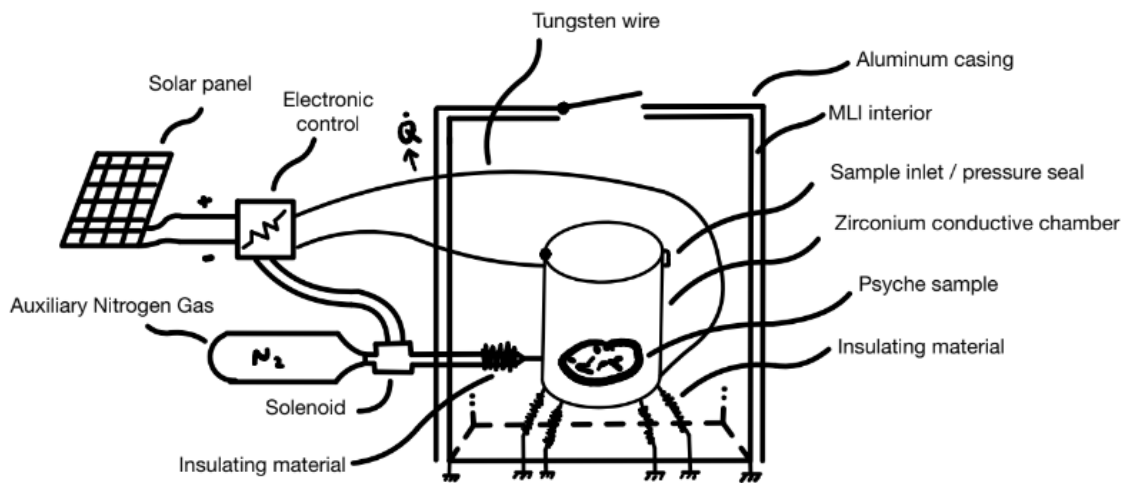


Figure 15: Full diagram for heating via conduction through resistors

This system would also be encased in aluminum but would have an MLI interior so the heat generated by the resistors could also reflect back to the crucible and therefore the sample. The wire material necessary for this is tungsten because tungsten has a higher melting temperature than iron. The crucible to hold this sample is theorized to be zirconia, due to its combination high melting point and high conductivity and would also be removable from the chamber.

The third full system also uses conduction, but through heated rods instead of resistors. A front view of this system is shown in Figure 16.

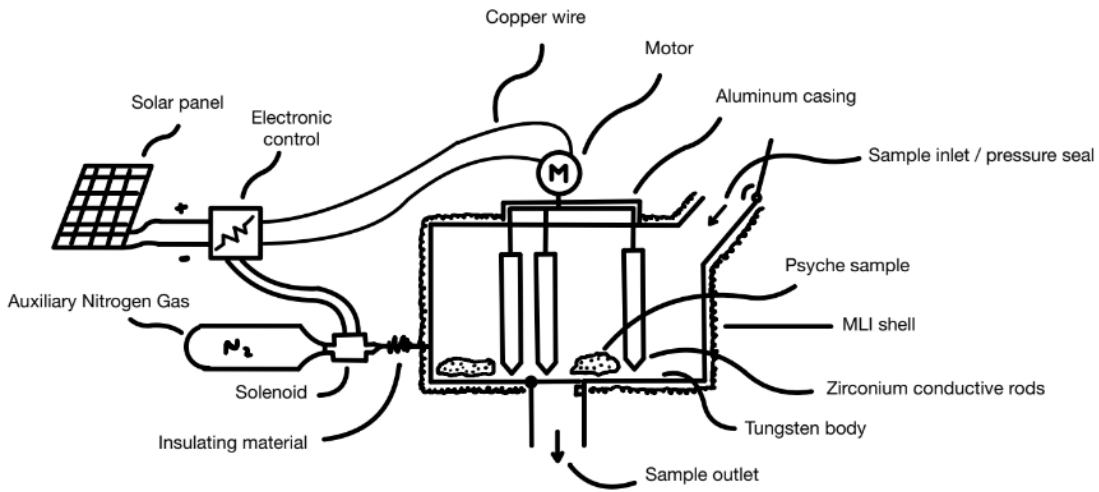


Figure 16: Full System diagram for conduction via heating rods

The encasement will have a constantly open sample inlet, and a hinged sample outlet. This chamber will also be encased in both aluminum and MLI, but this time the aluminum will be inside, because MLI's fragility will not allow it to be around moving parts like these rods.

The last full system relies on sintering, a method recommended to us during our external review. A figure of this mechanism is below in Figure 17.

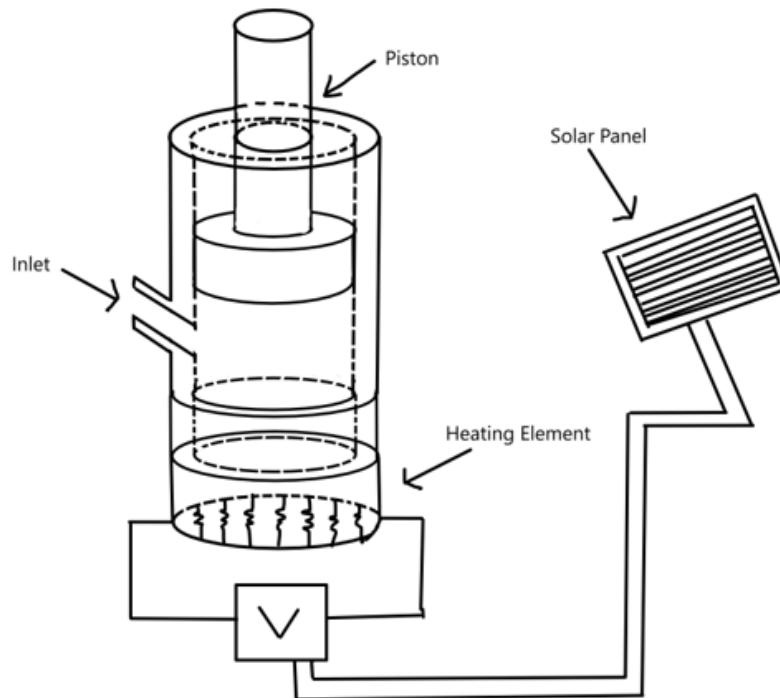


Figure 17: Full System diagram for forming via sintering

Sintering is a two-phase process, where powdered sample is first stamped into the mold, then the mold is heated until the sample is either liquefied or at the desired microstructure. We would create the stamping mechanism through a modified rack-and-pinion mechanism because the low temperatures this system would run at could cause issues for hydraulic liquid.

Rough sketches completed during our first couple of rounds of concept generation are located in Appendix A for reference.

Concept Selection

We created go/no-go constraints to eliminate some concepts before they made it to selection, to ensure we did not spend extraneous time on selection for a concept that would end up not working anyway. These restraints were as follows:

- Is the concept verifiable? Can we, as a senior capstone team of four, verify the success/failure of this system within nine months?
- Is the concept going to fit within volume constraints? If we choose one concept for a sub-system, will the combination of all sub-systems chosen fit within the volume benchmarked by the Mars Curiosity Rover (16m³)?
- Is the concept going to contain the sample at all potential phases (solid, gas, liquid)?

Concept selection for this project will take multiple rounds, as discussed in concept generation, so we can ensure we pick the best sub-systems for each function and create the best combined system. We will rate every function and system against the same criteria and rank them against each other. The criteria used for concept selection and their respective percentage weights for ranking are shown below, along with which technical specification(s) they satisfy:

- (25%) Low Complexity: How difficult will the design be to create? Is it a system the team will be able to fully account for and understand?
- (25%) Feasibility: How confident is the team that the design will work? How many critical assumptions must be made?
 - o Tech Specs: "Melting Point", "Temperature Maintenance"
- (10%) Modifiability/Scalability: Will the system be easy to adjust for different sample sizes if NASA requires more or less metal to be melted at a time?
 - o Tech Spec: "Melt a Significant Quantity"
- (10%) Energy Use: Does the system use a minimal amount of energy? Will this system justify its energy use through the amount of metal it can produce?
 - o Tech Specs: "Energy Constraint", "Melt a Significant Quantity"
- (20%) Weight of System: How heavy is the system? Will the system be able to justify its weight through the amount of metal it can produce?
 - o Tech Specs: "Weight Constraint", "Melt a Significant Quantity"
- (10%) High Insulation: How much heat will be likely to escape from the system?
 - o Tech Specs: "Thermally Isolate", "Heat Recycling"

We chose these as our selection criteria because they best encompassed our high-priority design objectives and technical specifications, while taking into consideration the limitations of the team. While low complexity does not have a technical specification linked to it, we still included it in our selection criteria and ranked it as one of the highest because we want to be confident explaining the system we choose without exceeding the scope of our undergraduate education. We also ranked feasibility as one of the highest because our major stakeholder is NASA, and we want to ensure that our final project is an idea NASA could consider in future missions to

Psyche. If we make too many assumptions, then the system may be rendered impossible when more data is discovered.

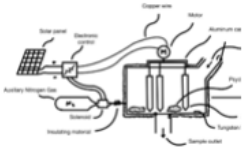
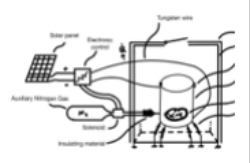
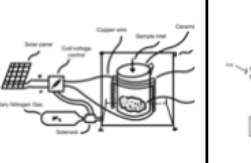
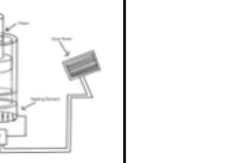
These criteria are organized using Pugh’s method, which organizes a decision matrix to compare different concepts. This matrix will allow us to evaluate the baseline strengths and weaknesses of each generated idea and identify which ideas merit further investigation. The values populating the design matrices will be generated by the team’s judgment, after background research and benchmarking (if applicable) each method.

Since the function to “heat the sample” is the primary focus of the project and is the function we focused on for concept generation, we did an initial concept selection matrix for four heating systems: induction, conduction (resistor), conduction (rod), and combustion. The matrix and analysis are in Appendix D. The main conclusion we drew from this decision matrix was to not focus on the combustion system due to its complexity and large amount of external materials.

The main concept selection we ran was on the full systems. These systems are categorized by the sample heating mechanism they contain, and the four that were considered were conduction – rods, conduction – resistance, induction, and sintering. These systems are explained in detail in the concept generation section.

Using the same selection criteria to evaluate these full systems produced our final weighted decision matrix, shown below in Table 3.

Table 3: Concept Selection Matrix with Full Systems

		Concepts							
		Conduction - Rod		Conduction - Resistor		Induction		Sintering	
									
Criteria	Weight	Rating	Score	Rating	Score	Rating	Score	Rating	Score
Low Complexity	25%	1	0.25	5	1.25	3	0.75	2	0.5
Feasibility	25%	2	0.5	4	1	3	0.75	2	0.5
Weight of System	20%	3	0.6	3	0.6	4	0.8	2	0.4
Energy Use	10%	3	0.3	1	0.1	5	0.5	2	0.2
Modifiability /Scalability	10%	2	0.2	4	0.4	2	0.2	3	0.3
High insulation	10%	2	0.2	1	0.1	4	0.4	3	0.3
Total		2.05		3.45		3.4		2.2	
Rank		4		1		2		3	

The results of this matrix eliminate the conduction via rod system and the sintering system, primarily due to their higher complexity, lower feasibility, and average scores in all other criteria. Both systems have a lot of

moving parts, which make them more difficult to model, and the conduction via rod method requires materials that are not easily obtainable. Sintering as a heating mechanism tends to work in two stages (the molded sample moves to a heating chamber), which means a larger system and a more complex design to insulate and recycle heat. Therefore, we are left with conduction – resistor and induction.

After further discussion about the results the decision matrix left us, it seemed our discomfort with induction came from our personal unfamiliarity with the system, shown by the average scores it received in low complexity and feasibility. However, the conduction via resistor method had the lowest scores in both energy use and high insulation (it would use a lot of energy and would be difficult to insulate), which shows deficits in the system itself rather than the team knowledge. From this, we chose to pursue the induction system.

We also considered three mechanisms to convert energy to heat: solar, nuclear, and optical. Solar panels are widely used in space because they do not require external fuel, and the sun consistently emits energy. However, not every deep space mission stays in constant sunlight, so while solar energy is highly reliable, the collection of the energy could be inconsistent on Psyche. An alternative could be nuclear energy, which involves either radioisotope thermoelectric generators (RTGs), or fission reactors. RTGs generate power by using the heat produced from the natural radioactive decay of isotopes such as plutonium-238 to generate electricity through thermoelectric conversion [20]. Fission reactors generate power using controlled nuclear reactions to produce heat, which is then converted to electricity [20]. Nuclear systems have the potential to harness significantly more energy than solar mechanisms but would require higher amounts of external material and have not previously been tested in space. The third possibility for energy harvesting would be optically, which uses multiple solar concentrators to transmit energy into a heating element using fiber optical cables [21]. However, further research showed these cables are meant to directly heat an object, rather than store energy, which means we would have no ability to store energy in an external battery.

Since the Psyche orbiter uses solar panels currently, and solar panels would be used to get any future Psyche missions to Psyche, we chose to stick with solar panels. This decision was further backed by our various proof-of-concept calculations that demonstrated the potential of solar panels to generate enough energy to melt the metal.

Design-to-Date

Our design to date consists of the induction system, which is repeated below in Figure 18. Rough calculations for the size of the system have been performed, utilizing the known sample diameter of 9 cm and height of 10 cm. We then ran thermal simulations on the temperature for the inside and outside of the ceramic crucible, and found the thickness of the crucible was best at 0.4 cm. Then, the insulating chamber was then sized to allow ample space for induction coils, wiring, and insulation, yielding a chamber diameter of 26 cm. The nitrogen canister was chosen based on a rough calculation for the gas required for 1000 cycles of 1 Pa of pressure, which is described further in Appendix EAppendix [22]. The electronic control and solar panels are not dimensioned as part of the system as they are outside of the project scope.

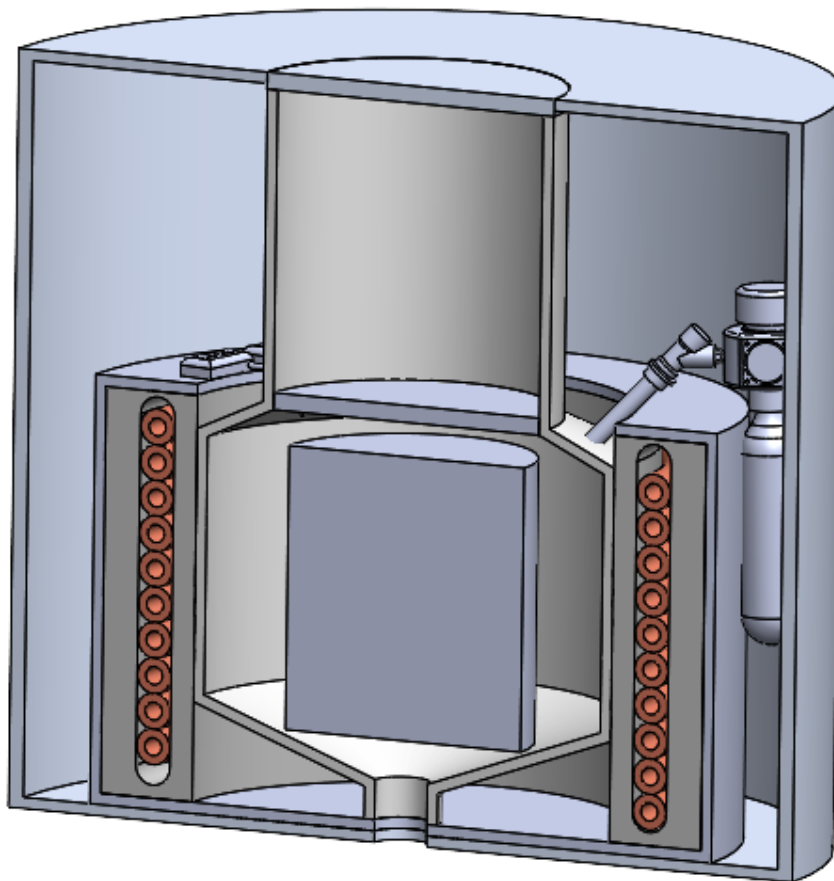


Figure 18: Full induction system design-to-date, sectioned to show gas canister, coils, and sensors.

Notable changes from the fall to winter quarter include the addition of an external gas canister, in case the chamber needs to be pressurized, and the addition of a temperature and pressure sensor to send data back to Earth if necessary. During winter quarter, we also changed the top of the crucible to include an airlock type of lid, which allows the solid sample to enter with minimal heat escaping, and changed the bottom half of the crucible to funnel so the molten metal can flow smoothly out of the system. Notable changes from the winter to spring quarter included rescaling the chamber to the dimensions mentioned above, to account for a larger sample size.

For the electrical control, we plan to utilize a control circuit and battery to store and deliver the power from Psyche's solar panels and direct the use of energy and auxiliary gas. This circuit can be seen in the previous drawings of our design-to-date but is shown with more detail in Figure 19.

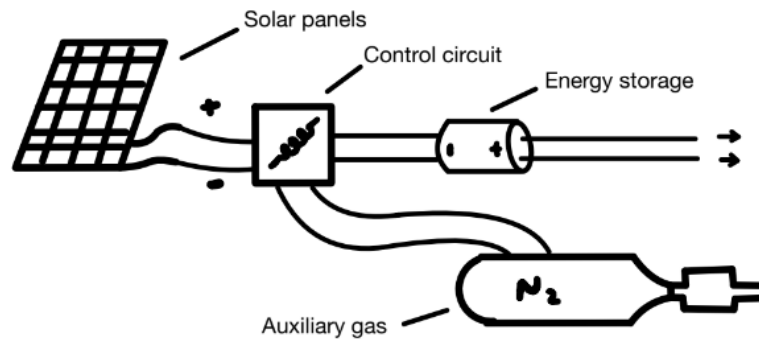


Figure 19: Electrical and auxiliary components to design. A battery has been included to ensure consistent energy delivery to the system.

We expect this design to be capable of melting the material with the given power constraint. This is backed by our initial proof-of-concept calculation yielding a low time to reach melting temperature for ideal conditions, and the preexisting induction metal melters that are capable of the temperature and metal quantity requirements this system needs. The proof-of-concept calculations are available for reference in the next section. Utilizing an insulating crucible will allow for heat to be conserved, and exclusively heating the sample via induction will yield high efficiency in energy use and minimal thermal losses. A simple 4-stage process for the induction melting is shown below in Figure 20.

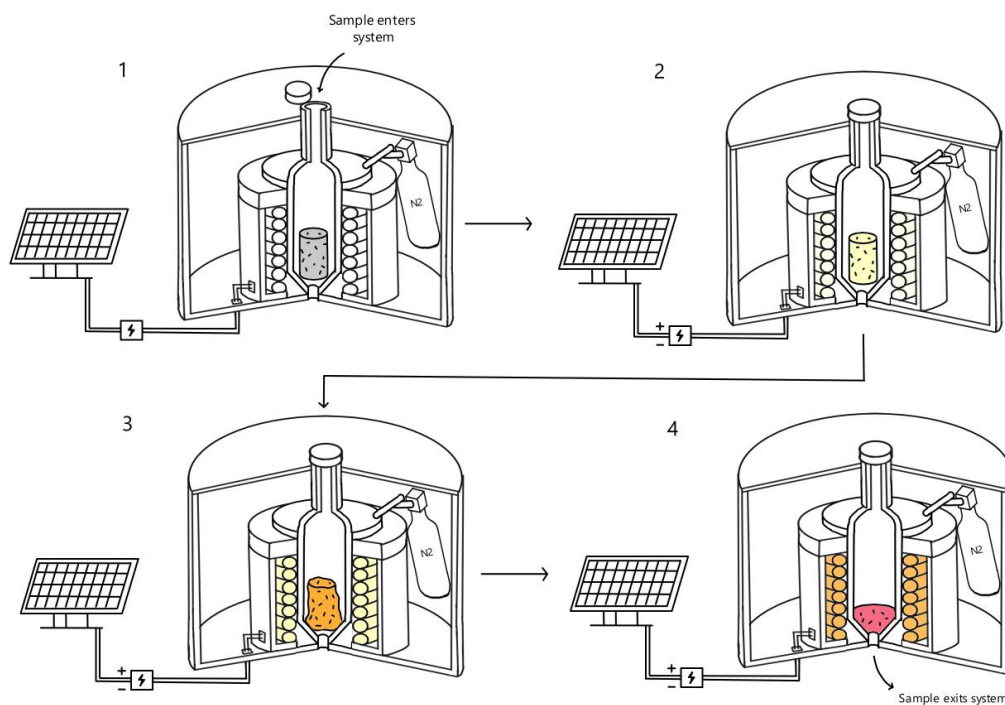


Figure 20: A 4-stage process for induction melting. The induction coils reach a lower temperature than the sample, shown using color gradients.

The proof-of-concept in the fall quarter proves that the system we chose will be able to reach 1810K and hold that temperature for the necessary amount of time to melt. We were able to look at the technical specification on how much metal the system should contain and compare it to the time it takes for metal to melt to find an optimal sample size, and therefore calculate the volumetric dimensions of the system. During the winter quarter, we proved sublimation negligible to our system and validated the system we created against a physical experiment and an experiment from the Los Alamos National Laboratory. Then, in spring quarter, we ran a breakeven analysis on the cost of launching the system versus the cost of launching the raw materials, and finalized the analysis on our technical specifications to see if they were met. We found that the amount of iron our system needed to manufacture to make launching the system (over the cost of sending just raw iron) worth it, the system needed to successfully melt four samples. This means it would take the system approximately three hours, based on the simulations we have run, to fully break even.

Our expected budget at the beginning of the year was minimal, due to student access to all the software we used. However, in the winter quarter, we received a budget of \$300 from the mechanical engineering department to help us create a physical experiment. We used \$228.79 of this budget to buy a handheld induction heater to run the experiment, results of which are discussed in sections below. Everything else necessary for the experiment and our spring quarter demonstration were able to be made on-campus for free, so we will return the remaining budget to the mechanical engineering department.

Conceptual Design Validation

Physical Experiment

Our winter quarter advisor, Dr. McCormack, recommended we run a physical experiment to answer some lingering questions we had about induction, so this was a major focus for the winter quarter. Our primary questions revolved around the difference that different sizes of metal would make (e.g. solid metal versus fine granules) and the difference that silicates would make when melting. Since iron has a high melting point on Earth and finding an induction heater to melt at temperatures that high would be difficult, we resorted to pewter, instead. The pewter used on our campus is 99.9% tin, which has a melting point of 505K, and will be easier to melt [23].

We had three learning objectives for this experiment: to determine the difference between melting times of solid pewter and powdered pewter, to determine the effects of silicates (gravel) on the melting time of pewter, and to create temperature vs. time graphs of the pewter melting to verify the mathematical and simulation modeling. We ran three different experimental setups, one with solid pewter, one with powdered pewter, and one with powdered pewter and mixed-in silicates (miniature gravel pieces).

Since the budget we received from the mechanical engineering department of Rose-Hulman was small, and induction heaters are expensive, we bought an induction bolt heater made by Solary. We set the pewter in a graduated cylinder, and then put the graduated cylinder in a crucible and surrounded it by casting sand to keep it upright and disperse the heat. We then measured the temperature of the pewter via a type K thermocouple, read by a UEI DT2000 digital thermometer. To record the temperatures for data analysis, we recorded the thermometer with a phone camera, and recorded the entire setup with a phone camera to visually observe melting. This setup required all four of us: one to hold the induction heater, one to hold the thermocouple in constant contact with the pewter, one to record the temperatures read on the thermometer, and one to record physical changes. A picture of the full setup is shown below, in Figure 21.

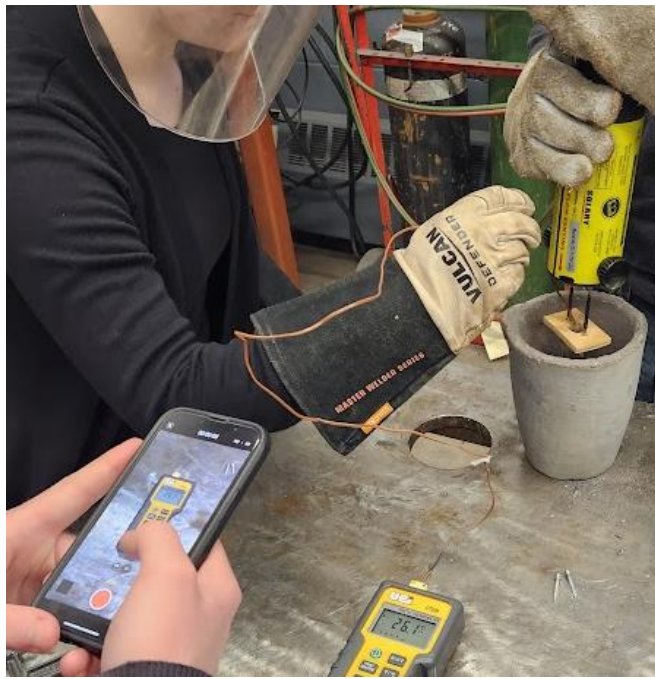


Figure 21: Physical Experiment Setup

The melting times of the solid and powdered (no silicates) pewter were recorded successfully, but the powdered pewter with silicates was not melting after the three-minute mark, so we scrapped that experiment. The induction heater we purchased is not meant to run more than about two and a half minutes, and we felt it necessary to prolong the life of the heater over the success of that experiment.

Therefore, to answer the first learning objective, the melting time of the solid pewter was 75 seconds, and the melting time of the powdered pewter was 156 seconds, which demonstrates that the melting time of solid pewter is significantly lower. This was further confirmed by discussion with our external reviewers, who explained that the air pockets in the powdered pewter interfered with the induction heating by decreasing the amount of internal conduction that could happen in the metal.

To answer the second learning objective, the powdered pewter without silicates fully melted in 156 seconds, and past 180 seconds, the powdered pewter with silicates did not show any signs of even starting to melt. Therefore, we determined that silicates do have a slowing effect on the melting time.

For the third learning objective, the temperature-time graph for a previously melted solid pewter chunk is shown below, in Figure 22. It is important to note the previously melted condition because it resulted in the solid pewter becoming more cylindrical, which is important for the math model and thermal simulation.

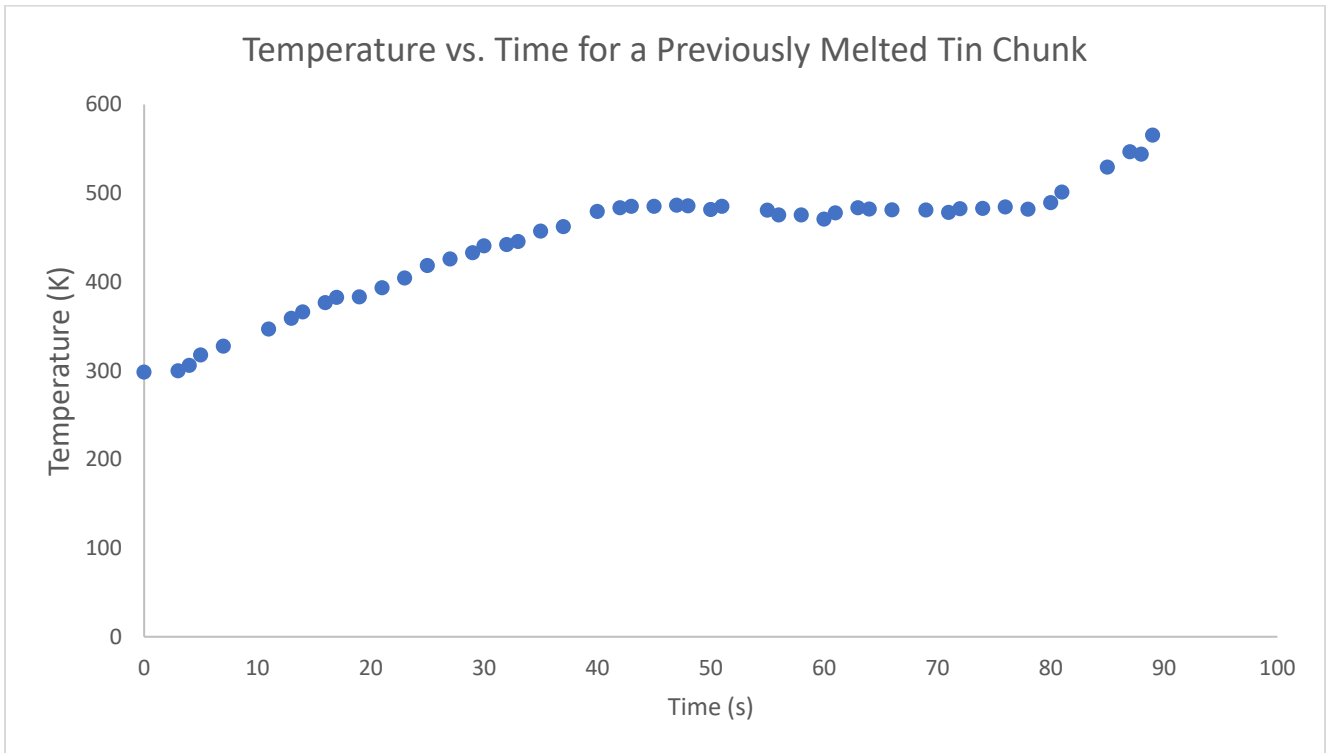


Figure 22: Temperature vs. Time Graph for Pewter

The most notable conclusion here is the flat line between 40 and 80 seconds of passed time, where thermal energy from the induction heater was used for the phase change of the pewter, rather than directly heating it. This was not previously accounted for in the math model, and will now need to be added, because 40 seconds of an approximately 85 second melt is significant.

Mathematical Model

We created a mathematical model that uses induction heating equations to estimate the response of the sample as it melts. This model was heavily influenced by a relevant approximation completed by researchers at Los Alamos National Laboratory, henceforth referred to as LANL [24]. The assumptions governing the mathematical model are shown below in Table 4.

Table 4: Assumptions made during the generation of the mathematical model.

#	Assumption	Rationale
1	The sample will be modeled as a solid cylindrical object	This sample type will enable the use of the approximation techniques performed by LANL.
2	Convection does not exist	Psyche is a pure vacuum, and within the chamber minimal atmosphere will exist.
3	The system passes lumped capacitance	The characteristic length of the sample is small enough to assume a small Biot number
4	The sample uses the highest possible emissivity for iron, $\epsilon = 0.95$	Results in the model representing worst-case conditions for melting
5	Sample radiates out to a large surface with a temperature of 75 K, Psyche's worst-case temperature	
6	Sample will be made of purely iron without any nickel	
7	The surroundings will have an absorptivity of 1	
8	Environment stays at a constant temperature	
9	Temperature dependent curves were created for applicable materials from limited data points (shown in Appendix)	Portrays the variation of the property with increasing temperature as best as possible
10	Finite difference approach is valid	Math model is iterated at multiple short time steps
11	The material holds a constant geometry as it melts	Lack of tools to model realistic behavior
12	Nagaoka coefficient can be obtained from Figure 23	System operates using an air-core solenoid

In addition to this set of ten assumptions that applies to Psyche, the individual calibration trials performed each come with their own set of assumptions, documented in their own section.

The variables utilized in the mathematical model are shown below in Table 5.

Table 5: A list of the relevant variables for the mathematical model.

Variable	Description
ρ	Density of sample
c	Specific heat of sample
A_s	Surface area of sample
R	Cylindrical radius of sample
l	Length of sample and coil
σ	Electrical conductivity of sample
k	Thermal conductivity of sample
c	Specific heat of sample
ϵ_R	Emissivity of surface of sample
T	Temperature of sample
T_∞	Temperature of surrounding environment
N	Number of turns of the coil
n	Turns per unit length, $\frac{N}{l}$
b	Distance between surface of cylinder and coil
β	Ratio between the surface distance and length, $\frac{b}{l}$
I	Peak amplitude of current
ω	Frequency of current
δ	Skin depth
μ_r	Magnetic permeability
ϵ	Ratio of radius and skin depth, $\frac{R}{\delta}$
σ_B	The Stefan-Boltzmann constant
K_n	Nagaoka coefficient

The foundation of the mathematical model is conservation of energy. For the remainder of this section, bolded property values indicate that a property is temperature dependent. This yields the following equation, reliant on the lumped capacitance and exclusively radiative heat loss assumptions:

$$mc \frac{dT}{dt} = q - A_s \epsilon_R \sigma_B (T^4 - T_\infty^4) \quad (1)$$

Following this, q , the heat energy introduced to the system, was derived. Key system parameters in q include the number of turns in the induction coil along with the frequency and magnitude of the alternating current running through it. The complex derivation was sourced from the LANL paper; the intricacies of this information are omitted for brevity [24].

$$q = \frac{\pi n^2 I^2 l}{\sigma \epsilon} K_n^2 \left(1 - \frac{\epsilon}{2}\right) \quad (2)$$

The two unique terms in this calculation are ϵ , the ratio of radius to skin depth ($\frac{R}{\delta}$), and K_n , the Nagaoka coefficient [24]. The skin depth of an induction heating system is the distance that the electromagnetic field

will penetrate the sample and directly heat the area with eddy currents. The larger the skin depth, the more effective the heating. The skin depth is calculated with the following equation [24],

$$\delta = \sqrt{\frac{2}{\omega \mu_R \sigma}} \quad (3)$$

where ω is the term incorporating the frequency of the current into the equation for q . The final unique term to induction heating is the Nagaoka coefficient. This coefficient is necessary to include because standard induction heating equations assume an infinite length induction coil, so the correction factor ensures the finite geometry is accounted for. Since the system we are modeling uses an air coil, the Nagaoka coefficient can be graphically approximated using Figure 23, below. Using the dashed “model” line, we determined a specific Nagaoka coefficient for each coil geometry.

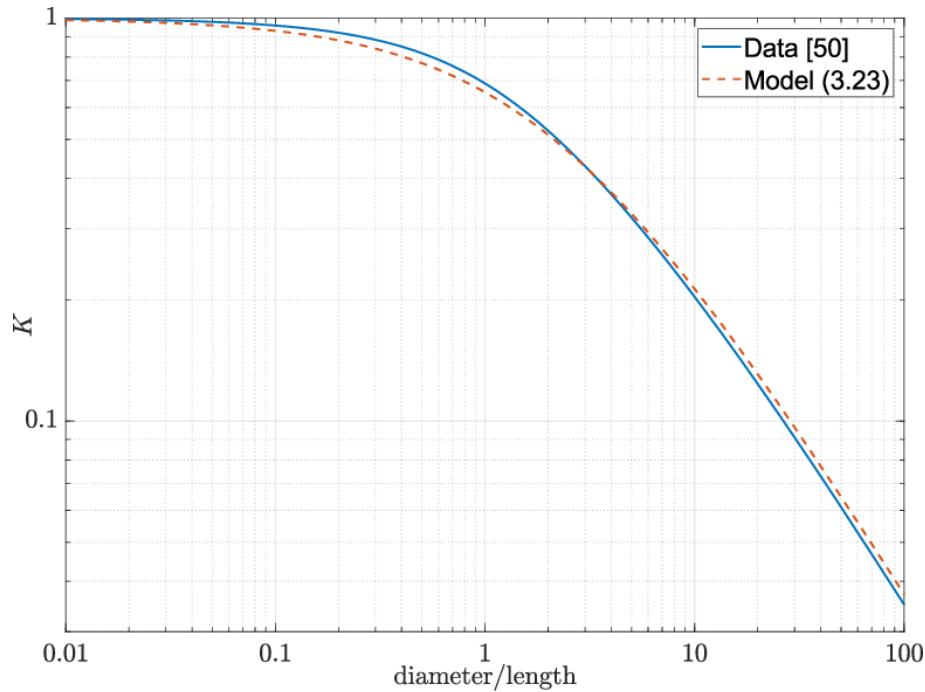


Figure 23: Correlation chart for the Nagaoka coefficient of an air-core solenoid [25].

Combining all of these factors together, a finite difference script was used to evaluate the overall heating of the sample. The form of this finite difference equation, below, is derived from equations 1-3,

$$dT = dt \left(\frac{\frac{\pi n^2 I^2 l}{\sigma \epsilon} K_n^2 \left(1 - \frac{\epsilon}{2}\right) - A_s \epsilon_R \sigma_B (T^4 - T_\infty^4)}{mc} \right) \quad (4)$$

where dT is the change in temperature, and dt is the time step. For each mathematical simulation performed, a time step of 0.10 seconds was used. This mathematical model will be validated using two separate metrics (the LANL data and the physical experiment run earlier), and then will be modified to demonstrate Psyche conditions.

Thermal Simulation

To analyze the thermal response of the full system, we used SolidWorks Thermal for finite element analysis (FEA) and simulation. The heat generated by the inductive method will be input as a temperature-dependent heat flux to the sample surface. The mesh size utilized for simulations will be the suggested SolidWorks default size, and this will be verified through a mesh convergence test on each simulation.

Some innate assumptions are made through the simulation software itself, notably that the surfaces are assumed grey and diffuse (no radiation transmits through surfaces) and the Kirchoff's Law is assumed true (absorptivity and emissivity of a surface is identical) [26]. These assumptions are viable so long as the materials utilized do not have high transmissivity or temperature differences. Since melting temperatures are present in our situation, the assumption of Kirchoff's law being true will result in some error in high-temperature analysis, but SolidWorks Thermal will remain the choice for analysis due to its intuitive interface and ability to clearly document all analysis. Additionally, all induction coils are converted to geometric shapes (8 sided for validating experiments, and 9-sided for the final design) due to limitations in computational hardware. Future attempts to analyze inductive heating should seek more traditional FEA software such as COMSOL, Abaqus, or ANSYS, which may be able to perform efficient simulations with less hardware requirements, enabling the removal of geometric induction coils and the innate assumptions of SW Thermal.

Application 1 – Los Alamos National Lab Experiment

The first validation of our mathematical model and thermal simulation was to the experimental setup completed by Jankowski et. al. in their efforts to validate their analytical approximation to inductive heating [24]. The experiment we will emulate is the one with a high frequency and fast startup conditions, because its high heat generation and deepest skin depth is the most applicable to Psyche. This experiment uses an Inductoheat SP16 to heat a graphite cylinder, as shown in Figure 24, and a detailed list of the relevant parameters for the experiment are shown below in Table 6. The wire diameter, D_{wire} , is measured as the outside diameter of the induction coil, and the coil radius around the crucible is D_{coil} . Not pictured are the type K thermocouple in the center of the graphite for temperature measurement and a clamp-on current probe for current analysis.

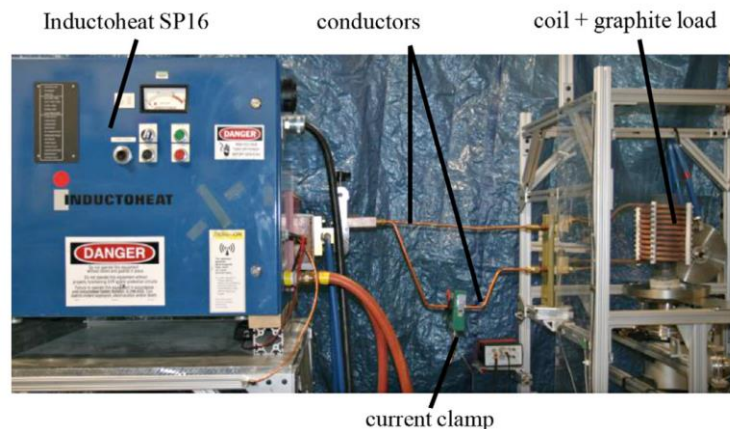


Figure 24: The experimental setup utilized for the LANL validating simulation [24].

Table 6: The physical parameters utilized in the high frequency fast startup experiment.

Variable	Value	Units
R_{cyl}	4.51	cm
L_{cyl}	19.8	cm
ϵ_R	0.9	--
b	6.65	cm
T_{∞}	293.15	K
N	11	--
σ_b	$5.67 \cdot 10^{-8}$	$\frac{W}{m^2 \cdot K^4}$
D_{coil}	18.0	cm
D_{wire}	1.27	cm
t_{wire}	0.32	cm
F	15983	Hz
I	467.72	A

The sample material was POCO graphite, whose temperature dependencies are located in Appendix G. Assumptions made in our math model to align the two are that the surrounding temperature is 293K, the only heat loss is radiative, and the coil is an air-core solenoid. Applying these parameters and assumptions to the mathematical model yields Figure 25 for the POCO graphite:

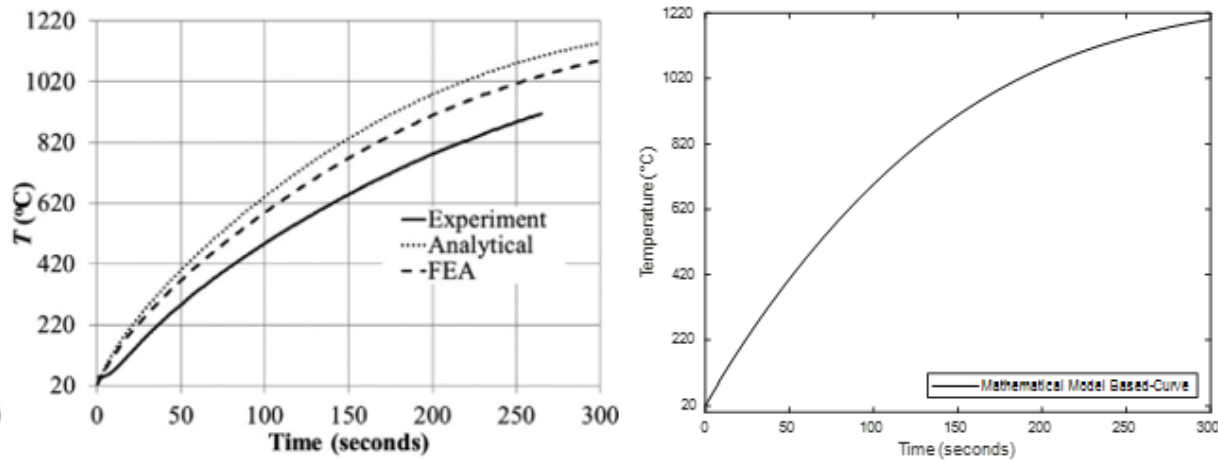


Figure 25: Comparison of the LANL produced temperature vs. time graph (left) and the math model produced graph (right). The math model seeks to recreate the analytical curve.

The math model's curve recreates the analytical curve created by the LANL researchers semi-accurately but tends to overshoot the temperature. Two of the worst points are at 100 and 300 seconds, where the math model overshoots the LANL analytical curve by roughly 100°C. One of the contributing factors to this difference is that the project's math model does not include convection heat loss, which likely decreased the LANL's analytical model. Our math model is designed to work under Psyche's conditions, which guarantees no convection, so it was not updated to reflect this disrupting factor. Overall, the comparison between the two

reinforces the strength of our mathematical model, and validates the process taken. The math model also produces a heat flux over temperature graph that is input to the thermal simulation to represent the system heating. This graph is shown in Figure 26.

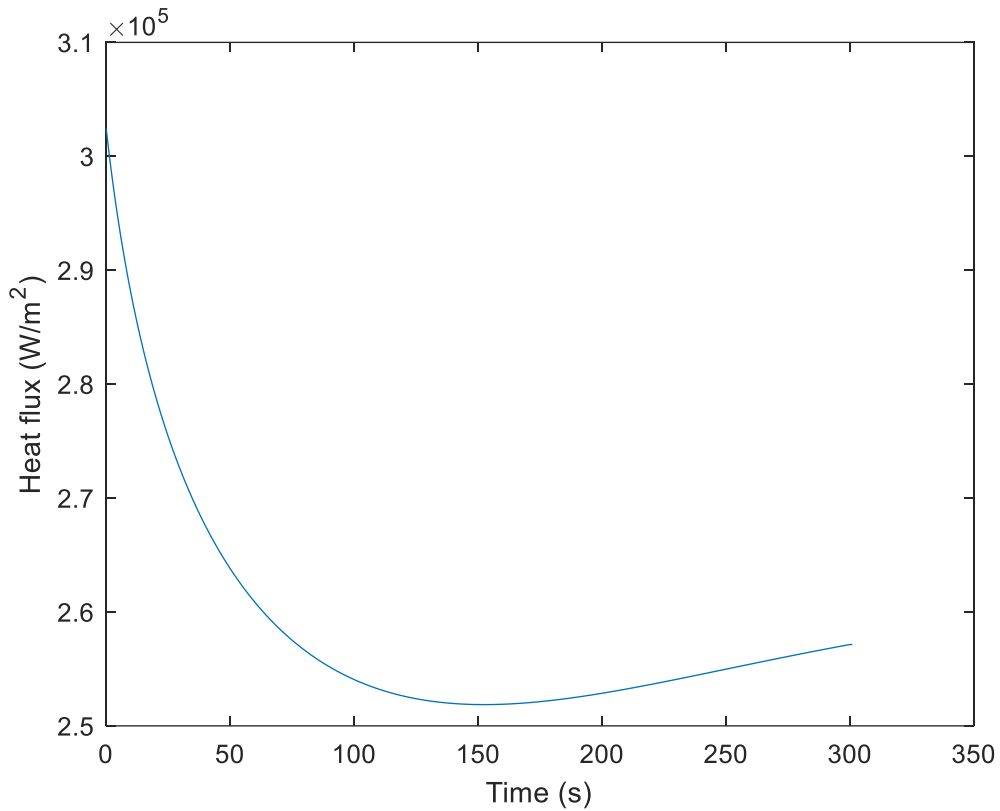


Figure 26: Heat flux vs. time graph for the mathematical modeling of the LANL data

The LANL experimental setup was then replicated in SolidWorks so thermal analysis could be performed, using the heat flux from the math model as the heat input to the simulation. An image of the model can be seen below in Figure 27.

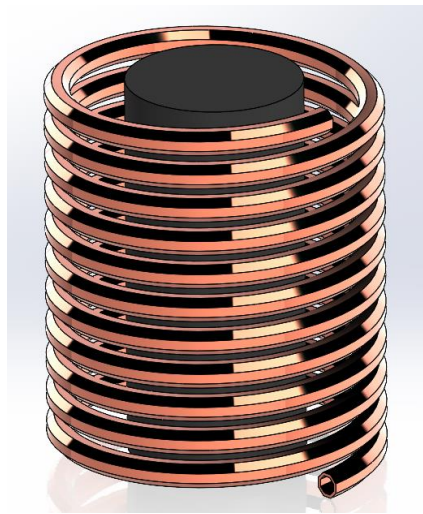


Figure 27: The 3D model utilized for the thermal simulation of the Los Alamos experiment.

Due to the limited computational power of the Rose-Hulman student laptops, the circular copper induction coils were converted to 8-sided polygonal coils, to ensure the mesh could accurately convey the faces of the coils and convergence could be achieved. This conversion was performed such that the octagonal coils have the same projected surface area as the circular wire, though the effective surface area differs.

The following parameters were defined for the thermal simulation:

- The simulation is transient, lasting 300 seconds with a 3 second timestep.
- The sample is a material of “POCO Graphite”, with a density of $1720 \frac{kg}{m^3}$ and temperature-dependent specific heat and thermal conductivity values defined according to Appendix H.
- A material of “[SW] Copper” for the induction coils.
- A blended curvature-based mesh of width 2.16 cm.
- An initial temperature of 293.15K to all solid bodies.
- A temperature-dependent thermal load of heat flux into the coil-facing surface of the cylinder, with values shown in Figure 26 Appendix G.
- A surface-to-surface radiation on the coil-facing surface of the cylinder, with an ambient temperature of 293.15 K and an emissivity of 0.9.
- A surface-to-surface radiation on the outside faces of the copper coil, with an ambient temperature of 293.15 K and an emissivity of 0.1.
- A surface-to-ambient radiation on the flat faces of the cylinder with an emissivity of 0.9 and a view factor of 1.

This results in the following transient response, with the animation of the system shown in Figure 28 and a plot of the transient data shown in Figure 29 below. Note that Figure 29 and Table 7 utilize units of Celsius to match the data from the Los Alamos National Lab experiment. At 300 seconds, the exterior of the sample is 3.3% hotter than the center, with a temperature of 1102.8°C (1375.8 K).

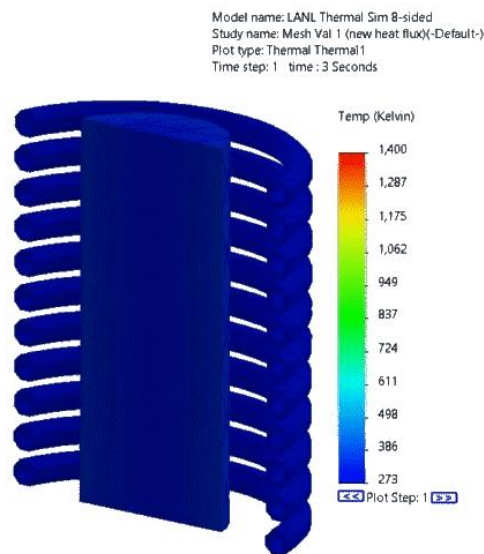


Figure 28: A cross-section animation of the LANL sample heating over time.

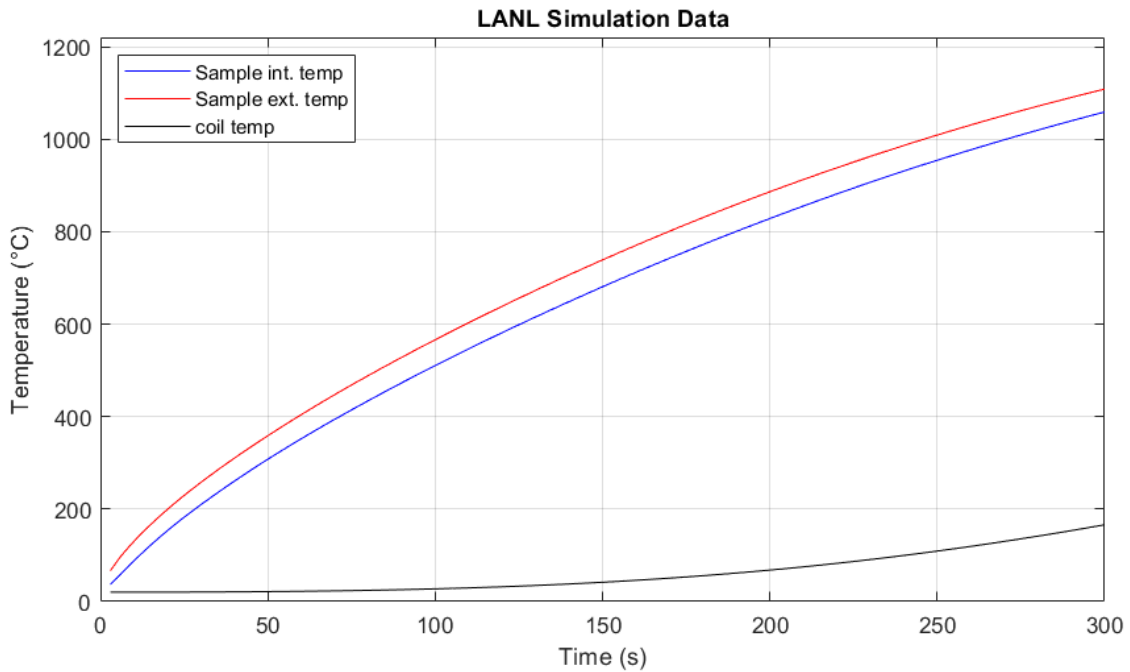


Figure 29: Transient temperature response data for the LANL sample and coil. The sample reaches a center temperature of 952.0°C (1225.15 K) after 250 seconds, and the coil reaches a temperature of 108.2°C (381.2 K).

The difference between the simulation and experiment performed at LANL is shown below in **Error! Reference source not found.** A percent difference of 5.30% indicates confidence that the mathematical model and SolidWorks Thermal combination is a viable method of analysis for inductive heating systems.

Table 7: Percent difference calculations for the response of the LANL simulation.

Measurement Type	Simulated Response	Experimental Value	Percent Difference
Temperature at 250s (°C)	951.9	888.6	6.87%

Mesh convergence was performed during a previous iteration by utilizing a finer and coarser mesh and analyzing the change in response. This data is shown below in **Error! Reference source not found.** Since the change in sample and coil temperature is less than 5%, the simulation mesh is considered converged.

Table 8: Percent difference calculations for mesh convergence of the LANL simulation

Mesh size	Sample Temp at 300s (K)	Sample Percent Difference (%)	Coil Temp at 300s (K)	Coil Percent Difference (%)
2.74 cm mesh	733.37	---	304.2	---
2.16 cm mesh	735.88	0.35	303.61	0.20
1.89 cm mesh	733.52	0.32	304.52	0.30

Application 2 – Physical Experiment

The sample utilized in the physical experiment is pewter, which consists of 99.99% tin. The relevant material properties for tin are shown in Appendix H. The experiment performed utilized a Solary inductive bolt heater, with temperature measured using a type K thermocouple placed on the outer surface of the tin, read by a UEI DT2000 digital thermometer. Relevant parameters for the experiment are shown below in **Error! Reference source not found.**

Table 9: The physical parameters utilized for the tin melting experiment

Variable	Value	Units
R	0.724	cm
l	1.113	cm
ϵ_R	1	--
T_∞	293.15	K
N	3.5	--
K_n	0.6	--
F	10000	Hz
I	6.3	A

We assumed that the heating was linear, based on the raw experiment data, to the point that heat of fusion started and once the heat of fusion was overcome. We also assumed that there was no heat loss in the experiment, and we ignored uncertainties in the measurements taken. Since the inductive bolt heater did not come with a specifications sheet, we assumed an output frequency of 10 kHz from benchmarking other induction heaters, and we modeled the electrical resistivity and density of materials were modeled as constant.

Since the raw data and general observations were discussed in the physical experiment section, the figure below (Figure 30) just shows the alignment between the smoothed data and the data gathered in the mathematical model.

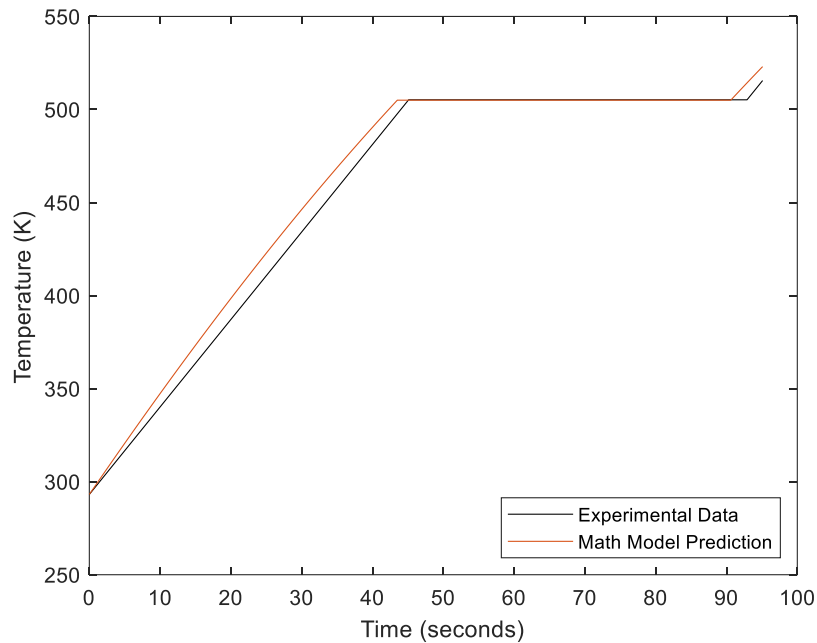


Figure 30: Comparison of measured data and experimental data for the physical experiment.

These curves match up very closely, which on the surface means the model is validated. However, tin's temperature-dependent electrical resistivity values could not be found because of its low melting point, which took out a significant variable used in the math model. We also had to assume the frequency value based on benchmarking similarly sized induction heaters, but this value could be incorrect. Altering this value can change the heating curve quite significantly, which detracts from the verification. However, the model aligned well with the Los Alamos experiment, which had more data included in it, so with similar alignment to the physical experiment, we still consider it validated.

Utilizing this mathematical model, the experimental setup was designed in SolidWorks so that a thermal simulation could be conducted. An image of the model can be seen below in Figure 31.

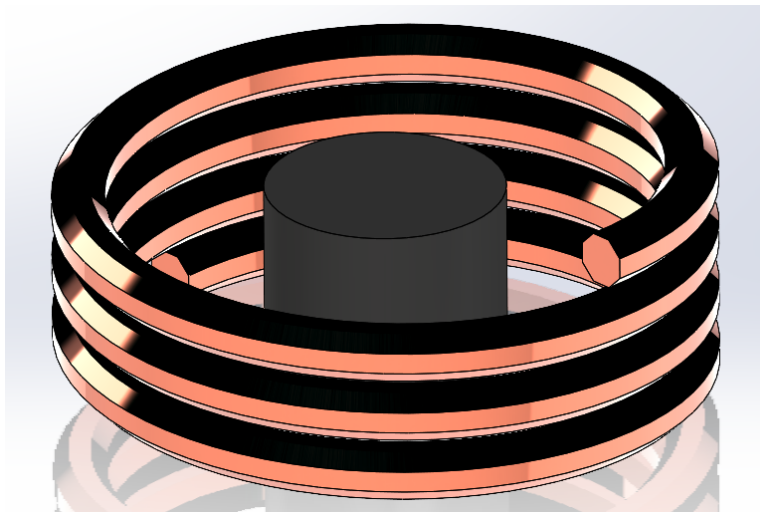


Figure 31: The 3D model utilized for the thermal simulation of the physical experiment.

The coils were converted to a 8-sided version in the same format as the LANL simulation, though the coils are assumed to be solid for the physical experiment. The following parameters were defined for the thermal simulation:

- The simulation is transient, lasting 90 seconds with a 1 second timestep.
- A material of “Pewter (tin)” for the sample, with a density of $7290 \frac{kg}{m^3}$ and temperature-dependent specific heat and thermal conductivity values defined according to Appendix H.
- A material of “[SW] Copper” for the induction coils.
- A blended curvature-based mesh of width 0.27 cm.
- An initial temperature of 293.15K to all solid bodies.
- A temperature-dependent thermal load of heat flux into the coil-facing surface of the cylinder, with values shown in Appendix G.
- A surface-to-surface radiation on the coil-facing surface of the cylinder, with an ambient temperature of 293.15 K and an emissivity of 0.9.
- A surface-to-surface radiation on the copper coils, with an ambient temperature of 293.15 K and an emissivity of 0.1.
- A surface-to-ambient radiation on the flat faces of the cylinder with an emissivity of 0.9 and a view factor of 1.

This results in the following transient response, with the animation of the system shown in Figure 32 and a plot of the transient data shown in Figure 33 below. Note that at the melting time of 75 seconds, the exterior of the sample is 0.4% hotter than the center, with a temperature of 507.48 K.

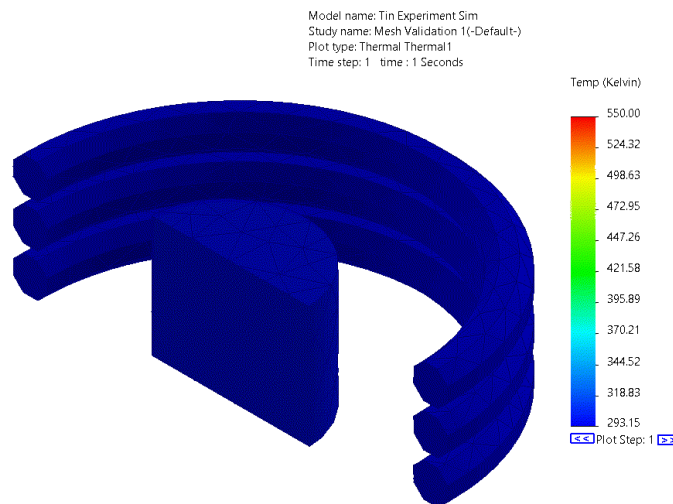


Figure 32: A cross-section animation of the physical experiment sample heating over time.

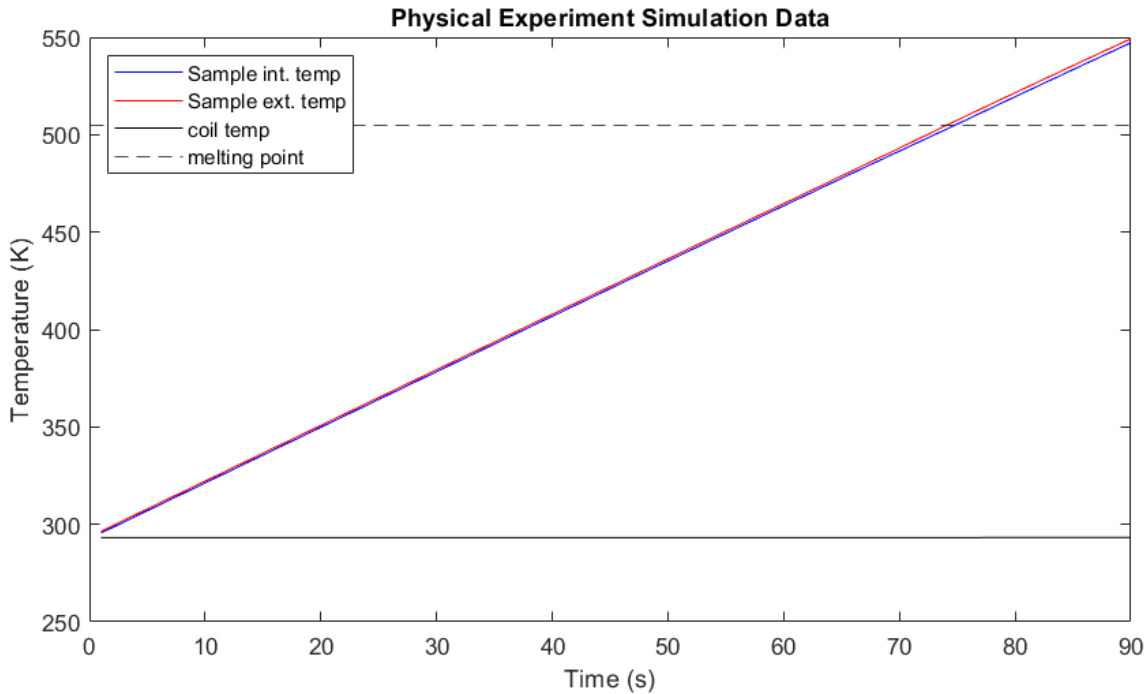


Figure 33: Transient temperature response data for the sample and coil. The sample reaches the melting temperature after 75 seconds with a temperature of 505.44 K, and the coil reaches a temperature of 293.23 K.

The difference between the simulation and experiment is shown below in **Error! Reference source not found.**

Table 10: Percent difference calculations for the response of the physical simulation.

Measurement Type	Simulated Response	Experimental Value	Percent Difference
Time to melt (s)	75	80	6.46%

Mesh convergence was performed by utilizing a finer and coarser mesh and analyzing the change in response. This data is shown below in Table 11. Due to the small size of this experiment in comparison to the LANL simulation, the mesh is significantly finer, leading to very small percent differences in response. Since the change in sample and coil temperature is less than 5%, the simulation mesh is considered converged.

Table 11: Percent difference calculations for mesh convergence of the physical simulation.

Mesh size	Sample Temp at 75s (K)	Melting Percent Difference (%)	Coil Temp at 75s (K)	Coil Percent Difference (%)
0.35 cm mesh	505.43	---	293.23	---
0.27 cm mesh	505.44	0.01	293.23	0.00
0.18 cm mesh	505.43	0.01	293.23	0.00

Simulated Psyche Model

After validating the mathematical model based on the previous two experiments, the model was applied to the Psyche inductive heating system. There are four necessary design parameters the math model seeks to produce for the selected design. These parameters are the number of coil turns, length of coil, current input, and current frequency. At this current stage, the parameters chosen for the induction heating system are:

Table 12: Chosen parameters for Psyche induction heating system

Variable	Value	Units
Number of turns (N)	7	--
Length of coil (L)	0.0972	m
Current input (I)	39	A
Current frequency (F)	200	kHz

These parameters were carefully selected to fit within various power and geometric constraints, while still successfully heating the sample. There are two additional key assumptions that this model is based off. Firstly, it assumes that the power of 1950 W is drawn from a 50 V battery. The specific battery referenced is an Ibeos 50V / 1 kW-hr lithium-ion battery, which has been classified as space-grade, with an acceptable mixture of voltage and power output [27]. This allows the magnitude of the current to be sufficient for the system to heat. If possible, further minimization of this voltage to maximize the current would improve the system efficiency. The second assumption is that the sample heated is a solid cylinder, with a height of 10 cm and radius of 4.5 cm. Under these parameters, the heating of the sample looks like the graph below, Figure 34.

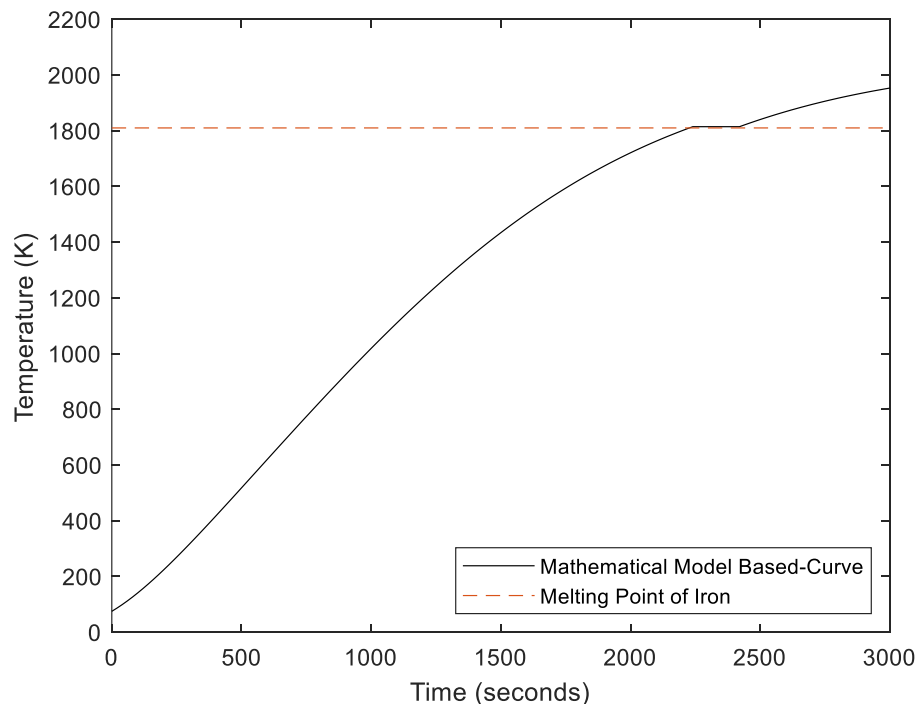


Figure 34: Temperature vs. time curve of iron sample with specific design parameters

This input fully melts the metal sample in approximately forty minutes, successfully accomplishing the mission’s goal. In addition, the fluctuation of the heat flux with temperature was recorded at each temperature spanned, and this information was translated into the thermal simulation. This output allows the heat energy input to the thermal simulation to be identical to that generated by the mathematical model.

Following from the mathematical model, a thermal simulation can also be performed using SolidWorks Thermal. The relevant material properties for the thermal simulation were acquired from three key sources. The temperature-dependent specific heat values for iron were approximated using data from Desai, and thermal conductivities were approximated using data from Powell et. al. [28, 29]. Emissivity values were acquired from Cole-Parmer, a laboratory equipment manufacturer [30]. A summary of relevant material properties is shown below in **Error! Reference source not found.**. Note that for unoxidized iron, the emissivity is stable until the liquid phase is reached, transitioning from 0.21 to 0.28.

Table 13: The material properties utilized for the Psyche design simulation.

Material	Density ($\frac{kg}{m^3}$)	Thermal Conductivity ($\frac{W}{m \cdot K}$)	Specific Heat ($\frac{J}{kg \cdot K}$)	Emissivity
Iron (unoxidized)	7874	Temp-dependent	Temp-dependent	0.21-0.28 (solid-molten)
Zirconia	5000	2.2	500	0.62
Copper	8900	390	390	0.1
1060 Aluminum	2700	200	900	0.04
Ceramic Porcelain	2300	1.4949	877.96	0.9

To simulate the Psyche system with available hardware, the changes below were made to the CAD model to reduce the computational power necessary to run the simulation:

- The circular copper induction coils were converted to a 9-sided polygon, in a method similar to the LANL simulation. Nine sides were chosen for the final simulation coils to avoid parallel faces between coils and surfaces, which would cause excessive radiative heat transfer.
- The temperature and pressure sensors and the external gas canister were removed to focus on gaining results from the sample, coils, and insulation.
- Mesh control was applied to the sample and coils to utilize a finer mesh necessary for achieving valid sample results.

A sectional view of the simplified model is shown below in Figure 35.

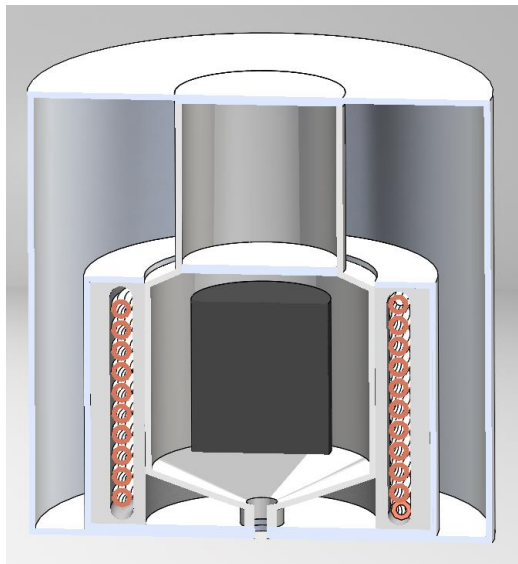


Figure 35: The 3D model utilized for thermal simulation of the Psyche system.

The following parameters were defined for the thermal simulation:

- The simulation is transient, lasting 3000 seconds with a 30 second timestep.
- The sample is a material of “Pure Iron (Unoxidized)”, relevant properties shown in **Error! Reference source not found.** and Appendix H.
- The crucible is a material of “Zirconia” with properties in **Error! Reference source not found.**
- The coil, system casings, and inlet caps are a material of “1060 Aluminum”, with properties in **Error! Reference source not found.**
 - o Note that the inlet cap closest to the sample should be modeled as zirconia in the future in order to handle the temperatures exposed to surfaces close to the sample.
- The induction coils are a material of “Copper” with properties in **Error! Reference source not found.**
- The SolidWorks default mesh option, a blended curvature-based mesh with a width of 4.67 cm.
 - o Mesh control applied to the sample with a width of 1.83 cm.
 - o Mesh control applied to the induction coil with a width of 1.77 cm.
- An initial temperature of 75K to all solid bodies.
- A temperature-dependent thermal load of heat flux into the coil-facing surface of the cylinder, with values obtained from the mathematical model results.
- Surface-to-surface radiation on the following areas, closed from the environment:
 - o All faces of the sample, with temperature-dependent emissivity $\varepsilon = 0.21$ (75-1810K) to 0.28 (1810K+).
 - o The exterior and interior of the zirconium crucible, with emissivity $\varepsilon = 0.62$.
 - o The interior and internal flat faces of the coil insulation, with emissivity $\varepsilon = 0.9$.
 - o The exterior of the copper induction coils, with emissivity $\varepsilon = 0.1$.
 - o The exterior of the induction coil casing, with emissivity $\varepsilon = 0.04$.
 - o The interior of the system casing, with emissivity $\varepsilon = 0.04$.
- A surface-to-ambient radiation on the exterior of the system casing with an ambient temperature of 75 K and emissivity $\varepsilon = 0.04$.

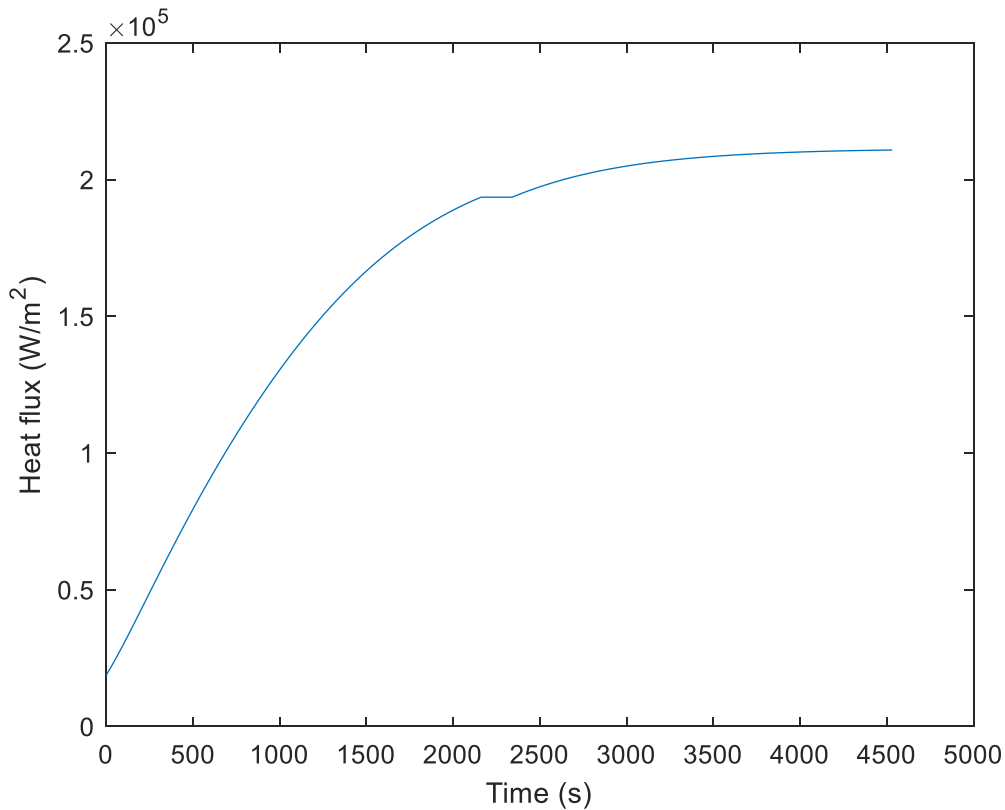


Figure 36: Heat flux vs. time for the final Psyche simulation

A final set of simulations were performed once the design was finalized, utilizing the same parameters described above, with updates to the geometry of the system and sample, and updated heat flux values as seen in Figure 36. During this simulation process, the system was evaluated for a longer length of time, and an additional simulation was performed at the warmest range of Psyche’s summer, an atmospheric temperature of 210 K. Due to time limitations with the computational hardware available at Rose-Hulman, the cold environment was only able to simulate over 3300s with a 90 second timestep, and the warm environment was simulated over 4500s with a 60 second timestep. Animations of the system heating over time are seen below in Figure 37 and Figure 38.

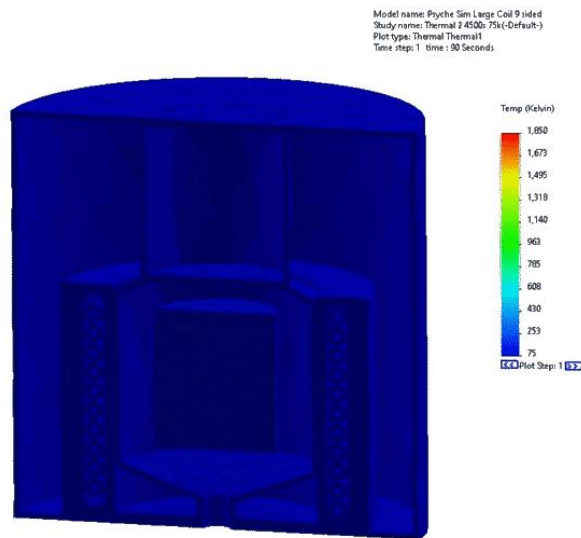


Figure 37: A cross-section animation of the Psyche system heating over time in cold atmospheric conditions.

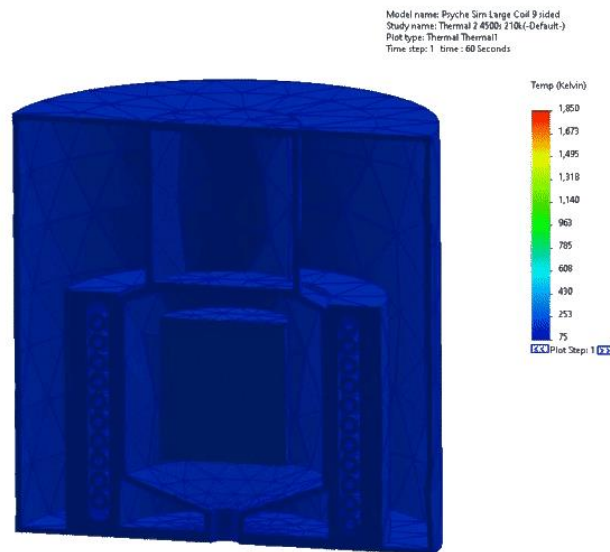


Figure 38: A cross-section animation of the Psyche system heating over time in warm atmospheric conditions.

Figure 39 and Figure 40 show the cold atmosphere response of the system, with the sample not reaching melting during the simulation’s timeframe. This is likely due to the reduction in size of the sample in the final design from a diameter of 9.72 cm to 9.00 cm, reducing the overall area heated on the outside radial face. Figure 41 and Figure 42 show the warm atmosphere response of the system, where the sample reaches melting after 3660s. Exterior temperatures for both atmospheric conditions are evaluated at the end of this section.

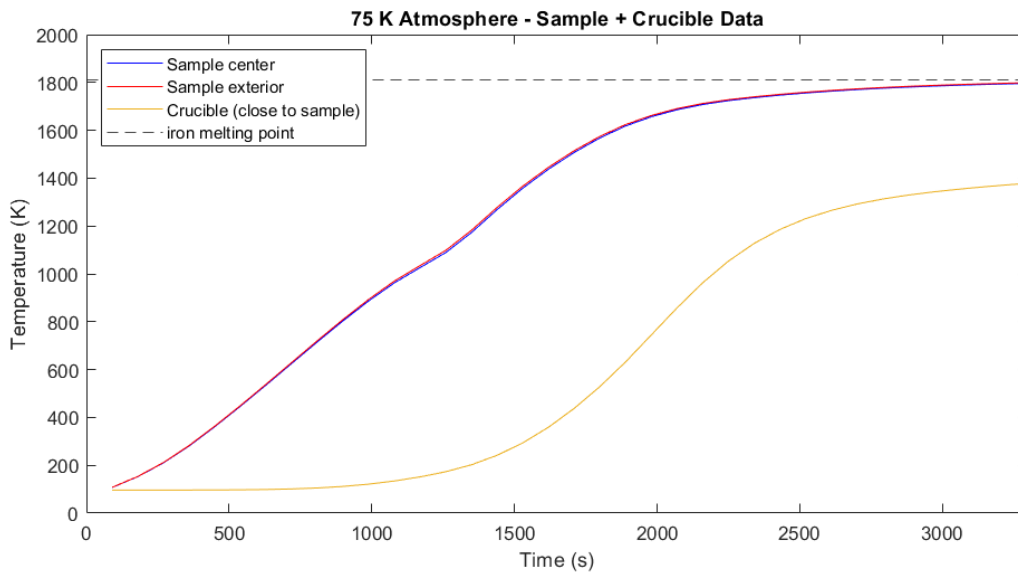


Figure 39: Transient temperature response data for the updated Psyche sample and crucible in cold atmospheric conditions. The sample does not reach melting within the 3300s range of the simulation, with a maximum temperature of 1797 K at 3300s.

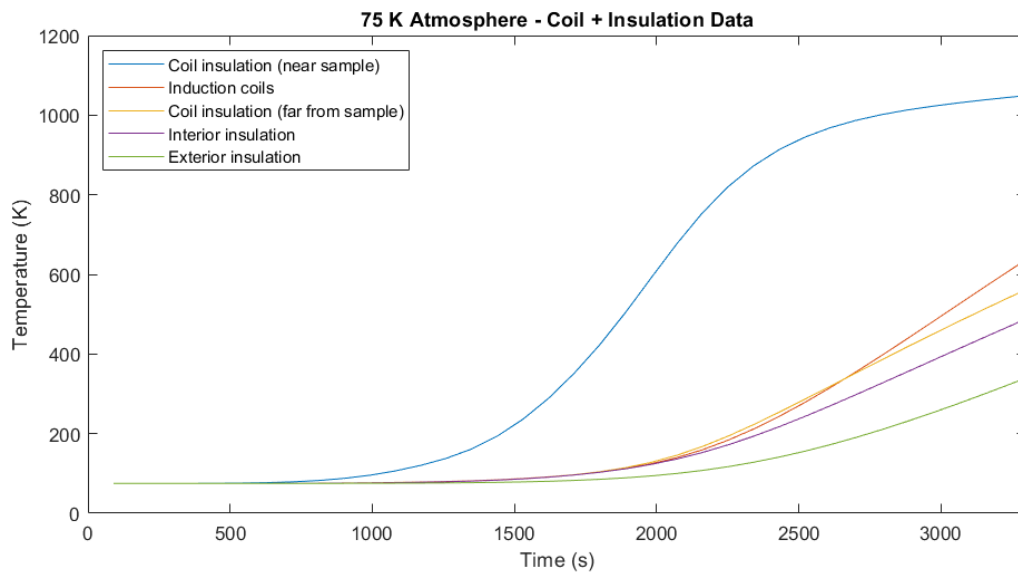


Figure 40: Transient temperature response data for the updated Psyche coils and insulation in cold atmospheric conditions. The coils reach a temperature of 651.01 K after 3300s of operation.

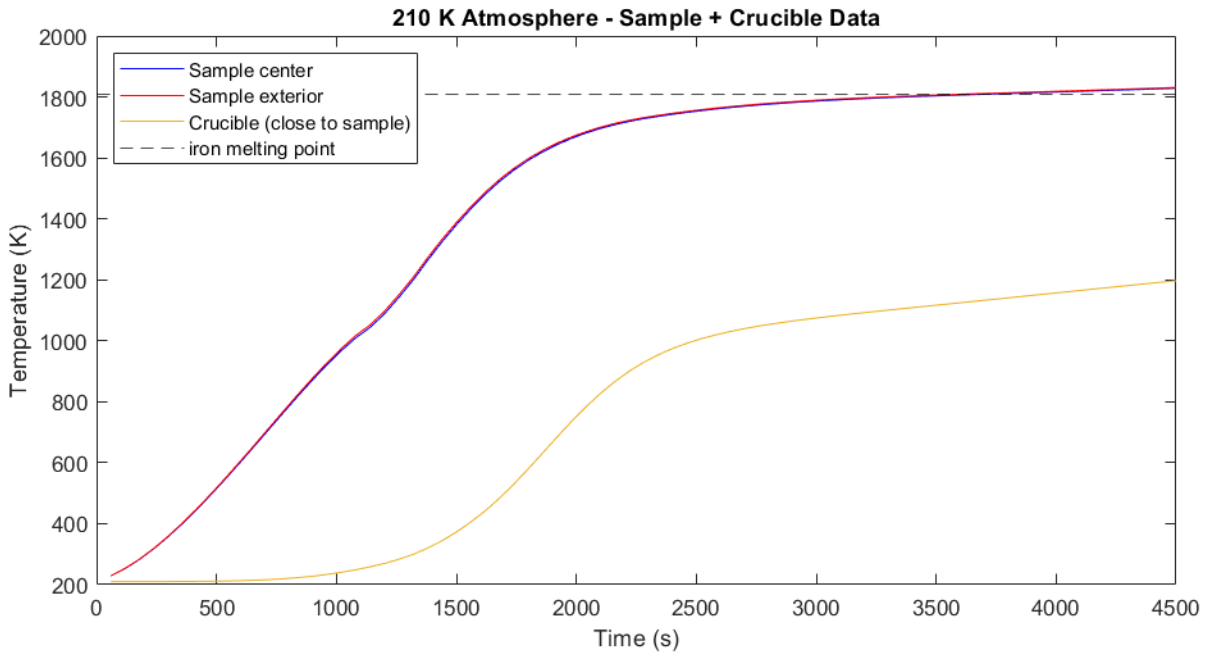


Figure 41: Transient temperature response data for the updated Psyche sample and crucible at warm atmospheric conditions. The sample reaches the melting point at 3660 seconds with a center temperature of 1810.3 K, and the crucible temperature reaches a temperature of 1129.6 K.

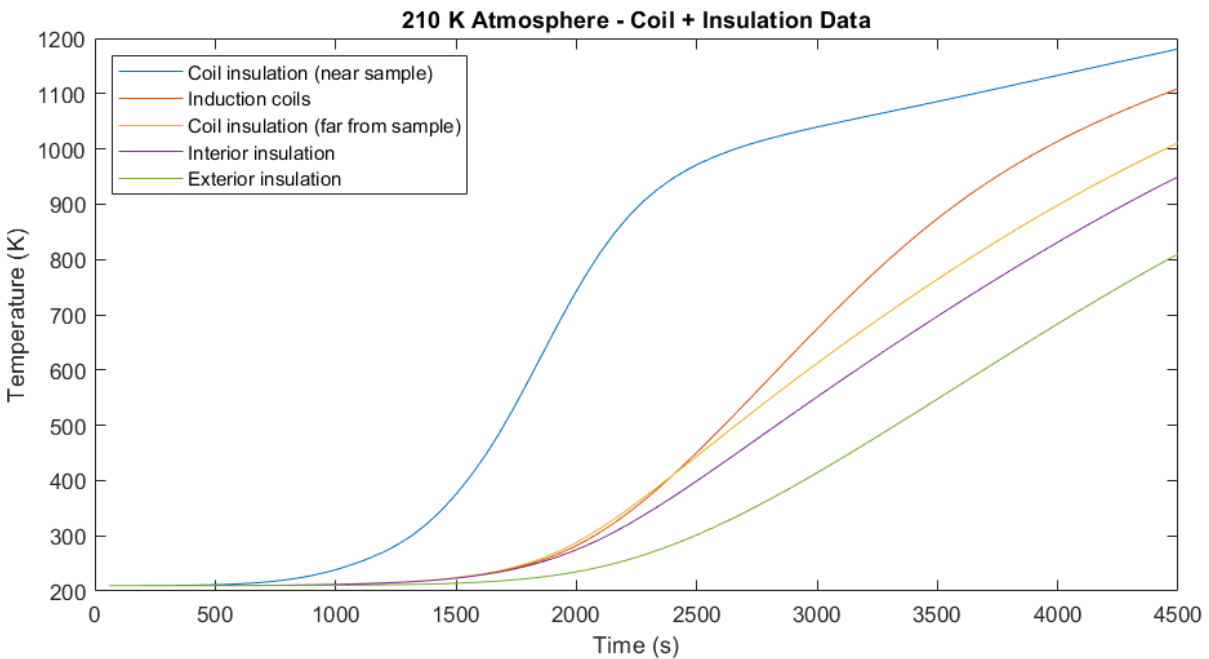


Figure 42: Transient temperature response data for the updated Psyche coils and insulation in warm atmospheric conditions. At the melting time of 3660s, the coil insulation reaches a temperature of 1100.7 K and the coils reach a temperature of 925.14 K.

External temperatures were evaluated for the finalized system to evaluate the safety of the system to external electronics. Only the radial face was evaluated for safety, due to the likelihood of modifications to the top and bottom of the system for inlet and outlet mechanisms. Figure 43 shows the transient response of two locations, the center of the outside insulation and the bottom edge of the outside insulation where the temperature was the highest for both cold and warm atmospheric temperatures.

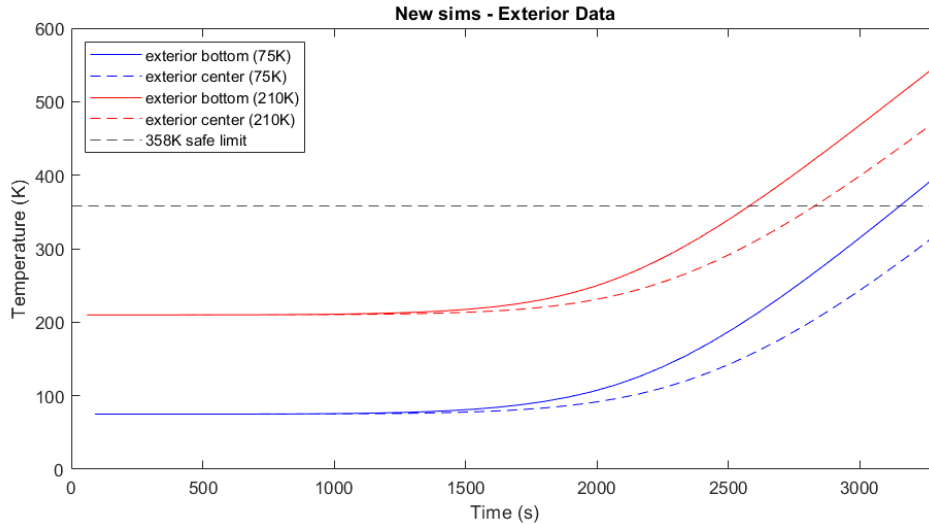


Figure 43: Transient response data for external temperature at two locations over the temperature range on Psyche. The safe limit is marked in black, with both systems breaching this threshold after approx. 2500s.

Mesh convergence was performed on a previous version of the system by using meshes that are approximately 10% finer and coarser than the chosen mesh and analyzing the change in system response. Ideally, to validate mesh convergence, minimal change should occur in the probed locations. This data is shown below in **Error! Reference source not found.** Mesh controls for the sample and coils were reduced by the same percentage as the overall mesh size. The sample mesh appears to be very well converged, while the coil mesh may require further minimizing in order to achieve consistent results. It is also possible that the change in mesh size resulted in slightly different locations probed, though the conductivity of the coils should minimize this effect. The 5% difference in the coils still gives indication that the data is useful to analyze, though it will not be as confident as the reported results for the sample.

Table 14: Percent error calculations for mesh convergence of the Psyche induction simulation.

Element size	Sample temp at 2610s (K)	Sample Percent Difference (%)	Coil Temp at 2610s (K)	Coil Percent Difference (%)
5.11 cm mesh	1810.8	---	314.36	---
4.67 cm mesh	1810.9	0.01%	332.87	5.72%
3.93 cm mesh	1808.2	0.15%	321.35	3.52%

For the previous system that mesh convergence was tested in, it is interesting to note that the sample reached melting temperature in 2610s under cold atmospheric conditions. The largest modification from the previous simulation to the final simulations was a reduction in size of the sample to allow more room between the sample and crucible inlet walls. This reduction in surface area on the radial face resulted in less area for the heat flux of the induction coils to act on the sample, reducing the overall heating capacity of the system. This is likely the cause of the change in melting time for the new simulation set. An image of the previous simulation model and the sample and crucible response over time from the previous simulation version is shown below in Figure 44 and Figure 45. Note the similarity in shape of the melting, though the melting point is reached before the change in temperature begins to slow down.

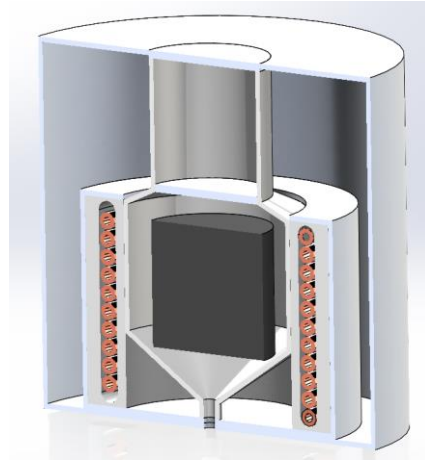


Figure 44: The 3D model utilized for the previous thermal simulations of the Psyche system. The outlet of the system and length of the inlet section are much smaller than the final model, and the sample is far wider with minimal distance between the sample and the inlet walls of the crucible.

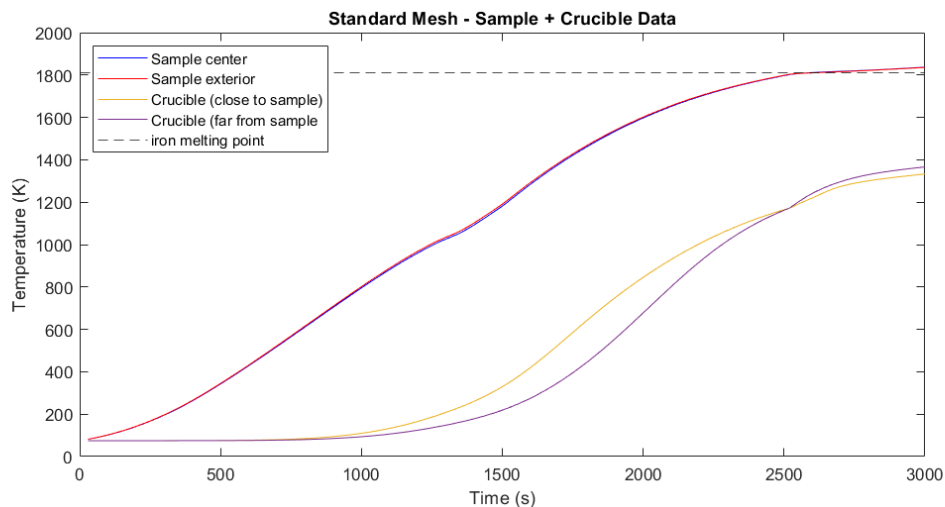


Figure 45: Transient temperature response data for the previous Psyche sample and crucible in cold atmospheric conditions. The sample reaches the melting point at 2610 seconds with a center temperature of 1810.9 K, and the crucible temperature reaches a maximum value of 1248.4 K.

Technical Specification Validation

To discuss the success of the system, we first start by analyzing how close we were to meeting all of our technical specifications. Table 15, below, shows how the design we created aligns with the technical specifications we created in the fall.

Table 15: Technical Specification Analysis

	Project Needs	Technical Specification	Value Hit	Met?
1	Melting Point	Melting chamber must reach 1810 K	1799.7 K	
2	Temperature Maintenance	Melting chamber temperature must hold steady until heat of fusion is overcome	3 min until fusion overcome, temperature holds	
3	Melt Significant Amount	Melting chamber must hold a minimum of 8 cm ³ of solid alloy	636 cm ³	
4	Contain Metal	Chamber must be fully sealed while melting	Yes	
5	Thermal Isolation	External temperature of system cannot exceed 358 K	330 – 410 K, radial outside center - bottom	
6	Weight Constraint	System must weigh less than 850 kg	25.17 kg	
7	Volume Constraint	System must take up less than 16 m ³	8289.2 cm ³	
8	Energy Constraint	System must be able to start with 1950 W or less	Yes – 1950 W	
9	Low Energy Consumption	System must be able to steadily operate on 500 W	No – 1950 W was only mathematically proven	

This table shows that we met over half our specifications, almost met the melting point specification, and only failed the thermal isolation and low energy consumption specification.

The first, and most important technical specification is the melting point, which our thermal simulation does not confirm we will reach, as seen in Figure 39. This conclusion differs from the heating predicted by the mathematical model's curve in Figure 34, which predicts melting in 2340 seconds. In previous thermal simulations, we also were able to prove melting in approximately 2600 seconds, which was shown in Figure 45. However, we had decreased the sample diameter slightly to allow it to fit inside the system easier, which had the unintended consequence of decreasing the surface area, making the heating less effective. The last simulation was the last one that was able to be run with the resources available, and we ran out of time to make further alterations. Recommendations to meet this specification would be to increase the surface area of the sample to increase the heat flux input.

The next technical specification that we failed is the thermal isolation of the system. As seen in Figure 43, above, the external insulation of the designed system increases to a level that is unsafe for electronics, which was the basis of that technical specification. This number was calculated by the thermal simulation results and relies on many of the assumptions that SolidWorks Thermal makes regarding insulation and heat transfer

values. Additionally, the full material properties of MLI were not able to be recreated inside of SolidWorks Thermal, reducing the overall effectiveness of our insulation. Recommendations we have to pass this technical specification are to change the simulation software so insulation can be correctly simulated, increase the amount of insulation in the system, and/or move electrical components away from the heating elements.

The final failed technical specification is that of low energy consumption, which was failed by a large margin, as the system requires the full 1950 W to reach the melting point of iron. This high power requirement was largely because of the resource limitations the team faced throughout the simulation process, and alternative solutions are discussed in the following section of the report.

Limitations and Next Steps

Although the data we have found has allowed us to draw useful conclusions, there are many limitations that we faced throughout this project that could be overcome with access to different resources. This mainly presented itself in the thermal simulation aspect of our project. All our simulation was done using SolidWorks Thermal, which is severely limited when it comes to dealing with material properties. In addition, our system was bound by the assumptions that SolidWorks Thermal is based on, which unfortunately cannot be removed. When talking to professionals in the material science field, we found that ANSYS or COMSOL could be a viable alternative to this, that will allow for a much more accurate modeling of our simulation. Unfortunately, we did not have the resources to swap to this software.

Along with SolidWorks Thermal being an ineffective modeling software, our team also faced severe hardware limitations. The computing power we had access to was severely limited compared to other facilities which may have access to supercomputers, and as a result, the solution that we could verify using our thermal simulation program was significantly worse than what is theoretically possible based upon our math model. A key aspect of our design is the size of the induction coils - the smaller the coils are, the more that can fit into the allotted space, and the more effective the heating is. Using geometric constraints, we found that we should be able to reduce our power consumption by slightly over 300% without any loss in system efficiency by increasing the number of usable coils from 7 to 21. However, this change necessitates much smaller coils, which would lead to significantly more computing power to simulate the heating. When attempting to simulate this more efficient system, we repeatedly ran into software crashes, and ultimately found that it would not be feasible to simulate considering our time and energy constraints.

There were also multiple aspects of this project that were deemed external to our scope, which simplified our project but may have taken out some of the realism. For example, we only focused on melting pure iron, rather than the hypothesized mixture of iron and nickel. While iron does have a higher melting point than nickel, so being able to melt iron should mean the system can also melt nickel, there is a possibility that nickel melting faster could affect the effectiveness of induction heating on the still partially solidified iron. Furthermore, the system we designed has the theoretical capacity to be cooled via liquid, which would be necessary to bring down the temperature of the coils after consistent use. However, because of the timeline we were under, to ensure we accurately modeled the sample heating, we had to take the design of the liquid cooling system out of our scope. Other elements of the design we were unable to fully design included the internal and external wiring, the power system, and the entry/exit procedures for the sample.

We learned a lot over the nine months we worked on this project, especially about induction heating and the limitations of design in deep space conditions, but if we were to continue to work on this project, we would more heavily dive into learning how Eddy currents work, how thermal expansion would work in the system, and how interactions in the iron-nickel alloy would actually work for induction heating. We would also expand the math model to account for heat loss and more accurately model induction, and then modify the

thermal simulation accordingly. Most likely, to modify the thermal simulation, we would need to switch the software to COMSOL Multiphysics or ANSYS

If this system were to be pursued by another team in the future, we would recommend further looking into the system shown below, in Figure 46. We were able to test this design via our mathematical model, but due to the computational limitations discussed above, we could not validate this through our thermal simulation and chose not to present this idea in the main body of our report.

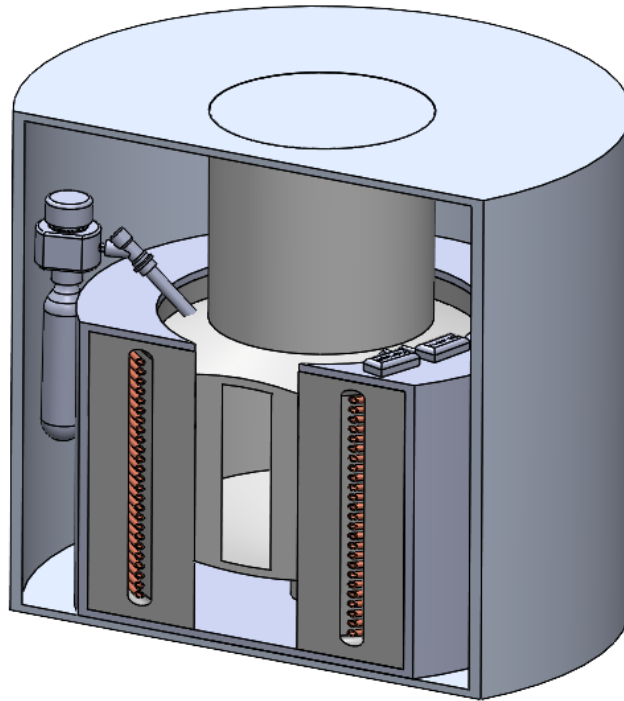


Figure 46: Optimized model, only proven mathematically.

This system, run at the same power level and with the same battery as the system presented in the main report, would melt the metal in three minutes (versus around forty minutes with the other system). Since three-minute melting would not be necessary when considering the time it presumably takes to gather the sample, we could decrease the power provided to the system and make the system run more efficiently. If this project were to continue past our stead, we would recommend this system be more thoroughly researched and simulated, because it is likely more effective.

References

- [1] NASA, "Psyche," [Online]. Available: <https://science.nasa.gov/mission/psyche/>.
- [2] NASA, "Ep 307: Psyche," 29 September 2023. [Online]. Available: <https://www.nasa.gov/podcasts/houston-we-have-a-podcast/ep-307-psyche/>.
- [3] C. Bizouard, "USEFUL CONSTANTS," 13 March 2021. [Online]. Available: <https://hpiers.obspm.fr/eop-pc/models/constants.html>. [Accessed November 2023].
- [4] L. T. Elkins-Tanton, E. Asphaug, J. F. Bell III, B. Bercovici, R. Bills and W. F. Bizen, "Observations, Meteorites, and Models: A Preflight Assessment of the Composition and Formation of (16) Psyche," *Journal of Geophysical Research: Planets*, vol. 125, no. 3, 2020.
- [5] C. J. Bierson, L. T. Elkins-Tanton and J. G. O'Rourke, "The Geologic Impact of 16 Psyche's Surface Temperatures," *Planetary Science Journal*, 2022.
- [6] A. C. Muscatello and E. Santiago-Malonado, "Mars in Situ Resource Utilization Technology Evaluation," NASA Technical Reports Server, 2013. [Online]. Available: <https://ntrs.nasa.gov/citations/20120001775>.
- [7] Boeing, "Active Thermal Control System (ATCS) Overview," NASA, February 2021. [Online]. Available: https://www.nasa.gov/wp-content/uploads/2021/02/473486main_iss_atcs_overview.pdf. [Accessed 25 November 2023].
- [8] "MARS Reconnaissance Orbiter," NASA, [Online]. Available: <https://mars.nasa.gov/mro/mission/spacecraft/parts/thermal/>. [Accessed October 2023].
- [9] Y. Y. Spirin N, "Development of heat-transfer circuits in the blast furnace," *IOP Conference Series: Materials Science and Engineering*, vol. 150, 2016.
- [10] R. Petrucci, F. Herring, J. Madura and C. Bissonnette, "23.3 Metallurgy of Iron and Steel," in *General Chemistry: Principles and Modern Applications*, 2022.
- [11] C. Emeodi and B. Animashaun, "Ferrous Metallurgy - Pig Iron, Wrought Iron, Steel, Cast Iron," [Online]. Available: <https://www.linkedin.com/pulse/ferrous-metallurgy-pig-iron-wrought-steel-cast-animashaun-bukola/>. [Accessed October 2023].
- [12] D. M. Wroughton, E. C. Okress, P. H. Brace, G. Comenetz and J. C. Kelly, "A Technique for Eliminating Crucibles in Heating and Melting of Metals," *Journal of the Electrochemical Society*, vol. 99, no. 5, p. p.205, 1952.
- [13] W. J. Kroll, "Melting and Evaporating Metals in a Vacuum," *Transactions of the Electrochemical Society*, vol. 87, no. 1, p. 571, 1945.
- [14] R. G. Budynas and K. Nisbett, "Metal Melting Temperatures of Common Engineering Materials," *Shingley Mechanical Engineering Design*, [Online]. Available: https://www.engineersedge.com/materials/metal_melting_temperatures_13214.htm.
- [15] P. Vinet, H. Schlosser and J. Ferrante, "Pressure dependence of the melting temperature of metals," *Physical review*, vol. 40, no. 9, pp. 5929-5935, 1989.

- [16] G. Hautaloma, A. Johnson, N. N. Jones and E. Morton, "NASA's OSIRIS-REx Spacecraft Collects Significant Amount of Asteroid," 23 October 2020. [Online]. Available: <https://www.nasa.gov/news-release/nasas-osiris-rex-spacecraft-collects-significant-amount-of-asteroid/>. [Accessed 11 October 2023].
- [17] "At What Temperature do Conventional Electronics Packages Fail?," TWI Global, [Online]. Available: <https://www.twi-global.com/technical-knowledge/faqs/faq-at-what-temperature-do-conventional-electronics-packages-fail>.
- [18] NASA, "Mars Curiosity Rover - Summary," 2019. [Online]. Available: <https://mars.nasa.gov/msl/spacecraft/rover/summary/>.
- [19] NASA, "The Psyche Spacecraft and Science Instruments," 13 October 2023. [Online]. Available: <https://blogs.nasa.gov/psyche/2023/10/13/the-psyche-spacecraft-and-science-instruments/>.
- [20] "Nuclear Reactors and Radioisotopes for Space," World Nuclear Association, May 2021. [Online]. Available: <https://world-nuclear.org/information-library/non-power-nuclear-applications/transport/nuclear-reactors-for-space.aspx>.
- [21] D. Liang, L. F. Monteiro, M. R. Teixeira and L. M. Monteiro, "Fiber-optic Solar Energy Transmission and Concentration," *Solar Energy Materials and Solar Cells*, 1998.
- [22] K. Smiths, "Nitrogen Threaded Beverage Grade Cartridges - 4.1 Gram," [Online]. Available: <https://www.kegsmiths.com/products/4-1-gram-threaded-nitrogen-cartridges>. [Accessed 3 November 2023].
- [23] E. Toolbox, "Metals and Alloys - Melting Temperatures," [Online]. Available: https://www.engineeringtoolbox.com/melting-temperature-metals-d_860.html.
- [24] T. A. Jankowski, N. H. Pawley, L. M. Gonzales, C. A. Ross and J. D. Journey, "Approximate Analytical Solution for Induction Heating of Solid Cylinders," *Applied Mathematical Modelling*, vol. 40, pp. 2770-2782, 2016.
- [25] P. A. Kyaw, "Efficient Power-Dense Passive Components for Next-Generation High-Frequency Power Conversion," *ResearchGate*, 2018.
- [26] D. Systems, "Thermal Analysis," Concord, 2010.
- [27] Hywel, "Satellite batteries – for CubeSats, nanosats, and other form factors," *satsearch*, 23 Jun 2021. [Online]. Available: <https://blog.satsearch.co/2021-06-23-satellite-batteries-for-cubesats-nanosats-and-other-form-factors>.
- [28] "Desai, P. D.," *Journal of Physical and Chemical Reference Data*, vol. 15, no. 3, pp. 967-983, 1986.
- [29] R. W. Powell, Y. C. Ho and P. E. Liley, *Thermal Conductivity of Selected Materials*, Washington, D.C.: United States Department of Commerce, National Bureau of Standards, 1966.
- [30] "Emissivity of Specific Materials," Cole-Parmer, 2018. [Online]. Available: <https://www.coleparmer.com/tech-article/emissivity-of-specific-materials#anchor63>.
- [31] "Nuclear Regulatory Commission," National Archives: Federal Register, [Online]. Available: <https://www.federalregister.gov/agencies/nuclear-regulatory->

commission#:~:text=The%20Nuclear%20Regulatory%20Commission%20licenses,Act%20of%201974%20(42%20U.S.C.. [Accessed 2023].

- [32] McGraw Hill, Encyclopedia of Science & Technology, 8th Edition, McGraw Hill, 1997.
- [33] S. P. Sahib Mohammad, "Reductants in Iron Ore Sintering: A critical review," *Fuel*, vol. 332, 2023.
- [34] L. L. Han Hongliang, "Effect of ore types on high temperature sintering characteristics of iron ore fines and concentrate," *Minerals Engineering*, vol. 197, 2023.
- [35] J. Hontas, "Binary Nickel Alloy Phase Diagrams Compilation and Critical Evaluation," *NASA Technical Reports Server*, 1982.
- [36] M. Shaw, "Vacuum Thermal Sublimation for Metal Production from Lunar Regolith," The Commonwealth Scientific and Industrial Research Organization, Melbourne, 2023.
- [37] A. J. G. Yunus A. Cengel, Heat and Mass Transfer | Fundamentals & Applications Sixth Edition, McGraw Hill, 2020.
- [38] E. K. a. A. Katelhon, "Carbon capture and utilization in the steel industry: Challenges and opportunities for Chemical Engineering," *Current Opinion in Chemical Engineering*, 25 October 2019. [Online]. Available: <https://www.sciencedirect.com/science/article/pii/S221133981930036X>. [Accessed 27 September 2023].
- [39] D. Steve, "Temperature uniformity survey (TUS) general practice for CQI-9 and ams2750e," *Thermal Processing Magazine*, 2020.
- [40] C. A. Boehler R, "Melting, thermal expansion, and phase transitions of iron at high pressures," *Journal of Geophysical Research: Solid Earth*, vol. 95, no. B13, 1990.
- [41] R. M. Boehler R, "Properties of rocks and minerals – high-pressure melting," *Treatise on Geophysics*, pp. 527-541, 2007.
- [42] H. K. Ahrens Thomas, "Phase diagram of iron, revised-core temperatures," Caltech, 13 April 2002. [Online]. Available: https://web.gps.caltech.edu/~asimow/TJA_LindhurstLabWebsite/ListPublications/Papers_pdf/Seismo_2079.pdf. [Accessed 27 September 2023].
- [43] S. Gordon, "Structural Design and Test Factors of Safety for Spaceflight Hardware," NASA, 2022. [Online]. Available: <https://standards.nasa.gov/standard/NASA/NASA-STD-5001>.
- [44] D. Oh, S. Collins, D. Goebel, B. Hart, G. Lantoine, G. Whiffen, L. Elkins-Tanton, P. Lord, Z. Pirkl and L. Rotlisburger, "Development of the Psyche Mission for NASA's Discovery Program," in *35th International Electric Propulsion Conference*, Atlanta, 2017.
- [45] NASA, "Crew Safety," 25 October 2023. [Online]. Available: <https://msis.jsc.nasa.gov/sections/section06.htm>.
- [46] "Sintering manufacturing process," Ames, 06 July 2018. [Online]. Available: <https://ames-sintering.com/basic-manufacturing-process/>. [Accessed 27 October 2023].

- [47] T. Nakamura and B. K. Smith, "Solar Thermal System for Lunar ISRU Applications: Development and Field Operation at Mauna Kea, HI," *Proceedings of SPIE*, 2011.
- [48] S. Z. Liu Weiqi, "Capacity and operation optimization of a low-temperature nuclear heating system considering heat storage," *Progress in Nuclear Energy*, vol. 161, 2023.
- [49] R. I. H. Solutions, "Ceramic Melting Crucibles for Casting," RDO Induction, Inc., [Online]. Available: <https://rdoinduction.com/ceramic-melting-crucibles.html>. [Accessed 3 November 2023].
- [50] B. Liu, Y. Wang, Z. Lin and T. Zhang, "Creating Metal Parts by Fused Deposition Modeling and Sintering," *Materials Letters*, vol. 263, 2020.
- [51] "Tin, Sn," MatWeb - Material Property Data, [Online]. Available: <https://www.matweb.com/search/datasheet.aspx?matguid=64d7cf04332e428dbca9f755f4624a6c>.

Acknowledgements

Dr. Elizabeth Melton is a physics professor at Rose-Hulman, specializing in astrophysics. She provided information on the general environment of space and launch conditions. She also clarified that minimal gravity should not be assumed to be zero gravity and helped us prioritize our design objectives.

Dr. Matt Riley is a mechanical engineering professor at Rose-Hulman, specializing in aerospace and materials engineering. Dr. Riley confirmed the possibility of sublimation, drew parallel between his research and ours to help us understand the challenges of material phases and conditions in space, and recommended we look at and/or extrapolate data from pressure vs. temperature graphs. He was also our spring quarter external reviewer and helped us ensure our project was feasible to finish.

Dr. Eduardo Vitral is a mechanical engineering professor at Rose-Hulman, specializing in materials science. He was our external reviewer for the fall and winter quarters. Dr. Vitral gave us insight into where our next steps should lead and recommended that we learn ThermoCalc so we could attempt to extrapolate pressure vs. temperature data of the metals on Psyche. He also confirmed our path during winter quarter, and further recommended looking into Abaqus or COMSOL for more advanced thermal simulation modeling.

Elliot Carol is the CEO of Lunar Resources, a company that aims to use in-situ resource utilization on lunar regolith for potential future lunar colonies. He was initially emailed about his research in ISRU techniques on the moon and put us in contact with one of his resource engineers, Mark Hinkel. Elliot also provided a general idea that 1950W was realistically a lot of power to consume, which will be kept in mind for future design considerations.

Mark Hinkel is a resource extraction engineer working under Elliot Carol at Lunar Resources. He affirmed our choice to use ThermoCalc, from Dr. Vitral's recommendation, and further recommended another source, FastWeb.

Dr. Amir Danesh-Yazdi is a mechanical engineering professor who has experience in heat transfer and thermodynamics. He helped us verify that our proof-of-concept model for Quarter 1 had merit and pointed us toward thermal simulation software that Rose-Hulman already has access to (SolidWorks, ANSYS, and ComSol). He also walked into the four of us sitting in his office and said, "Hello troublemakers", which eased our stress about the difficulties we had in our proof-of-concept calculations.

Dr. Shraddha Sangelkar is a mechanical engineering professor who advised us throughout the fall quarter. She reality checked us in the beginning, and then motivated and encouraged us through the

rest of the quarter. If we had not started with Dr. Sangelkar as our fall advisor, this project would not have advanced as far as it has.

Dr. Maarij Syed is a physics and optical engineering professor who specializes in magnetic materials and has experience with induction heating. He served as one of our external reviewers in the winter quarter and confirmed our models of induction heating were on the right path. His experience with induction heating has been invaluable throughout our research.

Dr. Jay McCormack is a mechanical engineering professor who advised us through the winter quarter. He procured a budget for us to experiment with an induction heater and pushed us to explore other means of validation.

Dr. Zac Chambers is a mechanical engineering professor who advised us through the spring quarter. He helped us find a new computer to run our thermal simulations on and has allowed us the freedom to finish our project how we wanted.

Ethical Considerations

Since this hypothesized mission is unmanned and operating in the asteroid belt light-minutes away from Earth, some ethical considerations are out of the scope of this project. Public health, safety, and welfare, for example, are all not considered for this project because no humans are launching with the mission or impacted by the performance on Psyche. In a similar vein, considering the global, cultural, and social ethics of choosing to delegate funds to this Psyche mission (rather than focusing on domestic issues) is outside our project scope. Ethical considerations that we will consider for this mission are listed in Table 16 below.

Table 16: Ethical considerations for the mission's scope.

	Considerations for the project
Environmental	<p>The system must function under the environmental conditions of Psyche. This includes near zero-gravity and zero-pressure conditions, along with a consistently fluctuating temperature. Should we pursue a nuclear method of generating energy for the system, we will follow the standards in place by the Nuclear Regulatory Commission to protect public and environmental health and safety, and both use and discard the fuel responsibly [31].</p> <p>Applicable Tech Specs: 1-12</p>
Economic	<p>To account for the astronomic cost of sending objects into space, we will design our system to be as lightweight as possible, ensuring our allocated resources are responsibly used. In addition, the system will use a minimal amount of fuel, such that it is not bringing unnecessary resources into space.</p> <p>Applicable Tech Specs: 3, 8-10</p>
Sustainability	<p>To best embrace sustainable thinking, our solution will focus on operating with renewable energy and multi-use batteries. This will allow our system to function for the entire duration of the Psyche mission.</p> <p>Applicable Tech Specs: 3, 11</p>
Engineering Standards	<p>NASA has numerous standards necessary to consider when constructing our design, including but not limited to: NASA-STD-5001 (Structural Design and Test Factors of Safety for Spaceflight Hardware); NASA-STD-5017 (Design and Development Requirements for Mechanisms); NASA-STD-8719.17 (NASA Standard for Ground-Based Pressure Vessels and Pressurized Systems)</p> <p>Applicable Tech Specs: 2, 5-7</p>

Appendix A

Concept Generation, Filtering

The first idea was using the magnetic properties of iron to help the iron separate from the nonmetallic slag. This would use a combination of Psyche's limited gravity and magnetism to allow the metal and silicate to separate naturally over time. Unfortunately, this idea was scrapped after further research exposed that molten iron is not magnetic. To melt iron, it must be heated past its Curie temperature, which is the point where metals lose their inherent magnetic properties. Iron's Curie temperature is 1043 K, which is significantly less than the necessary 1810 K for melting [32].

The second idea to filter was to use a centrifuge to create more of a gravitational force to help the sample separate quicker, a diagram of which is shown in Figure A1. This idea would work through the density differences that the molten iron and the slag would have, like how molten iron and slag separate on Earth.

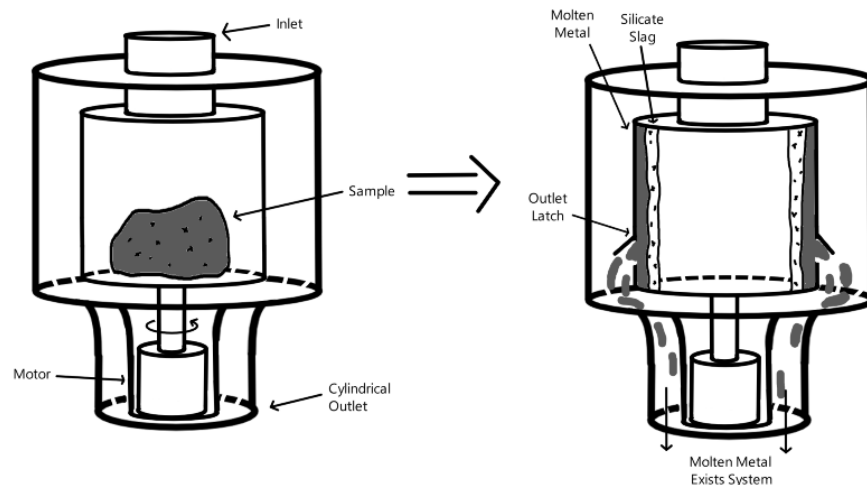


Figure A1: System utilizing centrifugal force to separate sample

The other consideration we have for filtration is completely passive, where the slight gravity of Psyche allows the molten iron to fall to the bottom of the container the sample is in over time. A diagram of this is shown in Figure A2. This idea is primarily time-dependent, we are currently unsure how long it would take for this to work, but it is still a viable concept.

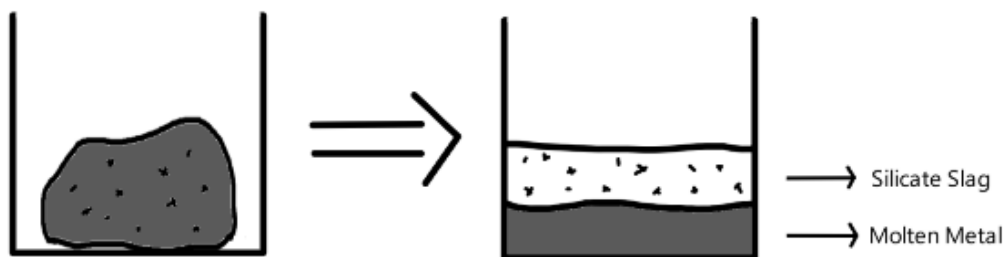


Figure A2: Sample separation using the available gravity on Psyche

Appendix B

Sintering Description

The process of sintering is shown in Figure B1, below:

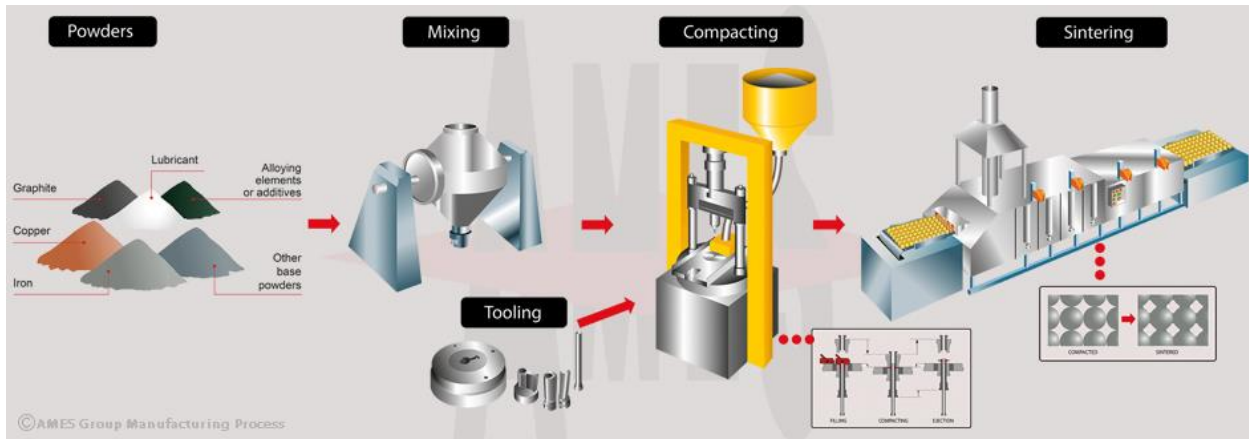


Figure B1: Four-step process of sintering

The sintering process starts with powder preparation. Once the powder is prepared, it is then compacted using a mold or a die to create the correct shape. The pressure can be applied using a variety of techniques, including cold pressing, isostatic pressing, and injection molding [33]. The point of compaction is to create the desired shape while the metal is still loose powder particles.

Once the powder is compacted, it can be heat treated in a furnace. A sintering furnace is heated to temperatures that allow for particle bonding without the metal completely changing phases. The vacuum conditions of Psyche would help this step, as the heating process tends to take place in a controlled vacuum environment to prevent oxidation and to control the final properties of the metal. During the heating process, adjacent particles will start to bond together (neck formation); atoms within the particles migrate, which allows for further bonding and densification (diffusion); and the compacted material shrinks as the particles draw closer together and the necks grow (shrinkage).

In some cases, sintering may add an additional step for controlled grain growth, which can enhance the material properties of the sample. This step allows grain to grow by recrystallization or coalescence. If this step is not added, then the sintered part is slowly cooled to room temperature to prevent the introduction of internal stresses. This step also ensures the final part's dimensional stability.

The result of sintering is a dense, solid material that retains the shape and dimensions of the compacted shape but has improved mechanical and material properties. The sintering process can be tailored to achieve specific material properties, such as density, hardness, and electrical conductivity, but also relies on the powdered metal being in a mold, which limits the shapes that can be created [34].

Appendix C

Initial Concept Generation Sketches

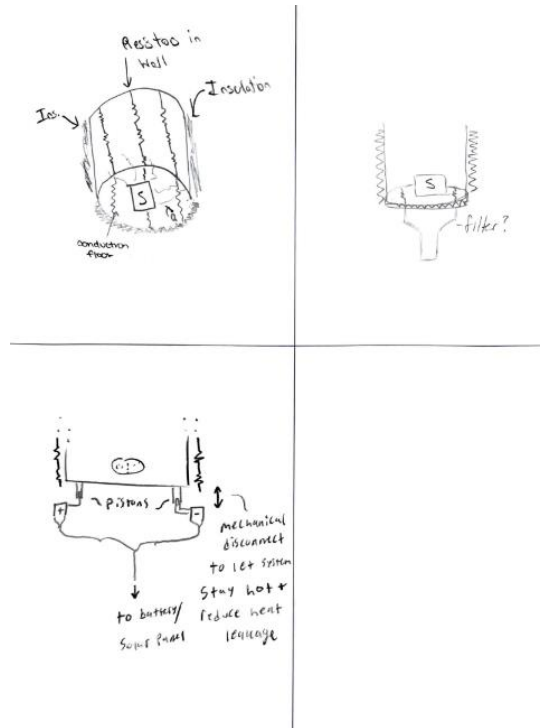


Figure C1: The sample here would be heated by a combination of radiation and conduction, through resistors embedded in the wall.

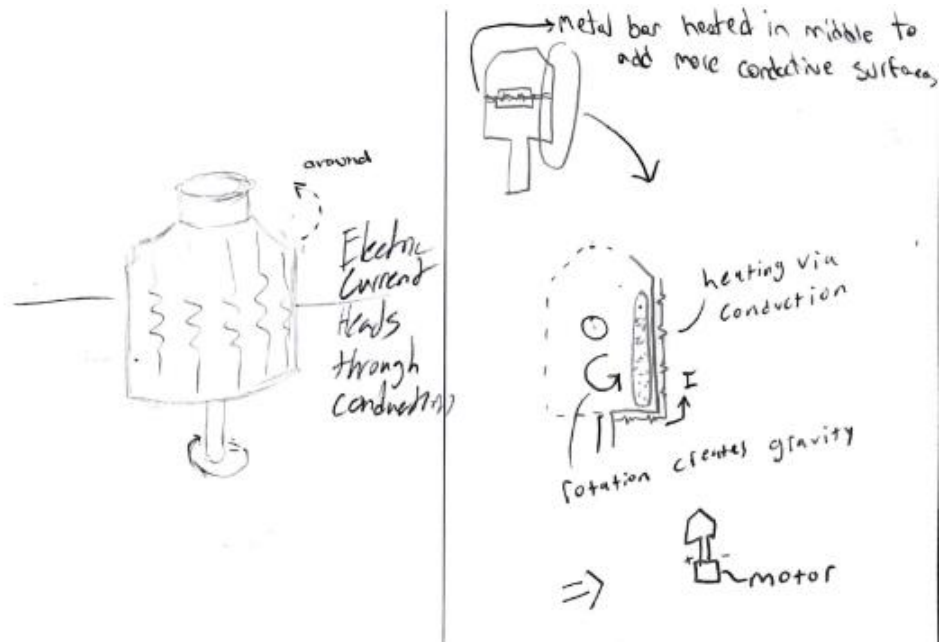


Figure C2: This system relies primarily on conduction, with resistor contact points in the walls and in the center.



Figure C3: This system uses conduction through one rod, constantly “stirring” the sample.

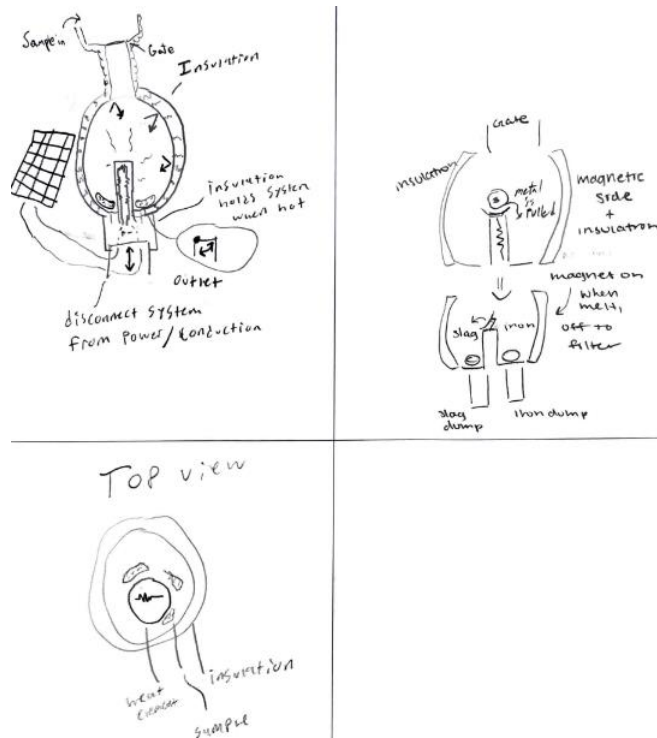


Figure C4: This system is powered by solar energy, uses the conduction stirring rod, and filters via a combination of magnetism and gravity.

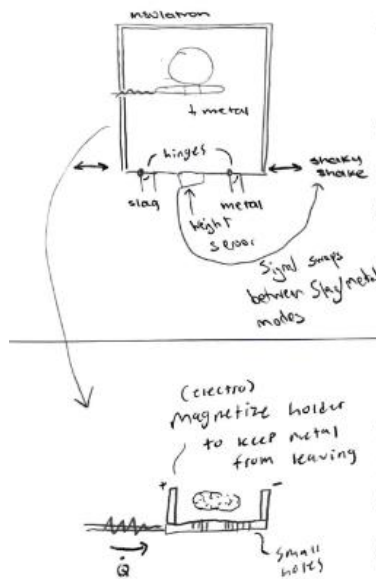


Figure C5: This system combines the induction/conduction idea, where the sample sits on a hot plate with a hole in the middle and molten liquid flows through the middle via gravity and is filtered using a shaker table.

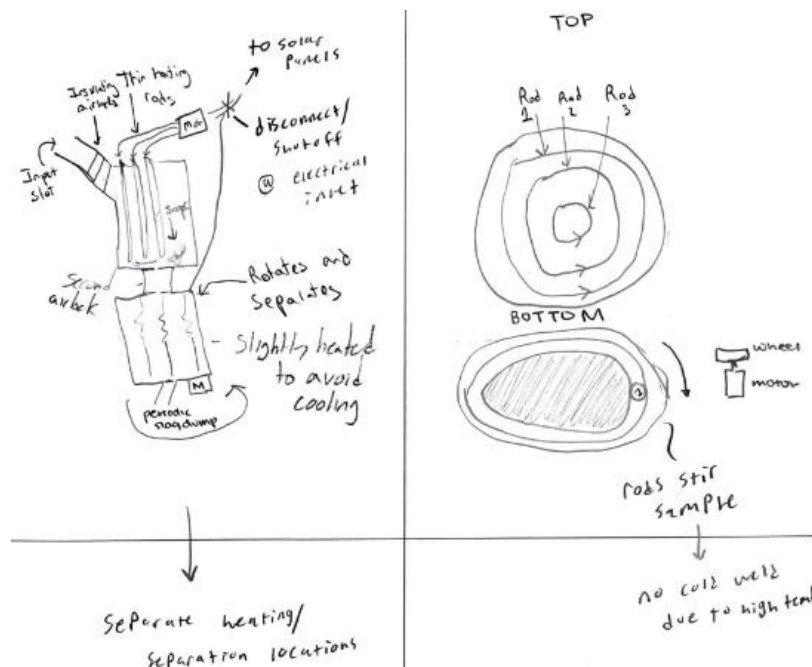
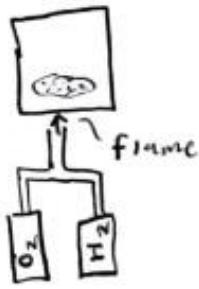


Figure C6: This system uses the idea of stirring heating rods to melt the sample into a sort of slurry.



Heat via fuel + combustion

Figure C7: Heating the sample via combustion using external fuel.

Heat material w/ high-powered laser

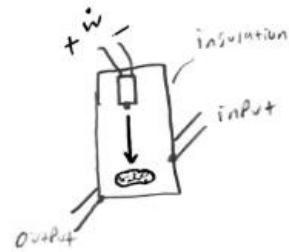


Figure C8: Heating the sample via high-powered laser.

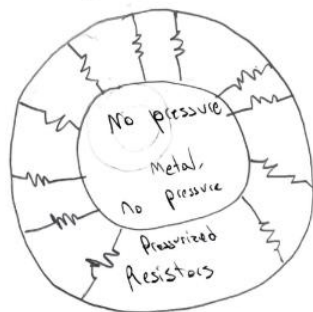
Purview
Induction heater above sample



Figure C9: Heating the sample via induction, coiled heater above sample.

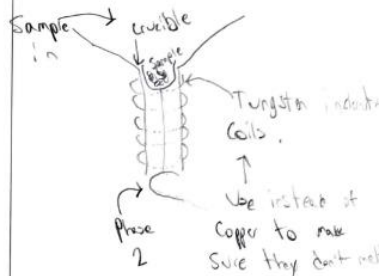
Idea 1:

Top:



Pressure difference should make resistors not melt, metal still melt

Idea 2:



Alternatively, have a really big crucible, no movement of crucible

Figure C10: Heating the sample via conduction (resistors), with and without a crucible.

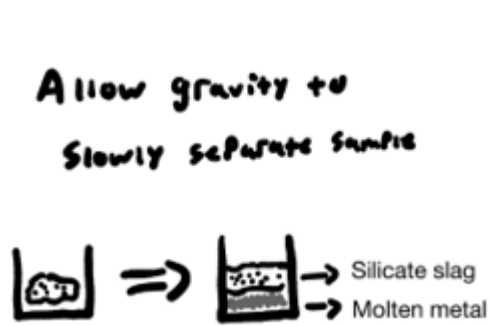


Figure C11: This is a passive system, relying solely on gravity.

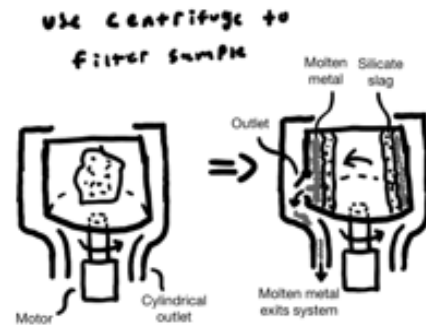


Figure C12: This system uses a centrifuge.

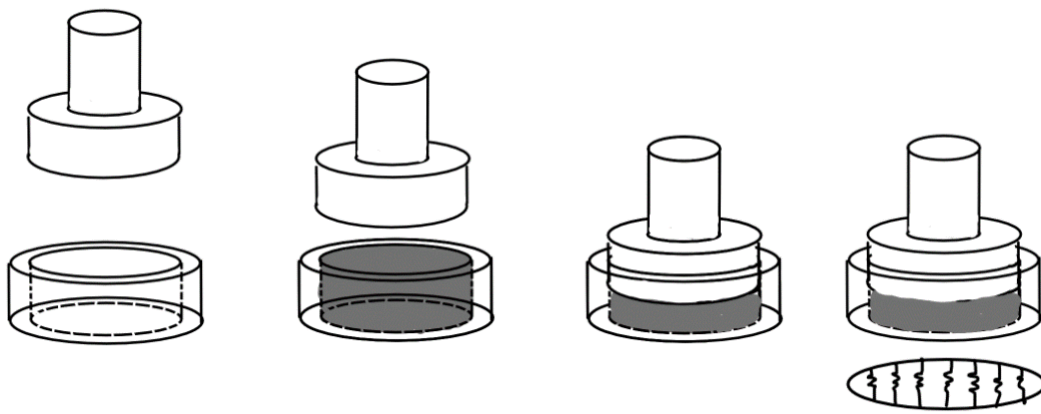


Figure C13: This demonstrates the principle of sintering, where we will mechanically operate a press that will pressurize a collection of powdered sample.

Appendix D

Concept Selection, Heating Systems

The weighted decision matrix for the sample heating function is shown below in Table D1.

Table D1: The weighted decision matrix for each heating element

Criteria	Weight	Concepts							
		Induction		Conduction (Resistor)		Conduction (Rods)		Combustion	
		Rating	Score	Rating	Score	Rating	Score	Rating	Score
Low Complexity	25%	1	0.25	4	1	3	0.75	2	0.5
Feasibility	25%	4	1	2	0.5	3	0.75	5	1.25
Weight of System	20%	2	0.4	4	0.8	3	0.6	1	0.2
Energy Use	10%	5	0.5	3	0.3	4	0.4	1	0.1
Modifiability/Scalability	10%	4	0.4	3	0.3	2	0.2	3	0.3
High insulation	10%	4	0.4	3	0.3	2	0.2	1	0.1
Total		2.95		3.2		2.9		2.45	
Rank		2		1		3		4	

The results of this decision matrix clearly rule out combustion for heating the sample, due to low scores in the weight of the system (the amount of external gas necessary to bring would add up), energy use (would lose heat potential to create steam), and high insulation (need vents to allow steam out, oxygen and hydrogen in). However, the other three systems are very close in score to each other, so even though conduction via resistors technically wins, all three will undergo closer consideration.

Appendix E

Calculations for Nitrogen Container Size

In order to calculate the nitrogen container size, we found the weight of nitrogen needed for 1000 full cycles of heating and cooling. We are unsure what pressure is necessary to limit sublimation, so we assumed a pressure of 1 Pa to be safe. Using the ideal gas law,

$$PV = nRT \quad (F1)$$

where P is the pressure in the system, V is the volume of gas, n is the number of moles of gas, R is the gas constant, and T is the absolute temperature in the system. To find the mass of the gas, the relationship between mass, m , molar mass, M , and number of moles, n ,

$$m = nM \quad (F2)$$

can be utilized once the number of moles is found. Assuming the gas takes up the entire volume of the 10x10x10 cm chamber and we desire 1 Pa of pressure at a temperature of 1000 K, and utilizing the molar mass of nitrogen, 28.01 g/mol, equations (C1) and (C2) respectively yield

$$n = \frac{1 \text{ Pa} * (10 \text{ cm} * \frac{1 \text{ m}}{100 \text{ cm}})^3}{8.314 \frac{\text{J}}{\text{K} * \text{mol}} * 1000 \text{ K}} = 1.203 * 10^{-7} \frac{\text{mol}}{\text{cycle}} = 1.203 * 10^{-4} \text{ mol for 1000 cycles} \quad (F3)$$

$$m = (1.203 * 10^{-4} \text{ mol}) * (28.01 \frac{\text{g}}{\text{mol}}) = 0.00336 \text{ g} \quad (F4)$$

Therefore, less than 0.01 grams of nitrogen are necessary to include in the design for 1000 cycles. A small nitrogen canister of 4 grams was found and chosen to incorporate in our design, due to the fact that it is still lightweight, however a smaller canister could be included in the future.

To understand the expected pressure at max temperature, this calculation was re-performed, using equation (C1) to find the pressure at melting temperature, 1810 K:

$$P = \frac{(1.203 * 10^{-5} \text{ mol})(8.314 \frac{\text{J}}{\text{K} * \text{mol}})(1810 \text{ K})}{(10 \text{ cm} * \frac{1 \text{ m}}{100 \text{ cm}})^3} = 1.8 \text{ Pa} \quad (F5)$$

We will need to design our system to withstand a nominal pressure of 1.8 Pa.

Appendix F

Sublimation Negligibility Justification

One of the tasks we wanted to accomplish this quarter was identification of sublimation as a legitimate design concern. We only found one paper that discussed the potential impacts of sublimation on melting metal in vacuum/space conditions, and further discussions with one of our external advisors pushed us to believe this was a necessary lead.

To identify if sublimation would be an issue, we started by learning ThermoCalc, a software to create phase diagrams. The goal was to create a phase diagram of pure iron at low temperatures and low pressures. However, ThermoCalc is often used for when there are multiple alloys within a material and a material property needs to be measured based on mass percentage of one of the alloys, and this analysis revolved around pure iron [35]. Figure G1, below, demonstrates the closest pure iron pressure-temperature graph we were able to create.

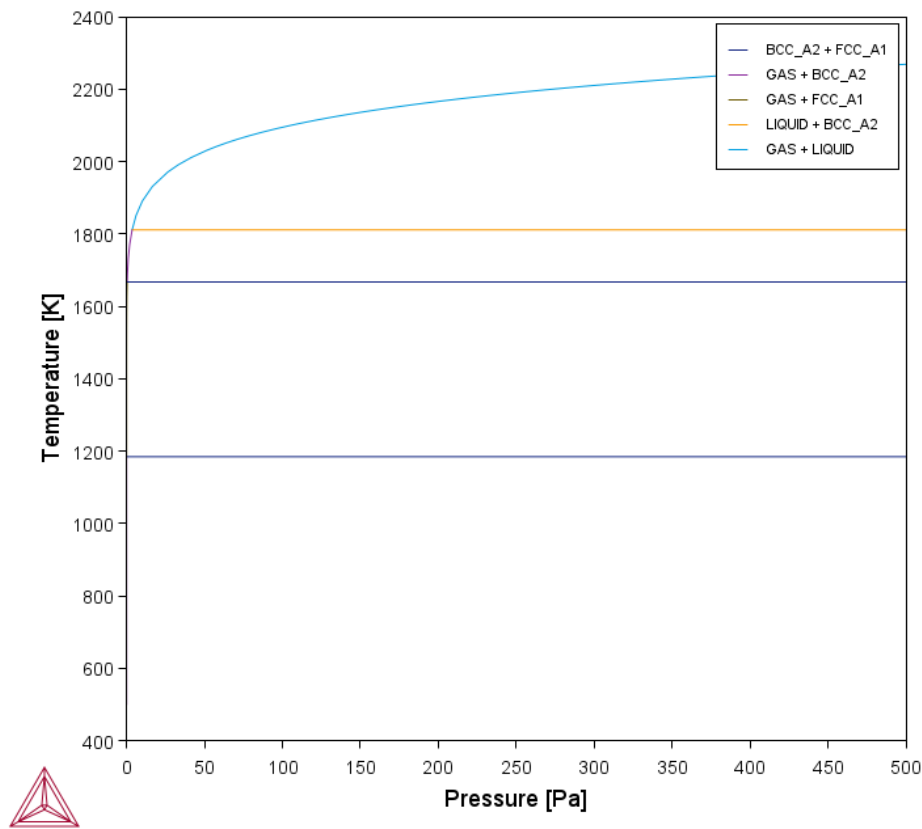


Figure G1: ThermoCalc Pressure v. Temperature Graph of Pure Iron

Notable in this figure are the axes; the smallest range of temperatures the graph was able to produce was 400-2400K, and the smallest range of pressures was 0-500 Pa. The ranges of temperatures and pressures we would expect on Psyche are 50-150K and 0-0.1 Pa respectively, so this software was unable to create any viable conclusions. We also cannot confirm the validity of the low-pressure range,

it is possible the software created the best graph it could and that the phase lines above are not representative of what iron would actually do on Psyche.

Since ThermoCalc was not going to work for our purposes, we went back to research on the properties of iron at low temperatures and pressures. We benchmarked off a study on metal production from lunar regolith to find justification that sublimation could be negligible. This paper found that iron sublimation requires at least 800C (1000K) at high vacuum (as close to 0 Pa as possible) conditions, and that under those ideal conditions the rate of sublimation would fall between 10^{-3} and 10^{-5} grams an hour [36]. While our system would reach 1000K in a vacuum condition as the temperature is raised to melt the iron, the overall process of melting iron is presumed to take no longer than fifty minutes, so sublimation can justifiably be assumed negligible for the purposes of our system.

Appendix G

Material Property Curves

To accurately track the temperature dependence of various material properties, various property databases were consulted to create curve fits. The four properties that vary based on the operating temperature range are electrical conductivity, thermal conductivity, specific heat, and magnetic permeability. Data on magnetic permeability's variation with temperature was unable to be found and was modeled as constant throughout the procedure. The curve fits for electrical and specific heat affected the mathematical model's output, along with the thermal simulation, while thermal conductivity exclusively affected the simulation.

The curves used for iron, the material expected to be found on Psyche, are as follows:

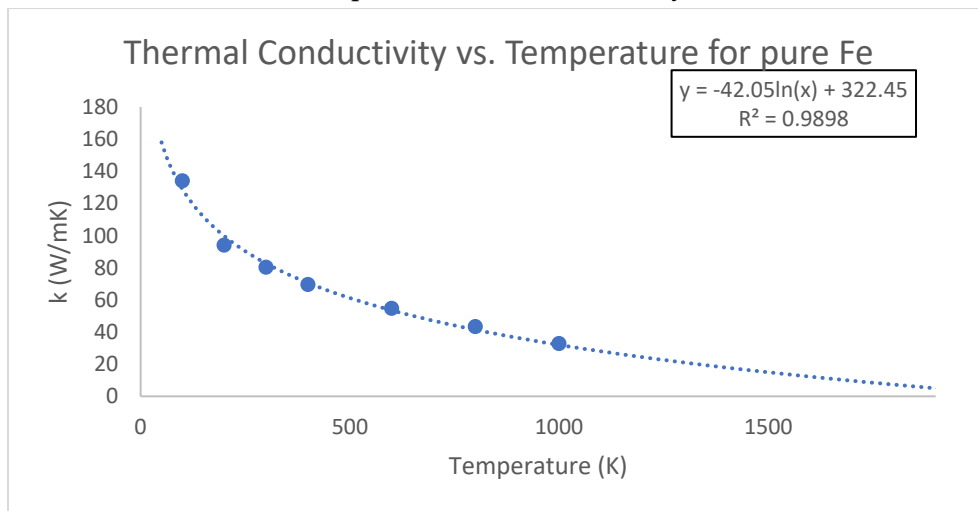


Figure H1: Thermal Conductivity vs. Temperature graph for pure iron [37]

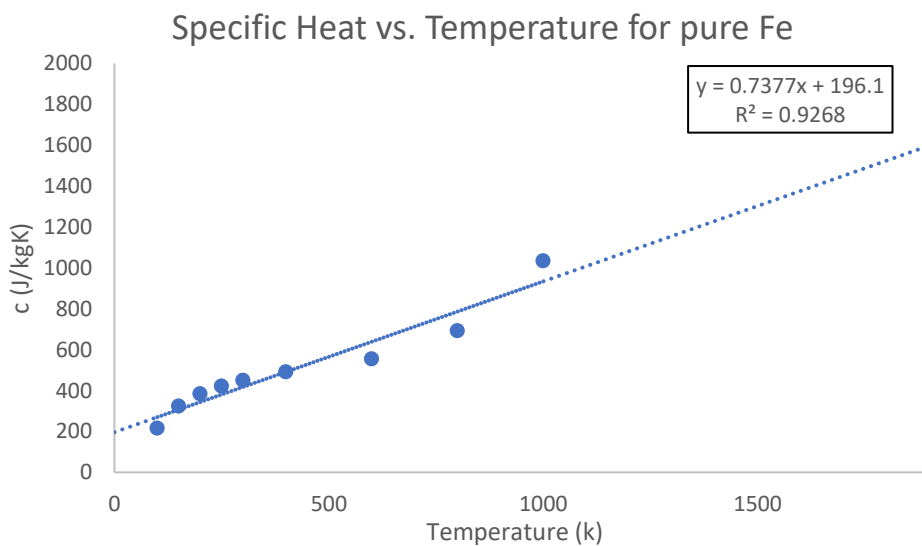


Figure H2: Specific Heat vs. Temperature graph for pure iron [37]

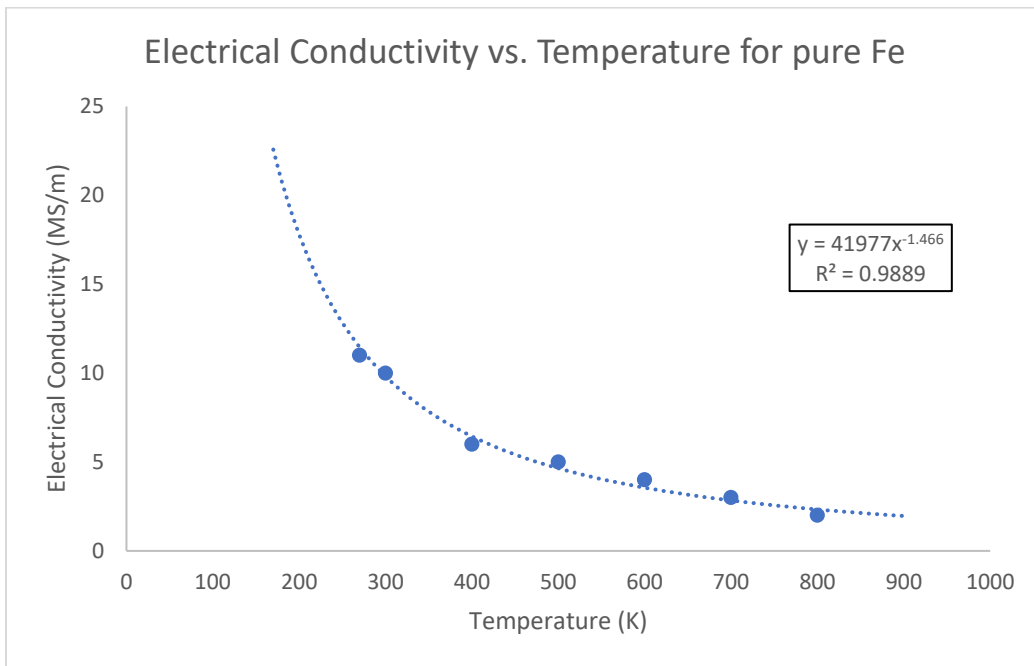


Figure H3: Electrical Conductivity vs. Temperature graph for pure iron [37]

In addition, curves for tin and graphite were found to calibrate the mathematical model and thermal simulations to the experimental data. For tin, information on electrical conductivity at various temperatures was unable to be found, likely due to its low melting point. The curve fits for tin are as follows:

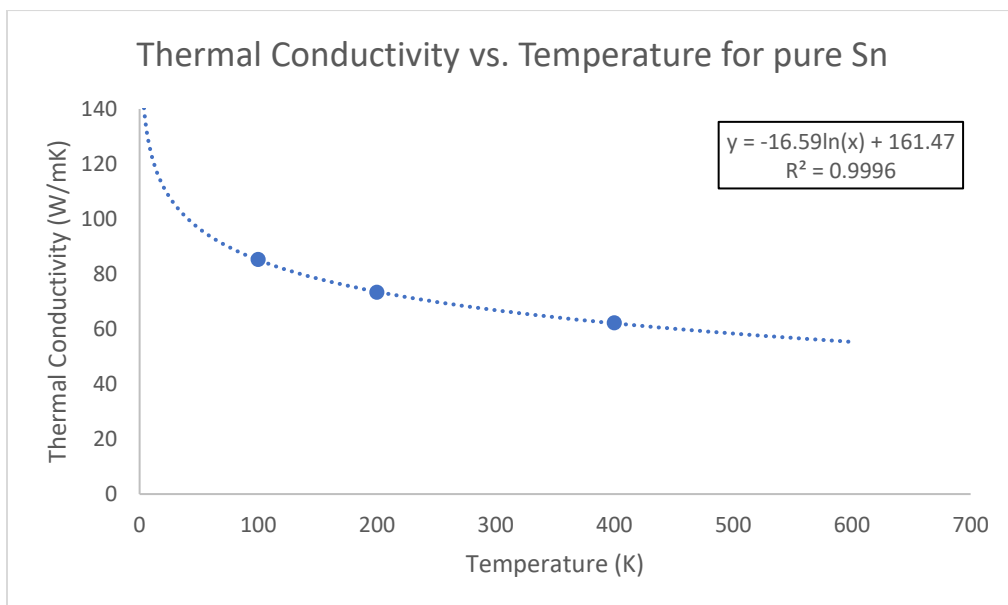


Figure H4: Thermal Conductivity vs. Temperature graph for pure tin [37]

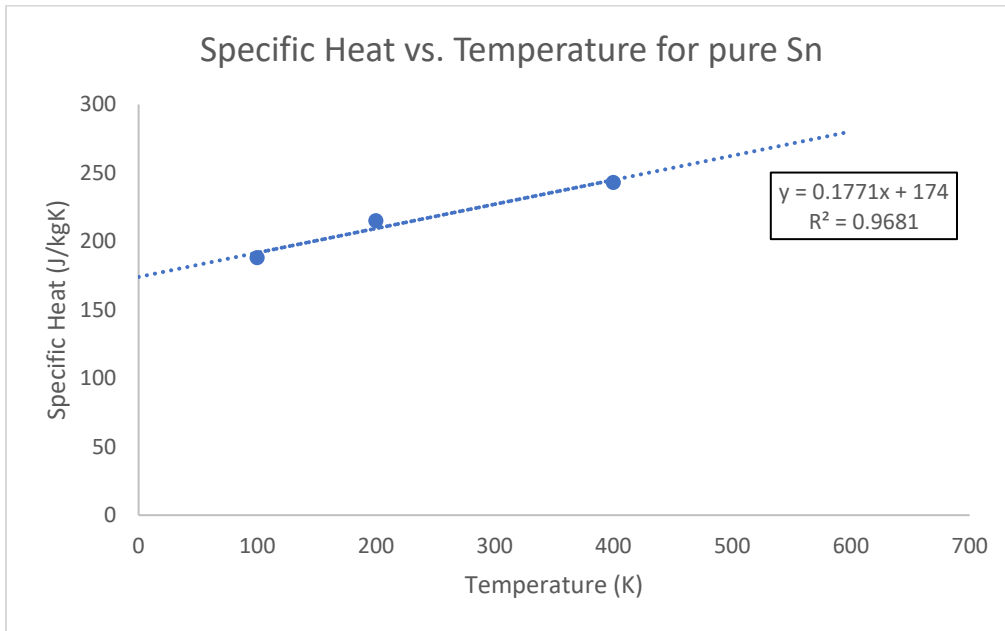


Figure H5: Specific Heat vs. Temperature graph for pure tin [37]

Finally, POCO graphite was examined, primarily from the data provided in the Los Alamos National Lab induction melting experiment [24]. Curve fits were recreated from this data and are as follows:

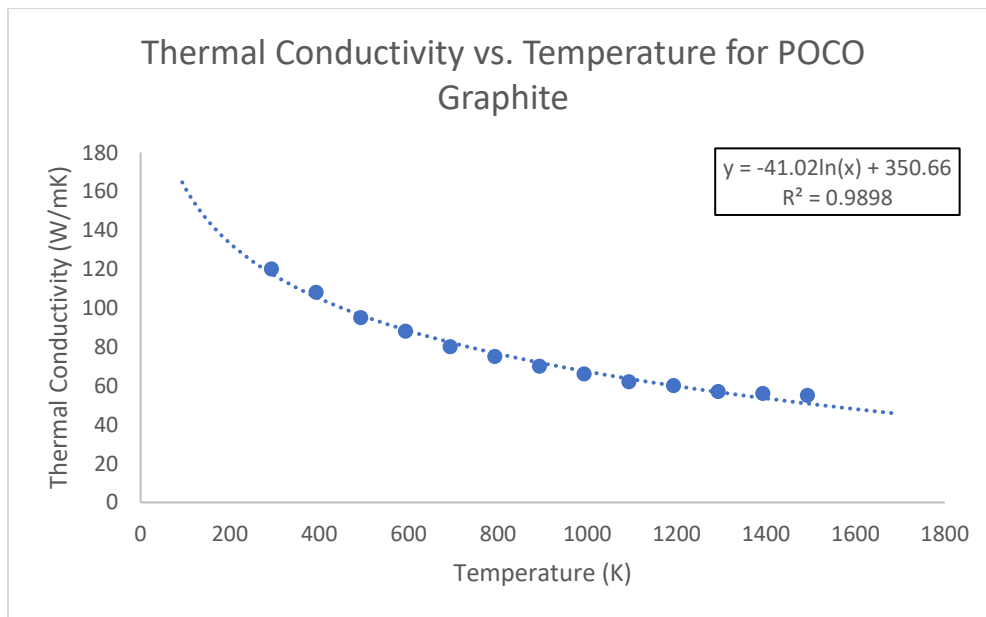


Figure H6: Thermal Conductivity vs. Temperature graph for graphite [24]

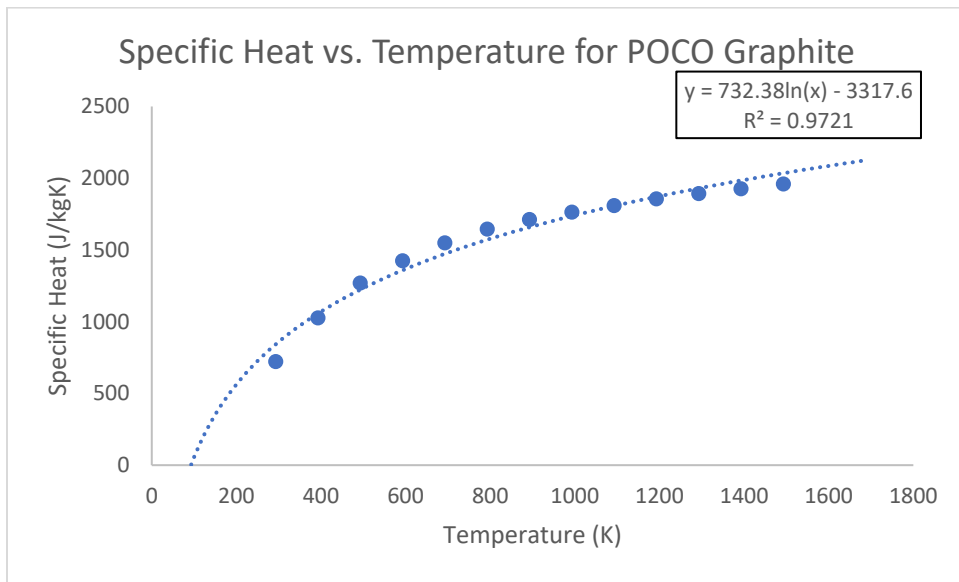


Figure H7: Specific Heat vs. Temperature graph for graphite [24]

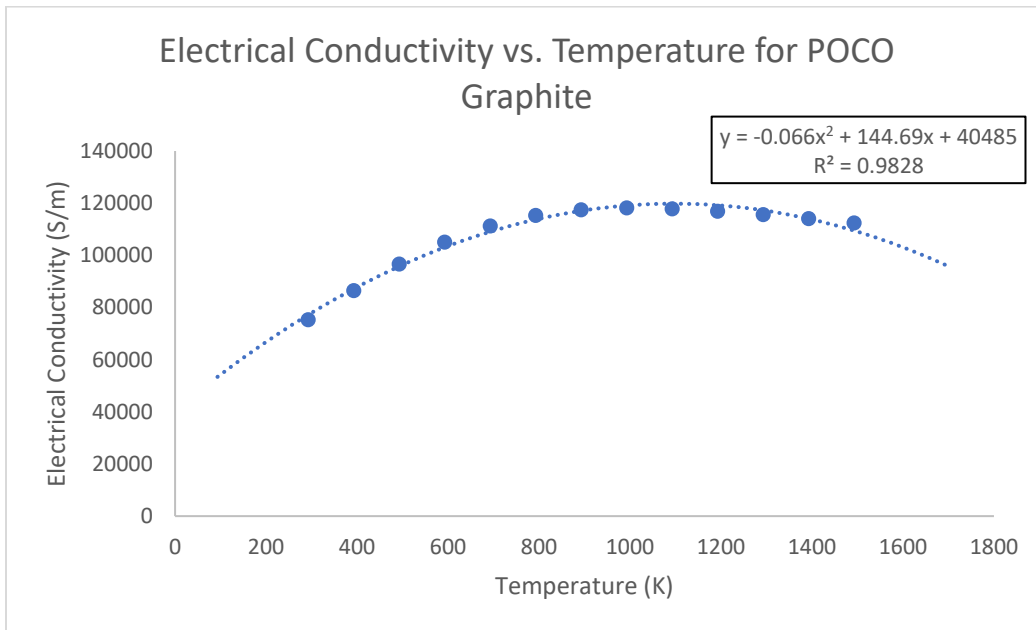


Figure H8: Electrical Conductivity vs. Temperature graph for graphite [24]

When modeling any material property in the mathematical model, the curve fit equations were used, and the property's value was iterated as the material heated, using a finite difference approach.